Validation of wind farm parameterisation in Weather Forecast Model HARMONIE-AROME Analysis of 2019

Dirksen, M.; Wijnant, Ine; Siebesma, A.P.; Baas, Peter; Theeuwes, Natalie E.

Publication date
2022

Document Version
Final published version

Citation (APA)
Dirksen, M., Wijnant, I., Siebesma, A. P., Baas, P., & Theeuwes, N. E. (2022). *Validation of wind farm parameterisation in Weather Forecast Model HARMONIE-AROME: Analysis of 2019*. Delft University of Technology. https://www.wins50.nl/publications

Important note
To cite this publication, please use the final published version (if applicable).
Please check the document version above.

Delft University of Technology

WINS50

Internal report WP5 & WP6

Validation of wind farm parameterisation in Weather Forecast Model HARMONIE-AROME

Analysis of 2019

Authors:
Marieke Dirksen[1]
Ine Wijnant[2]
Pier Siebesma[1,2]
Peter Baas[3]
Natalie E. Theeuwes [2]

July 1, 2022

[1]Delft University of Technology (TUD), PO Box 5, 2600 AA Delft, The Netherlands, www.tudelft.nl
[2]Royal Netherlands Meteorological Institute (KNMI), PO Box 201, 3730 AE De Bilt, The Netherlands, www.knmi.nl
[3]Whiffle, 2629JD Delft, the Netherlands, https://www.weatherfinecasting.com/

Abstract

In the next few decades climate mitigation efforts will transform the North Sea into one of the most important energy sources. The present wind energy capacity on the North Sea is expected to increase by almost a factor 5 in 2030 and almost a factor 10 in 2050. It is therefore of paramount importance to know how wind farms influence the atmosphere.

Wind farms extract kinetic energy from the atmosphere and in doing so decrease the wind speed and increase turbulence levels. More turbulence means more mixing of vertical layers in the atmosphere and a change in humidity and temperature profiles. This may lead to cloud forming or dissipation. Wind farms are also an obstacle to the flow, which is what is called the blockage effect, as opposed to the wake effect behind the wind farm. This report is about the wake effect, mainly on wind, but we also analysed temperature and humidity profiles.

In order to assess and quantify the wake effect, we compared two high resolution re-analyses for the year 2019 on a 2000 by 2000 km North Sea domain. The high resolution re-analyses with a 2.5 km horizontal grid spacing is based on global re-analysis ERA5 and downscaled with mesoscale weather model HARMONIE-AROME which is used operationally at KNMI. One of the re-analyses is without the effect of wind farms (referred to as control or HarmCY43-CTL in this report) and one with the Fitch wind farm parametrization that was recently incorporated in HARMONIE-AROME (HarmCY43-WFP). From the differences between the two we can isolate the wind speed deficits, or wakes, from the wind farms.

Earlier validation studies have shown that a previous version of the HARMONIE-AROME model (HarmCY40) produces accurate wind climatology for undisturbed wind fields (period 2008-2018) and validates well against disturbed tower, aircraft and lidar measurements from 2016. In these studies the wind climatology is not validated for different stability regimes. In this study we do make that distinction and use measurements from 2019 for validation of HarmCY43-CTL and HarmCY43-WFP.

- Generally HarmCY43-WFP outperforms HarmCY43-CTL in wake areas. HarmCY43-WFP even seems to capture the wind in wind farms reasonably well, although the WFP is not designed for that.
- The selection criterion that we used to select disturbed (in wakes) and undisturbed wind directions (outside wakes) seems to work well: the WFP reduces the wind speed bias for disturbed winds significantly, but hardly affects undisturbed winds.
- Our results confirm earlier studies that wakes are strongest for situations with stable stratification: we observed wake lengths as long as about 50 km. We can conclude that HarmCY43-CTL tends to underestimate the wind speed for stable stratification and overestimate the wind speed for weakly stable and unstable stratification, mainly for the lidar measurements. As expected HarmCY43-WFP reduces the wind speed in the wake. This means that HarmCY43-WFP validates better against measurements for weakly stable and unstable stratification. However, for stable stratification HarmCY43-WFP makes the underestimation of the measurements worse (note that this does not imply the wake deficits are biased). This could even become worse if wind turbines are not performing according to the power curve or are not turning at all because of maintenance or legislation, the WFP will not be aware of that and will extract too much energy, overestimate the wake effect and underestimate the wind speed.
- Earlier studies have shown that HarmCY40-CTL captures the diurnal cycle well. HarmCY43-CTL does as well and including the WFP does not seem to affect that.

The results of this study give us confidence that the present HARMONIE-AROME model configuration, including the Fitch WFP, can be used to assess the influence of the anticipated wind farm infrastructure in 2050 on the wind climatology.

1 Introduction

European and British climate mitigation efforts will transform the North Sea into one of the most important energy sources during the next few decades. At the end of 2020 the six wind farms[4] operational in the Dutch waters had a total rated power of 2.44GW. Offshore wind energy is expected to grow fast: on the Dutch part of the North Sea to at least 11.5-21.5GW by 2030 and even 38-72GW by 2050. Ambitions for offshore wind energy change all the time, but with the current plans from the national governments, the total wind energy capacity on the whole North Sea is expected to be 65-100GW in 2030 and 170-210GW by 2050 (in the WINS50 2050 scenario we assume about 190GW). Plans for offshore wind energy on Dutch waters include the *Hollandse Kust* wind farm sites that will become operational between 2022 and 2026, *Ten noorden van de Waddeneilanden* scheduled to become operational in 2027 and the *IJmuiden ver* sites scheduled to become operational in 2028-2029.

Over the years wind turbines have become larger. In less than 20 years they have become more than twice as big. The 80 Vestas V80-2MW turbines in Hornsrev I, one of the first offshore wind farms commissioned on the North Sea (2002), have a 70m hub height and a 80m rotor diameter (tip height 110m). The largest wind turbine in the world at this moment is the 12MW Haliade-X. It was built in 2019 in Rotterdam and has a hub height of 153m and a rotor diameter of 214m (tip height 260m). There are plans to use a turbine with even more power and larger turbine blades in North Sea wind farm *Sofia* (100 14MW turbines with rotor diameter 222m; to be build 2023/24 and commissioned 2024/25).

The increase in number and size of wind farms and the fact that turbines are getting larger, means that the effect on the atmospheric boundary layer (ABL) will only get larger (Fitch et al., 2013; Porté-Agel et al., 2020). Wind farms extract kinetic energy from the atmosphere and in doing so, cause the wind speed to decrease and turbulence levels to increase. Wind farms also affect temperature and humidity profiles and may influence the formation and dissipation of low clouds and fog.

The Dutch Offshore Wind Atlas (DOWA)[5] (Wijnant et al., 2019) provides undisturbed (no wind farm effects) North Sea wind climatology for the period 2008-2018. Validation against wind measurements with cup anemometers on wind masts (Knoop et al., 2019), satellite measurements (Duncan et al., 2019a) and (floating) lidar measurements (Duncan et al., 2019b; Knoop and Wijnant, 2019; Valk and Wijnant, 2019) showed an improvement compared to its predecessor, the KNW-atlas[6] (Stepek et al., 2015; Wijnant et al., 2015). The KNW atlas also provides undisturbed wind climatology and covers the years 1979-2019. DOWA not only performs well offshore (Knoop and Wijnant, 2019; Knoop et al., 2020). Both DOWA and KNW-atlas are based on ERA5 reanalysis downscaled with HARMONIE-AROME to hourly weather data on a horizontal resolution of 2.5 by 2.5km. Although not included in the DOWA atlas, one of the innovations in the DOWA project was to include the effect of wind farms in HARMONIE-AROME using the most commonly used wind farm parametrisation (WFP) by Fitch et al. (2012). Validation, with a.o. aircraft measurements, shows that at all validation locations the bias decreased compared to the reanalysis without WFP (van Stratum et al., 2021).

Whiffle, TU Delft and KNMI are part of the WINS50 consortium. For the WINS50 project KNMI extended the DOWA climatology with three years (2019-2021) and provided a future hypothetical wind farm scenario for 2050 (with 2020 weather). The WINS50 project provides two different climatologies: one with and one without wind farm effect. The DOWA and WINS50 domain are the same and cover the UK, a large part of Europe and the whole North Sea.

The goal of this report is to validate the Fitch-WFP in HARMONIE-AROME. In order to validate the wind speed deficit behind the wind farm we compared the two HARMONIE-AROME runs, the one with (HarmCY43-WFP) and the one without WFP (HarmCY43-CTL). Figure 1 shows the wind speed deficit averaged over 2019 at a height of 100m. The largest wind speed deficit is near the wind farm, $\sim$2m/s. We did not use the 2019 averaged values for the actual validation but we distinguished between disturbed (less than 50km behind a wind farm) and undisturbed wind directions. Also, we distinguished different atmospheric stability regimes.

We did a quality assessment of all publicly available wind measurements and selected only the best ones for the validation of HarmCY43-WFP. These include cup anemometer, vane and (floating) lidar measurements. The WFP validation is done for 2019. The main objectives of this report are: (1) Evaluation of the Fitch-WFP (2) Quantify the wind speed deficits caused by wind farms.

For the validation of HarmCY43-WFP and HarmCY43-CTL we will answer the following questions:

- *Q1: How well is the wind (speed, direction) represented over the North Sea by HARMONIE-AROME?*
- *Q2: How well is the diurnal cycle of the wind represented by HARMONIE-AROME?*
- *Q3: How does the wake effect depend on vertical stability and wind speed?*

[4] OWEZ, Luchterduinen, Prinses Amalia, Gemini and Borssele 1&2

[5] https://www.dutchoffshorewindatlas.nl/

[6] https://www.knmiprojects.nl/projects/knw-atlas

- *Q4: How strong and how long is the wake effect of the wind farms?*

The outline of this report is as follows: chapter 2 provides an overview of literature on wake development behind wind farms and measurements that are used for wake validation. Chapter 3 provides an overview of the publicly available measurements on the North Sea in 2019 and a description of the necessary post-processing of model data and measurements for validation. Chapter 4,5 and 6 describe the results of the WFP validation: chapter 4 for the offshore KNMI/RWS measurements, chapter 5 for the FINO1 and FINO3 measurements and chapter 6 for the (floating) lidar measurements. This includes validation of wind speed profiles for different stability regimes, the diurnal variation of the wind speed and the validation of the wind directions. The results will be discussed in chapter 7 and the conclusions will be drawn in chapter 8. Appendix A provides an overview of the WP6 deliverables of the WINS50 project. Appendix B provides background information on other types of wind measurements and validation studies. Appendix C provides background information on the directional correction for the Zephir300 lidars.

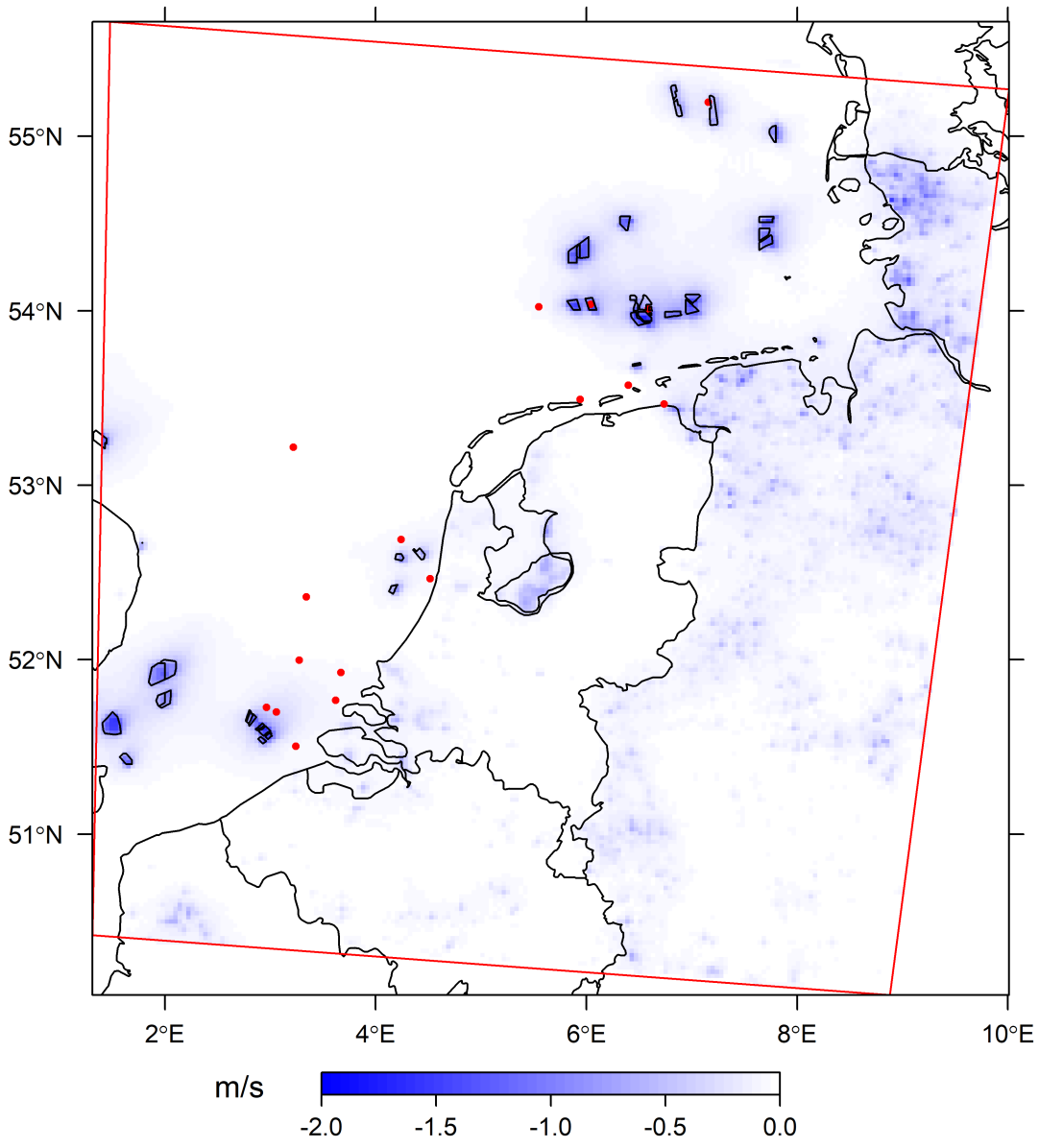

Figure 1: An overview of the validation domain with in red the measurement sites (the total model domain is approximately four times the size of the validation domain). The red square denotes the validation domain where the output is saved and made publicly available. In the background the yearly averaged difference between HARMONIE-AROME with and without wind farm parametrisation at a height of 100m is plotted. On Sea the operational wind farms from 2019 were included as black polygons (over land the operational wind farm areas were not included in this figure). Within the operational wind farms the wind speed is up to 2m/s slower. Around the wind parks a typical average velocity deficit is 0.5m/s.

2 Literature Background

In this section we provide a brief literature overview of the wake formation and measurements that are used for wake model validation.

2.1 Wake formation

The flow from across a wind farm can be distinguished in the following flow zones (Porté-Agel et al., 2020):

- *Induction zone*: As the wind flow approaches an obstacle it will slow down and divert around it, which is referred to as the blockage effect. The wind farms turbines will decelerate the upstream flow, resulting in a reduction of the energy production (Bleeg et al., 2018). This effect is more pronounced when the neutral boundary layer has a strong inversion.
- *Development zone*: The wake development begins with wakes behind individual turbines. Further downstream into the wind farm, as the wakes grow, they start to interact with other wakes. The internal boundary layer (IBL) of the wind farm starts to grow.
- *Fully developed zone*: When the internal boundary layer of the wind farm has fully grown, i.e. reaching the top of the atmospheric boundary layer (ABL), the flow becomes homogeneous. A wake velocity deficit of approximately 6% was estimated from SAR and Doppler radar measurements (Ahsbahs et al., 2020). For small wind farms this zone can develop several kilometres downstream of the wind farm (Nygaard and Christian Newcombe, 2018).
- *Wake zone*: Downwind the flow starts to accelerate until the momentum is fully recovered. The wakes can grow up to tens of kilometres downwind of the wind farm (Christiansen and Hasager, 2005; Nygaard and Christian Newcombe, 2018; Siedersleben et al., 2018b). The wake length depends on the stability of the flow. Wakes can grow up to 70km or longer under stable conditions (Hasager et al., 2015; Platis et al., 2018). During unstable conditions the wake recovery is much faster (Schneemann et al., 2020).

For very large wind farms an additional exit region was observed (Porté-Agel et al., 2020). In this case the wake recovery already started before the flow is downstream of the wind farm.

The WFP of Fitch et al. (2012) only parametrises the far-wake flow, i.e. at a distance of more than 5 rotor diameters downstream (Fitch, 2016). With a HARMONIE-AROME horizontal grid spacing of 2.5km we expect to solve regional wake effects on scales of ∼10km. Therefore, the model validation with measurements close to or within a wind farm does not hold.

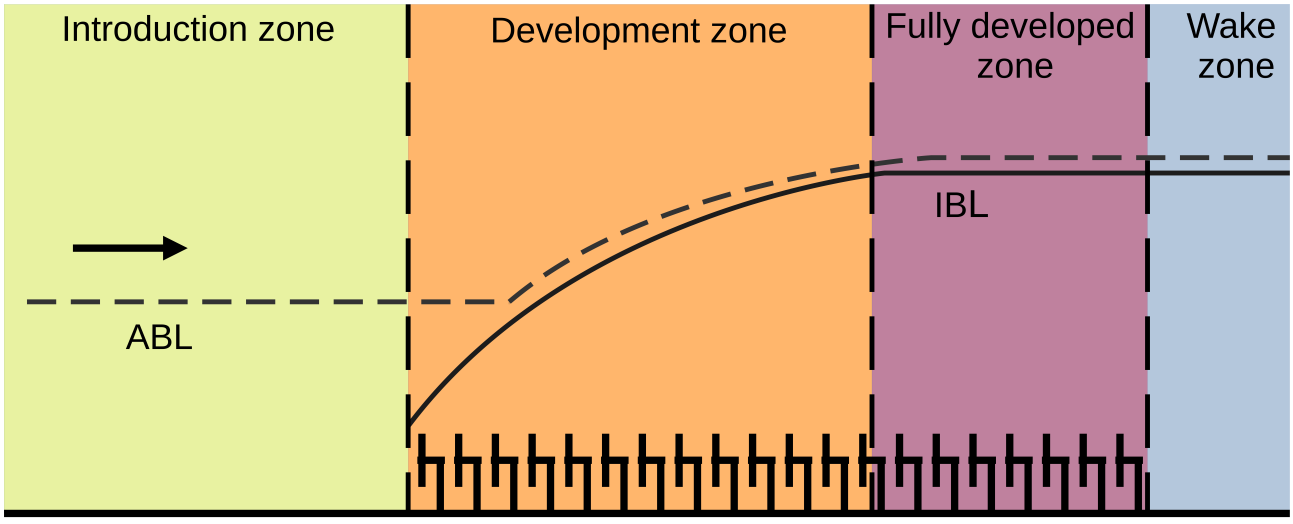

Figure 2: Schematic overview of the wake development from upwind to downwind of the wind farm, adapted after (Porté-Agel et al., 2020). The black arrow indicates the wind direction. The dotted horizontally curved line represents the Atmospheric Boundary Layer (ABL) and the solid curved line represents the Internal Boundary Layer (IBL).

2.2 Validation Measurements

We used lidar and cup anemometer and vane measurements for validation of HarmCY43-WFP. There are other measurement on different temporal and spatial resolutions and with a different coverage that are also used for (wake) model validation. For an overview we refer to Appendix B.

There are few reasons why we only used lidar and cup anemometer and vane measurements. For example, the availability of data from Doppler radars (Ahsbahs et al., 2020), Synthetic aperture radar (SAR) (Hasager et al., 2005) and aircraft flight (Lampert et al., 2020) is limited. Also the SAR data requires complicated post-processing in order to reduce the noise. The ASCAT data, with a grid box of 12.5km, is too coarse for wake detection.

With the lidar measurement we can validate the wind profiles up to 300m, which is very relevant for wind energy. The number of lidar measurements is however still quite low, which is why we also used KNMI and FINO measurements, despite the fact that they only measure at one or a few heights.

Compared to DOWA, the bias of the lidar and cup anemometer measurement is in the order of 0-0.3m/s (Duncan et al., 2019b), but cup anemometer measurements are generally more precise than lidar measurements. Valk and Wijnant (2019) estimated the precision of the cup anemometer and the lidar around 0.21m/s and 0.36m/s, respectively.

The wind directions from the lidar type Zephir300 are measured with Doppler technique and can be 180^o off. Knoop et al. (2021) found an error in 9% of the Cabauw lidar measurements, mainly at low wind speeds. After correcting the error with wind mast measurements from the same site the wind direction bias found by Knoop et al. (2021) reduces to less than 2^o.

Cup anemometer wind measurements may be disturbed by a vent stack on a oil rig (Joosten and Stepek, 2019) or by the mast itself. At FINO1 and FINO3 mast corrections should be applied to the raw measurements (Westerhellweg and Neumann, 2019).

3 Methodology

The methodology chapter starts with a description of the validation domain (paragraph 3.1). Next, the instrumentation and positioning of the wind measurements is described (paragraph 3.2). Paragraph 3.3 provides an overview of the availability of the measurements. After providing background information on the measurements the methodology continues with a description of the HARMONIE-AROME setup (paragraph 3.4). The implementation of the wind farm parametrisation (WFP) according to Fitch et al. (2012) is included.

During the data processing (paragraph 3.5) mast corrections for the cup anemometer are described. Next, the selection of grid points and temporal interpolation of the data for the validation is described. The last paragraph 3.5.3 introduces the Bulk Richardson number (Ri). With the Ri we will compare the model performance between stable and unstable atmospheric conditions.

3.1 Research area

The reanalysis domain covers the UK, a large part of Europe and the whole North Sea. The validation domain is denoted by the red square in Figure 1. Within the Dutch part of the validation domain several offshore wind farms were operational in 2019:

- Amalia: 120MW
- Luchterduinen: 129MW
- Offshore Windpark Egmond aan Zee (OWEZ): 108MW
- Gemini: 600MW
- Belgium wind farms: 1.6GW

Figure 3 provides an overview of the operational wind farms in 2019 and the locations of the wind measurements. BSA lidar is in the south-western part of the validation domain near the Belgium wind farms (Fig.3B). Further away from these farms are the KNMI/RWS measurement sites Vlakte van de Raan, Oosterschelde, Lichteiland Goeree and Europlatform. Just offshore, in the middle of the validation domain, near three smaller wind parks are the lidars of HKNW and HKNA as well as the KNMI/RWS measurement site IJmond (Fig.3C). The K13A lidar and K13 KNMI/RWS measurement site are positioned in the central north-western part of the validation domain. On the northern part of the shore the Eemshaven lidar is mounted. The KNMI/RWS measurement sites Huibertgat and AWG-1 are not far offshore near the northern islands. Further offshore in the North are the FINO1 tower, KNMI/RWS measurement site BG-OHVS-2 and TNWB lidar, in or close to the productive Gemini and German wind farm clusters (Fig.3C). With the German wind farm cluster we refer to the operational wind farms Alpha Ventus, Borkum Riffgrund and MEG Offshore. The FINO3 tower is near the northern border of the validation domain on the edge of a wind farm.

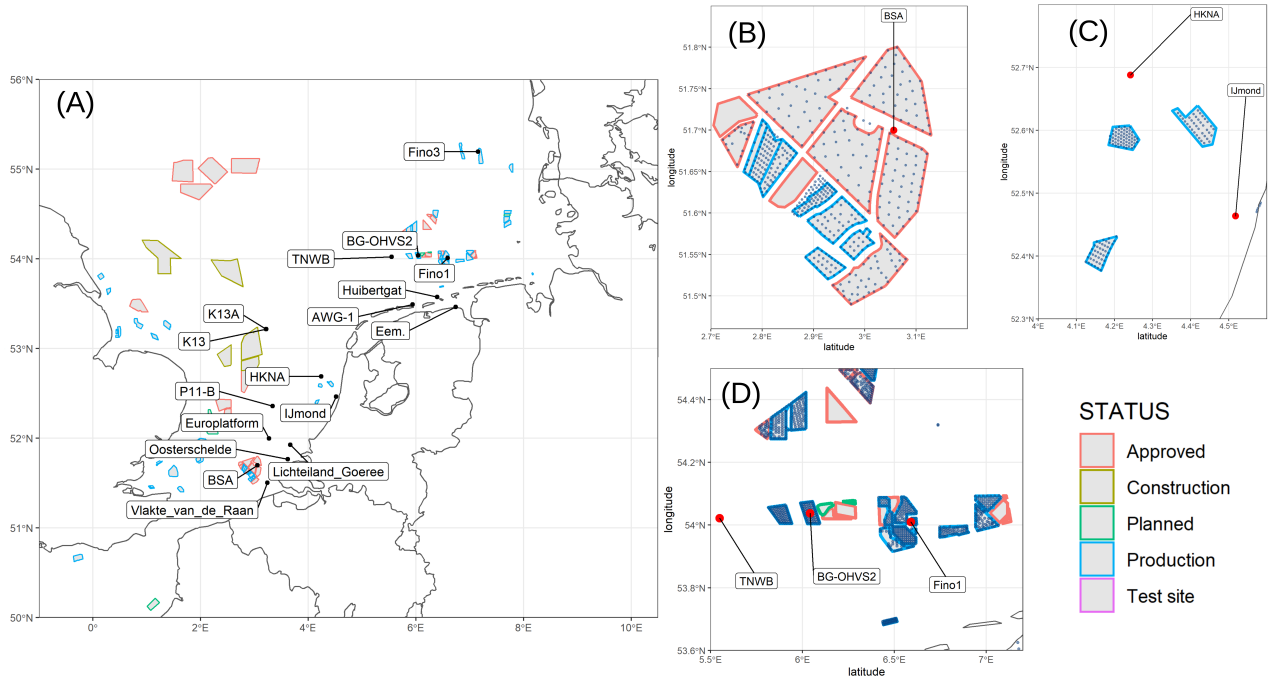

Figure 3: Measurements on the North Sea in 2019 and status of the wind farms (blue is operational in 2020). (A) Overview of the entire research area. Within the validation domain the modelling parameters are easily accessible. The lidars are BSA, HKNA, TNWB, K13A and Eemshaven. The FINO1 and FINO3 instrumentation is mounted on a meteorological tower. The other locations are KNMI/RWS measurement sites. (B) Zoom in at the Belgian wind farm zone. (C) Zoom in of the *Amalia*, *Luchterduinen* and *OWEZ* operational wind farms. (D) North of the *Waddenzee* with the TNWB lidar west of the wind farm clusters. The operational *Gemini* wind farm has the KNMI meteorological station BG-OHVS2 inside the farm. Further east the FINO1 tower is positioned inside the German wind farm cluster (including the operational wind farms Alpha Ventus, Borkum Riffgrund and MEG Offshore).

3.2 Wind farms and positioning of the measurements

From the KNMI/RWS measurement sites[7] the best quality wind speed measurements include AWG-1, BG-OHVS2, Europlatform, Huibertgat, IJmond, K13 and Lichteiland Goeree (Tab.1). At each location the wind speed is measured with cup anemometers on a single height. The measurements from AWG1 mounted on a vent stack and have been corrected for the disturbance caused by the vent stack. BG-OHVS2, Europlatform, K13 and P11-B are all mounted on large oil rigs. The measurements on the oil rigs are at a minimum height of 50m. The remaining measurements are on wind masts and all measure lower than the ones on the oil rigs (Tab. 1).

The measurement towers of FINO1 and FINO3 measure up to approximately 100m. The temperature and humidity were validated at the FINO1 and FINO3 locations. The FINO1 tower is located in the middle of the wind farm allowing the validation of the wakes within the park. The FINO3 tower is on the western edge of an operational wind farm. FINO3 is also close to a second farm west of the tower (Tab.2).

The KNMI/RWS measurements sites all have the cup anemometer instrumentation. From the FINO1 and FINO3 tower the cup anemometer measurements were used for the model validation (since these can be corrected for disturbances of the mast). The uncertainty in the cup anemometers depends on the calibration, operational characteristics and mounting. The calibration uncertainty of the cup and ultrasonic anemometer are typically 0.031m/s and 0.1m/s. The uncertainty related to the operational characteristics depends on the class of the anemometer (in the order of 0.1m/s up to 0.2m/s). The uncertainty due to the mounting can be estimated from multiple measurements at different angles. The total uncertainty is expected to be in the order of $3-4\%$ (Duncan et al., 2019b).

The lidars BSA, HKNA, K13A, TNWB and Eemshaven are ideal for the validation of wind profiles (Tab.2). The lidar measurements give reliable data up to a maximum height of approximately 300 m. The lidars HKNA and Eemshaven measure up to 200 m. BSA and Eemshaven are positioned close to wind farms. The BSA lidar is located north-east of the Belgian wind farm zone. The lidar at Eemshaven is positioned on the coastline near its harbours wind farm on its eastern side. The lidars at HKNA and TNWB are measuring around 20km from

[7] https://dataplatform.knmi.nl/dataset/windgegevens-1-0

Table 1: Overview of the selected 10 minute KNMI/RWS wind speed data in 2019. The measurement height has been rounded off in meters above mean sea level. The WF column denotes the angles of operational wind farms within 50km range. The coordinate reference system is WGS84.

name	height	type	lat	lon	WF
Oosterschelde/BG2	17m	cup anemometer	51.77	3.62	243-255
Vlakte van de Raan	17m	cup anemometer	51.50	3.62	277-309
P11-B	51m	cup anemometer	52.36	3.34	-
Huibertgat	18m	cup anemometer	53.57	6.40	0-36
AWG1	60m	cup anemometer	53.49	5.94	55-59
IJmond	17m	cup anemometer	52.46	4.52	249-261
					300-311
					330-348
K13	74m	cup anemometer	53.22	3.22	-
Lichteiland Goeree	38m	cup anemometer	51.93	3.67	-
Europlatform	29m	cup anemometer	52.00	3.38	202-228
BG-OHVS2	50m	cup anemometer	54.04	6.04	0-360

Table 2: Overview of the 10 minute tower and lidar measurements in 2019. The WF column denotes the angles of operational wind farms within 50km range. The coordinate reference system is WGS84.

name	type	lat	lon	WF
FINO1	cup anemometer	54.01	6.59	0-360
FINO3	cup anemometer	55.20	7.16	7-175
				240-298
BSA	zephIR300	51.70	3.06	192-298
K13A	zephIR300	53.22	3.22	-
HKNA	zephIR300	52.69	4.24	115-136
				173-200
TNWB	zephIR300	54.02	5.55	27-93
Eemshaven	leosphere	53.46	6.74	93-160

operational farms. South and south-east of the HKNA lidar there are two small wind farms. The TNWB lidar is West of the FINO1 tower outside the Gemini parks. The K13A lidar is not in the proximity of operational farms.

The Eemshaven measurement site was equiped with the leosphere windcube. The other measurement sites at BSA, HKNA, K13A and TNWB measured with the ZephIR300 instrumentation. The leosphere windcube and ZephIR300 generally have a wind speed uncertainty of less than 0.2m/s. Notorious to the the Doppler-shift method of the ZephIR300 is the 180^o shift in wind direction. Because of the homodyne detection method a single frequency is employed. Therefore the ZephIR300 relays on meteorological wind measurements from a nearby station. Although relaying on the anemometer for the wind direction, in some cases the incorrect direction is assigned (Knoop et al., 2018,0). Using the modelled directions from HARMONIE-AROME we will correct for the 180^o directional error of the ZephIR300.

3.3 Data availability

Figure 4 provides an overview of the available wind measurements within the validation domain for the year 2019. The lidars BSA and FINO1 have data available in the autumn. The HKNA and Eemshaven lidar have been measuring in the first months of 2019. The TNWB lidar has data spread over the summer, autumn and last months of 2019. The FINO3 tower and K13A lidar have data whole year round. Also the data availability of the other cup anemometers and buoys is generally more continuous.

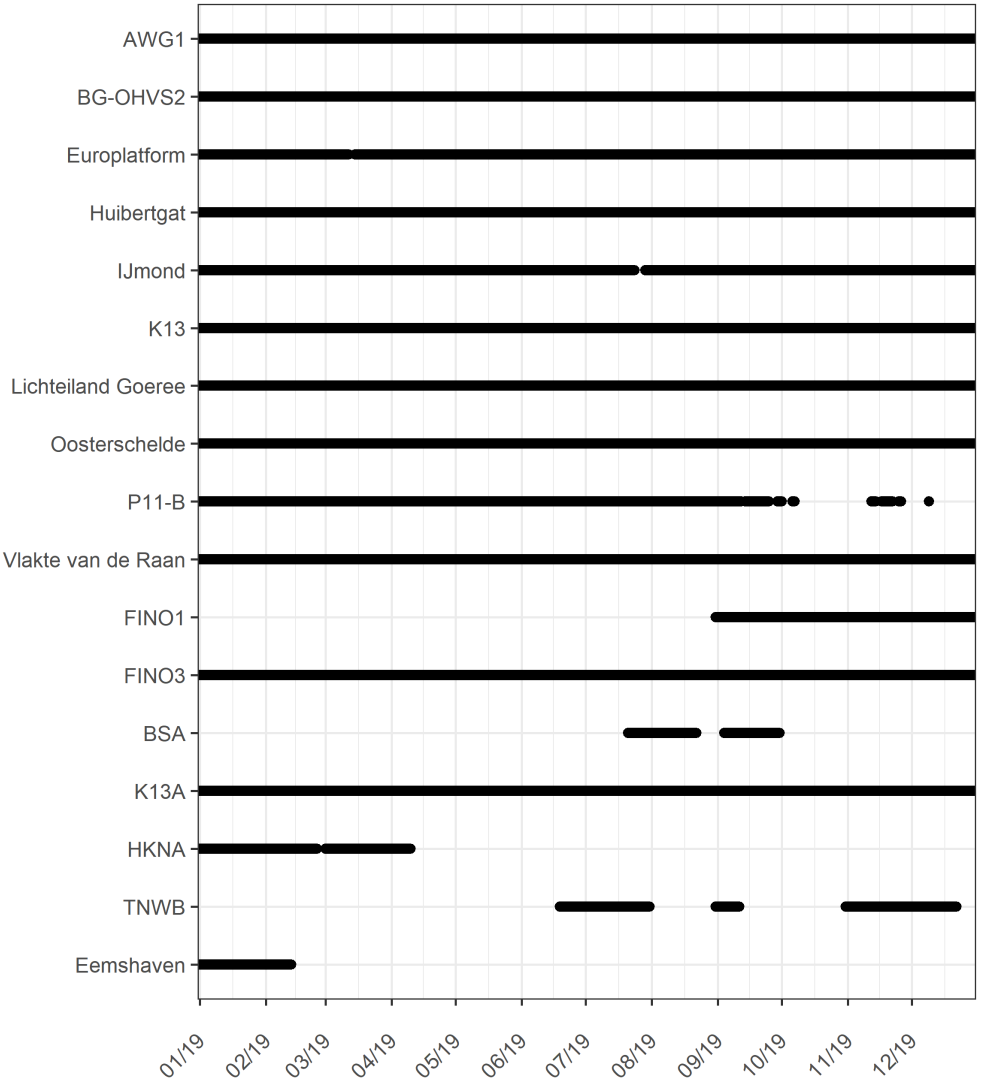

Figure 4: Availability of wind measurements on the North Sea and lidar measurements in 2019. The KNMI/RWS measurement sites are AWG-1, BG-OHVS2, Europlatform, Huibertgat, IJmond, K13 and Lichteiland Goeree. The FINO1 and FINO3 towers measure besides wind also temperature and relative humidity up to approximately 100m. The lidars at BSA, K13A, HKNA, K13A, TNWB and Eemshaven provide wind profiles from ∼50m up to a maximum height of 300m on the North Sea.

3.4 HARMONIE-AROME CY43

HARMONIE-AROME is a non-hydrostatic convection-permitting weather forecast model, based on the NWP models ALADIN and HIRLAM (Brousseau et al., 2011; Seity et al., 2011). In these experiments HARMONIE-AROME used ERA5 for the initial and boundary conditions. For a detailed escription of the HARMONIE-AROME-physics the reader is referred to Bengtsson et al. (2017). In the next section we will provide background on the WFP. At the end of this section the simulation set-up for the WINS50 project of the HARMONIE-AROME runs is included.

The wind farms parametrisation interacts with the Planetary boundary layer (PBL) by adding the TKE and momentum sink from the turbines (Bengtsson et al., 2017).

3.4.1 Wind Farm Parametrisation

The wind turbines in HARMONIE-AROME are parametrised with the (Fitch et al., 2012) scheme. Each model grid cell can contain multiple wind turbines, with the force acting at the rotor area of the turbines at hub height. The limitation of this approach is that the wind speed within a grid cell, and thus the effect of an individual turbine is unknown (Fischereit et al., 2021). Including the WFP in HARMONIE-AROME has resulted in a wind speed bias reduction of approximately 0.5m/s up to a height of $300m$ (Stratum et al., 2019).

The WFP is modelled as a thrust force acting at the turbines rotor area. Part of the thrust force C_T is converted into electrical energy, which is referred to as the power coefficient C_P. The energy that is converted into C_{TKE} is given by $C_T - C_P$.

The kinetic energy (KE) is transferred into electricity power, for a single grid cell $\Delta_k = (\Delta x \Delta y \Delta z)$, equals:

$$\left.\frac{\delta KE_k}{\delta t}\right|_{\text{cell}} = \frac{\delta}{\delta t}(\frac{1}{2}\rho_k|\vec{V_k}|^2)\Delta_k, [Js^{-1}] \tag{1}$$

where ρ is the density and $\vec{V}$ is the horizontal wind vector and, $|\vec{V}| = \sqrt{u_2 + v^2}$. The amount of energy extracted from the atmosphere depends on the mills specifications and the wind speed. Equation 1 can be rearranged into the velocity change with time:

$$\frac{\delta|\vec{V_k}|}{\delta t} = -\frac{1}{2}C_T|\vec{V_k}|^2 A_k \Delta_k^{-1}, [ms^{-2}] \tag{2}$$

where δV_{ijk} is a horizontal wind vector and A_k is the rotor area intersect at the k-th model level, where the total rotor area is defined as $A_T = (\pi/4)D^2$. The (Fitch et al., 2012) scheme assumes that the KE which is not transferred into electrical produces turbulent kinetic energy TKE :

$$\frac{\delta TKE_k}{\delta t} = \frac{1}{2}C_{TKE}|\vec{V_k}|^3 A_k \Delta_k^{-1}, [m^2 s^{-2} s^{-1}] \tag{3}$$

3.4.2 Simulation setup

During the WINS50 project HARMONIE-AROME cycle 43 (HarmCY43) will cover the years 2019, 2020 and 2021. Besides the applied model cycle the setup and WFP is similar to Stratum et al. (2019). The reanalysis also uses a three hourly 3D-VAR data assimilation scheme and in addition to the standard measurement MODE-S (De Haan, 2011,0) and ASCAT (Marseille and Stoffelen, 2016) were assimilated.

The HarmCY43 domain size is 2000x2000km with a horizontal grid spacing of 2.5km. The central coordinates are $51.96N, 4.9E$, this location is in the south-western part of the Netherlands. The variables of the model runs are saved at the 65 model height levels and 17 interpolated height levels (10m, 20m, 40m, 60m, 80m, 100m, 120m, 140m, 150m, 160m, 180m, 200m, 220m, 250m, 300m, 500m, 600m). The interpolated levels, which will be used for the validation, are more easily accessible and stored in smaller files for the validation domain[8]. Besides the standard meteorological output the WINS50 project also stores the turbulent kinetic energy (TKE) and fluxes (sensible and latent heat).

In order to analyse the wakes in HarmCY43 both a control run, without WFP (HarmCY43-CTL) and a run with wind farms as parametrised in Fitch et al. (2012) (HarmCY43-WFP) will be evaluated. The difference between the runs HarmCY43-CTL and HarmCY43-WFP in Figure 1 shows the averaged wake effects. In this report we will not evaluate the future hypothetical run for the year 2050 (with the 2020 weather) WFP.

Table 3 summarizes the model configuration for the WINS50 simulations. This set-up is as close as possible to that of the DOWA simulations, but some modifications could not be avoided. For details on the differences between the DOWA and WINS50 simulations, including an assessment of the consequences for the modelling results, we refer to (Theeuwes et al., 2021b).

[8] https://dataplatform.knmi.nl/

Table 3: Model settings for for the WINS50 simulations and domain specifications. The coordinate reference system is WGS84.

Model specifications	
Model	HARMONIE-AROME CY43h2.1
Initial & Boundary conditions	ERA5
Data assimilation	3D-VAR
$XRIMAX$	0.2
$XSCALE_H$	~ 0.68
Domain specifications	
Central coordinates	$51.96N, 4.9E$
Domain size	2000x2000km
Validation domain	500x500km
Horizontal resolution	2.5x2.5km
Vertical levels	65
Interpolated levels	17
Validation domain corners	**[lon,lat]**
North-west	[1.480,55.656]
North-east	[10.011,55.270]
South-east	[8.880,50.078]
South-west	[1.311,50.421]

3.5 Data processing

First, we will describe the mast corrections which have been applied to the wind measurements of FINO1 and FINO3. Second, the spatial assumptions and temporal interpolation to match the measurements with the HarmCY43 model output are described. Finally, the atmospheric stability calculations are included.

3.5.1 Mast corrections

The FINO1 and FINO3 towers measure the wind speed at several angles of the mast. When positioned downwind of the tower the cup anemometers are in the wake of the mast. Since we are interested in the *'free'* wind and not the local mast effects we have to correct for the mast wake. The procedure differs between the FINO1 and FINO3 tower: FINO1 measures at two sides of the mast and has a top anemometer while FINO3 measures the wind speed at three sides of the mast. The FINO1 cup anemometers (sensor type R3-50) are installed at the heights 41m, 51m, 61m, 71m, 81m and 91m. The wind speeds were corrected for the boom angles $135 - 143^o$. In 2019 a top anemometer was installed at 102m.

The measurements were corrected using the uniform ambient flow mast correction scheme (UAM-scheme) (Westerhellweg and Neumann, 2019; Westerhellweg et al., 2012). We assume similar wind speeds at all measurement heights during unstable uniformly stratified conditions. These conditions are here defined by a minimum velocity of 4m/s and a minimum temperature difference between the 3m water temperature and 30m air-temperature of $-1\,°C$). After making this selection of the data the correction factor was calculated as ws_{top}/ws_{bottom}, where ws stands for the horizontal wind speed. The uncertainties of the correction are in the order of 1-4 %. The mast correction of (Westerhellweg and Neumann, 2019) was extended to the entire time-series. At the height levels 41m, 51m, 61m, 71m, 81m and 91m the mast corrections were in good agreement with the more recent measurements (Fig.5). The mast corrections were applied when the the sensor was in the wake of the mast, which was for the wind directions 285° up to 340° (varying slightly depending on the boom angle variations).

At the FINO3 location a simple mast correction was applied. At the heights 51m, 71m and 91m cup anemometers are installed with boom angles of 105°, 225° and 345°. Depending on the wind direction the boom which was not in the wake of the mast was selected (Leiding et al., 2016).

3.5.2 Interpolation

The HarmCY43 output is averaged over a 2.5 x 2.5km area and instantaneous. The measurements from both the lidars and cup anemometers are at a single location and often time averaged. Since the HarmCY43 output is available at more height levels than the measurements it makes sense to interpolate the model data to the measurement heights. The next challenge is to match the differences in time and area with the model. One can

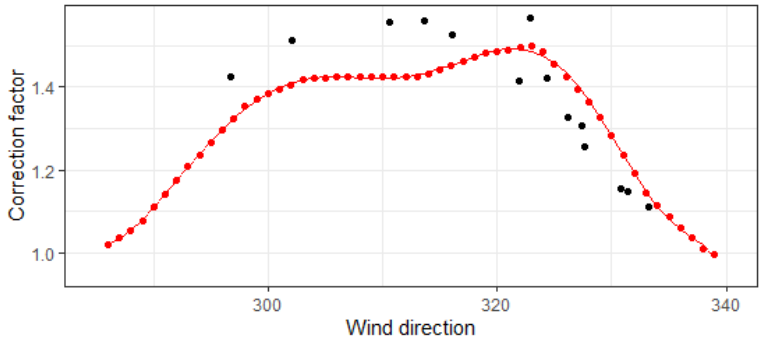

Figure 5: Mast correction of FINO1. In red the mast corrections at a height of 91m from (Westerhellweg and Neumann, 2019) and in black the estimates from the top anemometer at 102m measuring in 2019. Note that due to the limited amount of data from the top anemometer we have not been able to calculate the correction factor for all angles.

argue that if the measurements are averaged over approximately an hour this would be similar to the time for the wind to pass trough the 2.5 x 2.5km grid box (Stepek et al., 2015).

Height: To match the location of the measurements the closest HarmCY43 grid point was selected. The HarmCY43 output from the interpolated height levels (10m, 20m, 40m, 60m, 80m, 100m, 120m, 140m, 150m, 160m, 180m, 200m, 220m, 250m, 300m, 500m, 600m) was interpolated to the measurement heights. For the validation the HarmCY43 data was interpolated using a 5^{th} order polynomial function.

Time: Because of the spatial difference between the measurement point and grid averaged model output the measurements have been time-averaged. Previously, the FINO1 measurements have been used to verify the optimal time-averaging period (Stepek et al., 2015). The time-averaging period has been derived from the once a year wind speed at 100m, approximately 28m/s. The best comparison was found between 40 and 60 minutes. Here, the measurements have been smoothed using a 60 minute window function.

Diurnal and directional profiles: For the diurnal and directional plotting routines used for the figures in section 6 (wind speed as a function of time or angle on the x-axis and height on the y-axis) the HarmCY43 data and the time-averaged lidar measurements were interpolated to heights between 50m (lidar measurements are too uncertain below this height) and the highest measurement level and with a vertical spacing of 20m. The minimum number of measurements at each time-step for the 5^{th} order polynomial interpolation is set to 6.

3.5.3 Atmospheric stability

The wake lengths strongly depend on the stability of the atmosphere (Schneemann et al., 2020). Therefore it is essential to compare the performance of HarmCY43-WFP under various stability regimes. We derived the stability from HarmCY43-CTL, i.e. the background flow without disturbances of the wind farms. We used the Bulk Richardson number to define the atmospheric stability because it can be calculated for a layer around hub height. The Bulk Richardson number (Ri) is defined as:

$$Ri = \frac{\frac{g}{\overline{\theta_v}} \frac{\Delta \overline{\theta_v}}{\Delta z}}{\frac{\Delta \overline{u}}{\Delta z}^2 + \frac{\Delta \overline{v}}{\Delta z}^2}, \tag{4}$$

where the overline denotes the average, g the gravitational constant, θ_v the virtual potential temperature, z the height and, u and v are the eastern and northern wind components. The Richardson number was estimated around hub height at the interpolated model levels 60m, 80m, 100m, 120m and 140m. Here, $\Delta\overline{\theta_v}$, $\Delta\overline{u}$ and $\Delta\overline{v}$ were calculated as the temperature and wind gradient over each $\Delta z = 20$m, and averaged over the various model levels. The mean Ri was calculated from the averaged gradients. The flow is dynamically unstable and turbulent when the Richardson number is lower than the critical Richardson number ($Ri < Rc$). The transition to a stable regime is around $Rc \approx 0.20 - 0.25$ (Baas et al., 2007; Grachev et al., 2013; Lenderink and Holtslag, 2004). It should be noted that this is not the transition to laminar flow. Here, the following flow regimes are distinguished based on the Richardson number:

- Stable: $R_i > 0.25$
- Weakly stable: $0.0 <= R_i <= 0.25$
- Unstable: $R_i < 0.0$

The analysis of the different flow regimes will be combined with the disturbed and undisturbed wind directions (Tab.2).

4 KNMI/RWS measurements on the North-Sea

We have validated the WINS50 runs of HarmCY43 with a selection of the better wind speed measurements with cup anemometer from KNMI: AWG1, BG-OHVS2, Europlatform, Huibertgat, IJmond, K13, Lichteiland Goeree, Oosterschelde, P11-B and Vlakte van de Raan. An overview of the instrumentation and location of these sites is included in table 1 and figure 3.

The cup anometers on the KNMI wind masts are mounted at 17m or higher. In order to be able to compare these with HarmCY43 data we interpolated the HarmCY43 data to measurement height. The measured wind speeds were averaged over an hour around the HarmCY43 output. More details about the data processing are included in section 3.5. We calculated the 95% confidence intervals of the measured values, modelled values, bias, R^2 and $RMSE$ with 10.000 bootstrap repetitions.

The validation results of HarmCY43-CTL and HarmCY43-WFP are summarized in table 4 and 5, respectively. Here the bias is the modelled value (denoted by CTL or WFP) minus the measured value (denoted by OBS). Only at K13 the wind speed is underestimated by the model (negative bias). At all other selected KNMI sites the wind speed is overestimated. K13, Lichteiland Goeree and P11-B are nowhere near a wind farm so HarmCY43-CTL and HarmCY43-WFP are the same. At other sites there are wind direction dependent effects from nearby wind farms. In table 4 and 5 we do not distinguish between disturbed and undisturbed winds and put them all together. In table 6 we do make that distinction.

BG-OHVS2 is surrounded by turbines from wind farm Gemini with a hub height of 89m. At BG-OHVS2 the model overestimates the wind speed most (+1.5m/s), but the difference gets significantly smaller when the effect of the wind farm is included in the model (+0.5 m/s). The difference between model and measurements is nowhere larger than 0.55m/s when the effect of the wind farms is included. The mean squared correlation coefficient (R^2) is hardly affected by including wind farm effects: its value remains fairly high (between 0.8 and 0.9). The RMSE values are between 1.3m/s and 2.1m/s and slightly better when wind farms are included.

Table 4: Validation of HarmCY43-CTL in 2019. The 95% confidence intervals are calculated with 10.000 bootstrap repetitions. The measured values are denoted by OBS, the modelled values by CTL and WFP.

name	nr.	OBS	CTL	bias	R^2	$RMSE$
AWG1	8709	8.54 (8.46,8.61)	8.77 (8.69,8.85)	0.24 (0.2,0.27)	0.78 (0.77,0.79)	1.84 (1.81,1.88)
BG-OHVS2	8742	8.04 (7.95,8.13)	9.51 (9.43,9.6)	1.47 (1.44,1.51)	0.87 (0.86,0.88)	2.14 (2.11,2.17)
Europlatform	8655	8.65 (8.56,8.74)	8.79 (8.7,8.88)	0.14 (0.11,0.17)	0.88 (0.88,0.89)	1.46 (1.42,1.49)
Huibertgat	8739	8.11 (8.04,8.18)	8.23 (8.15,8.3)	0.12 (0.09,0.15)	0.86 (0.86,0.87)	1.32 (1.29,1.35)
IJmond	8619	7.79 (7.71,7.87)	8.16 (8.08,8.25)	0.37 (0.34,0.4)	0.87 (0.86,0.88)	1.46 (1.43,1.49)
K13	8715	9.81 (9.71,9.9)	9.37 (9.28,9.47)	-0.43 (-0.46,-0.4)	0.89 (0.89,0.9)	1.53 (1.49,1.57)
Lichteiland Goeree	8739	8.67 (8.59,8.76)	8.8 (8.71,8.89)	0.13 (0.1,0.16)	0.89 (0.88,0.89)	1.42 (1.39,1.46)
Oosterschelde	8723	7.75 (7.67,7.82)	8.37 (8.29,8.46)	0.63 (0.6,0.66)	0.87 (0.86,0.88)	1.56 (1.52,1.59)
P11-B	6489	8.4 (8.3,8.5)	8.67 (8.56,8.77)	0.27 (0.22,0.31)	0.83 (0.81,0.84)	1.84 (1.79,1.9)
Vlakte van de Raan	8724	7.71 (7.64,7.78)	8.3 (8.22,8.38)	0.59 (0.56,0.62)	0.86 (0.85,0.87)	1.57 (1.53,1.6)

Table 5: Validation of HarmCY43-WFP in 2019. The 95% confidence intervals are calculated with 10.000 bootstrap repetitions. The measured values are denoted by OBS, the modelled values by CTL and WFP.

name	nr.	OBS	WFP	bias	R^2	$RMSE$
AWG1	8709	8.54 (8.46,8.61)	8.76 (8.68,8.84)	0.23 (0.19,0.27)	0.78 (0.77,0.79)	1.85 (1.82,1.89)
BG-OHVS2	8742	8.04 (7.95,8.13)	8.55 (8.46,8.64)	0.51 (0.48,0.54)	0.88 (0.88,0.89)	1.56 (1.52,1.6)
Europlatform	8655	8.65 (8.56,8.74)	8.75 (8.66,8.84)	0.1 (0.07,0.13)	0.88 (0.88,0.89)	1.45 (1.41,1.48)
Huibertgat	8739	8.11 (8.04,8.18)	8.22 (8.15,8.29)	0.11 (0.08,0.14)	0.86 (0.85,0.87)	1.33 (1.3,1.37)
IJmond	8619	7.79 (7.71,7.87)	8.11 (8.03,8.19)	0.32 (0.29,0.35)	0.87 (0.86,0.88)	1.45 (1.42,1.48)
K13	8715	9.81 (9.71,9.9)	9.38 (9.29,9.48)	-0.42 (-0.45,-0.39)	0.9 (0.89,0.91)	1.49 (1.46,1.53)
Lichteiland Goeree	8739	8.67 (8.59,8.76)	8.74 (8.65,8.83)	0.07 (0.04,0.1)	0.89 (0.88,0.89)	1.41 (1.38,1.44)
Oosterschelde	8723	7.75 (7.67,7.82)	8.3 (8.21,8.38)	0.55 (0.52,0.58)	0.88 (0.87,0.88)	1.51 (1.48,1.54)
P11-B	6489	8.4 (8.3,8.5)	8.69 (8.58,8.79)	0.28 (0.24,0.33)	0.82 (0.81,0.83)	1.86 (1.81,1.91)
Vlakte van de Raan	8724	7.71 (7.64,7.78)	8.23 (8.16,8.31)	0.53 (0.5,0.56)	0.86 (0.86,0.87)	1.52 (1.49,1.55)

In table 4 and 5 we do not distinguish between disturbed and undisturbed wind directions whereas including wind farm effect should have (1) no effect for undisturbed wind directions and (2) improve the model performance for disturbed wind directions. We expect wind farm effects to be largest for stable stratifications and in order to study this, we also distinguish three stability regimes: ($Ri > 0.25$) stable, ($0.0 <= Ri <= 0.25$) weakly stable and ($Ri < 0.0$) unstable (see sec.3.5).

Table 6) shows the model performance for different stability regimes and for disturbed and undisturbed wind

directions. The disturbed wind directions correspond to WF wind directions in table 1 based on the operational wind farm polygons of 2019.

The results per station can be summarized as follows:

- **BG-OHVS2:** The measurements are in operational wind farm *Gemini*, so wind measurements are disturbed from all directions. The wind speeds of HarmCY43-CTL are overestimated by 1.4-1.7m/s, but with the WFP the overestimation is reduced to 0.3-0.8m/s, with the largest bias for weakly stable conditions.

- **AWG1:** There are not enough disturbed measurements to draw robust conclusions about including the wind farm effect. For undisturbed winds HarmCY43-WFP and HarmCY43-CTL perform similar, which is what is supposed to be the case. HarmCY43 slightly overestimates the undisturbed wind speed under stable conditions and gives an overestimation of about 0.3m/s in unstable and about 0.5m/s in weakly stable conditions.

- **Europlatform:** Although there are significantly more undisturbed (> 1000 per stability class) than disturbed measurements ($267 - 499$ per stability class) there are still enough measurements to draw conclusions about the performance of the WFP. For undisturbed wind the bias does not change significantly if wind farm effects are included in the model. This is what we expect. What we also expect to see is an overestimation of the wind speed by HarmCY43-CTL and a wind speed closer to the measurements for HarmCY43-WFP. That is what we find for weakly stable and unstable stratification, but not for stable stratification: HarmCY43-WFP underestimates the wind speed with 0.3m/s, while HarmCY43-CTL is almost unbiased. Europlatform is 45km from the nearest wind farm and this is almost at the 50km limit that we assume for disturbed winds. So, where the WFP in HarmCY43 still predicts a small average wake effect (0.2m/s), we do not measure it.

- **Huibertgat:** At Huibertgat there are not enough disturbed measurements to draw robust conclusions on the performance of the WFP. For undisturbed wind directions HarmCY43 is unbiased for stable and weakly stable conditions. There is only a small bias for unstable conditions of 0.3m/s, comparable to the measurement error.

- **IJmond:** Although there are significantly more undisturbed ($2000 - 3000$ per stability class) than disturbed measurements ($147 - 317$ per stability class) there are still enough measurements to draw conclusions about the performance of the WFP. We observe an improvement of the bias with the WFP for all measurements, though the largest improvement was for disturbed conditions. For stable conditions HarmCY43-WFP is unbiased, the disturbance of the wind farms is around 0.2m/s. For unstable conditions the 0.5m/s bias of HarmCY43-CTL is reduced to 0.4m/s with the WFP. The largest differences with the measurements are under weakly stable conditions, even with the WFP the wind speeds were overestimated with almost 1m/s.

- **Oosterschlede:** Although there are significantly more undisturbed (> 1700 per stability class) than disturbed measurements ($148 - 252$ per stability class) there are still enough measurements to draw conclusions about the performance of the WFP. The biasses of HarmCY43-WFP are in all cases smaller than HarmCY43-CTL, also for the undisturbed wind directions. For undisturbed winds the differences in bias are less than 0.1m/s. Under disturbed conditions the bias of HarmCY43-CTL was approximately 1m/s, with the WFP the bias was reduced to 0.5, 0.6 and 0.7m/s for respectively stable, unstable and weakly stable atmospheric conditions.

- **Vlakte van de Raan:** Most of the measurements were under undisturbed conditions (> 1700 per stability class). There are still enough measurements under disturbed conditions ($131 - 353$ per stability class) to drawn conclusions about the performance of the WFP. The bias of HarmCY43-CTL under disturbed conditions was 0.7-1.1m/s. With the WFP the bias was reduced with 0.4m/s. The resulting bias was approximately equal to the bias of the undisturbed winds.

- **P11-B:** There are no wind farms within 50km from P11-B. The undisturbed measurements show similar results for HarmCY43-WFP and HarmCY43-CTL. The model bias was smallest for weakly stable and stable conditions $\sim$0.2m/s. For unstable conditions the bias was larger $\sim$0.7m/s.

- **K13:** The measurements at the K13 station were all undisturbed, there are no productive wind farms in the proximity of the station. The bias is similar for both HarmCY43 runs. We observe an overall underestimation of the wind speeds. Under stable conditions the underestimation was around 0.9m/s, while for weakly stable and unstable conditions it was only 0.2-0.3m/s.

- **Lichteiland Goeree:** Also for Lichteiland Goeree all the measurements are undisturbed. The results are similar for HarmCY43-WFP and HarmCY43-CTL, on average the bias of HarmCY43-WFP was 0.06m/s smaller. The best correlation was found during stable and unstable conditions. Under weakly stable conditions the models overestimate the wind speed with 0.3-0.4m/s.

From this analysis we can conclude that in 7/10 cases HarmCY43-WFP had the largest biasses under weakly stable conditions. In all of these cases we see a clear overestimation of the wind speed of >0.5m/s. For 6/9 stations for stable undisturbed conditions the wind speed was underestimated, though in most of the cases the error was within the measurement uncertainty. The 0.9m/s bias from K13 is an exception. The largest difference between HarmCY43-WFP and HarmCY43-CTL was found for the BG-OHVS2 station, which is located in the middle of a operational wind farm. The Fitch WFP is not actually meant to be used in a wind farm. The wake effects were around 1.5m/s; HarmCY43-WFP estimates the wake intensity around 1m/s.

Table 6: Validation of the HarmCY43 runs for the different stability regimes: ($Ri > 0.25$) stable, ($0.0 <= Ri <= 0.25$) weakly stable and ($Ri < 0.0$) unstable (see subsection 3.5.3 for more details). The disturbed and undisturbed wind directions are according to table 1. The number indicates the amount of hourly averaged measurements which were available for the validation per category. The measured values are denoted by OBS, the modelled values by CTL and WFP.

Stability	Wake	nr.	OBS	WFP	CTL	bias WFP	bias CTL	R^2 WFP	R^2 CTL	RMSE WFP	RMSE CTL
BG-OHVS2											
Disturbed	Stable	2203	5.55	5.85	7.07	0.29	1.52	0.7	0.69	1.58	2.29
Disturbed	Unstable	4756	8.26	8.76	9.65	0.5	1.39	0.9	0.89	1.43	1.96
Disturbed	Weakly stable	1783	10.6	11.43	12.27	0.83	1.67	0.87	0.86	1.86	2.39
AWG1											
Disturbed	Stable	15	5.4	5.9	5.84	0.51	0.44	0.72	0.77	1.86	1.77
Disturbed	Unstable	28	5.46	6.86	6.96	1.4	1.5	0.8	0.8	2.05	2.13
Disturbed	Weakly stable	10	8.14	9.95	10.66	1.81	2.51	0.48	0.55	3.1	3.83
Undisturbed	Stable	3185	6.89	6.83	6.82	-0.06	-0.07	0.64	0.65	1.77	1.76
Undisturbed	Unstable	3006	8.62	8.93	8.95	0.31	0.33	0.82	0.83	1.64	1.62
Undisturbed	Weakly stable	2465	10.68	11.18	11.19	0.5	0.52	0.7	0.7	2.18	2.17
Europlatform											
Disturbed	Stable	267	6.31	6.03	6.25	-0.28	-0.05	0.74	0.73	1.54	1.62
Disturbed	Unstable	499	11.19	11.13	11.3	-0.06	0.12	0.92	0.92	1.31	1.35
Disturbed	Weakly stable	446	12.67	12.71	12.89	0.04	0.22	0.86	0.85	1.59	1.67
Undisturbed	Stable	2215	6.19	6.08	6.09	-0.11	-0.1	0.66	0.67	1.67	1.66
Undisturbed	Unstable	4059	8.95	9.11	9.13	0.16	0.18	0.91	0.91	1.24	1.24
Undisturbed	Weakly stable	1169	10.28	10.7	10.73	0.42	0.45	0.82	0.83	1.62	1.61
Huibertgat											
Disturbed	Stable	88	4.23	4.04	4.3	-0.19	0.07	0.67	0.7	1.26	1.23
Disturbed	Unstable	162	6.98	7.18	7.32	0.2	0.34	0.88	0.89	1.1	1.09
Disturbed	Weakly stable	19	7.59	7.89	7.84	0.31	0.26	0.77	0.88	1.57	1.2
Undisturbed	Stable	3409	6.56	6.55	6.53	-0.01	-0.02	0.72	0.73	1.41	1.4
Undisturbed	Unstable	2688	8.41	8.71	8.74	0.3	0.34	0.88	0.89	1.21	1.19
Undisturbed	Weakly stable	2373	10.29	10.37	10.37	0.08	0.08	0.86	0.86	1.38	1.35
IJmond											
Disturbed	Stable	136	4.51	4.53	4.67	0.02	0.16	0.54	0.48	1.52	1.7
Disturbed	Unstable	312	8.59	8.99	9.1	0.4	0.51	0.88	0.89	1.29	1.3
Disturbed	Weakly stable	165	10.03	10.92	11.02	0.89	0.99	0.89	0.85	1.6	1.84
Undisturbed	Stable	2947	5.67	5.7	5.75	0.03	0.08	0.66	0.67	1.46	1.44
Undisturbed	Unstable	3022	8.58	9.04	9.11	0.46	0.53	0.89	0.89	1.38	1.4
Undisturbed	Weakly stable	2037	9.65	10.14	10.16	0.5	0.51	0.86	0.86	1.54	1.54
Oosterschelde											
Disturbed	Stable	147	4.96	5.43	5.88	0.47	0.91	0.53	0.57	1.72	1.92
Disturbed	Unstable	252	8.72	9.32	9.68	0.59	0.96	0.83	0.85	1.52	1.63
Disturbed	Weakly stable	186	9.69	10.4	10.89	0.71	1.2	0.85	0.86	1.67	1.86
Undisturbed	Stable	2909	5.68	5.96	6.04	0.28	0.35	0.7	0.67	1.52	1.61
Undisturbed	Unstable	3477	8.5	9.08	9.13	0.58	0.62	0.9	0.9	1.39	1.4
Undisturbed	Weakly stable	1752	9.59	10.53	10.56	0.94	0.96	0.87	0.86	1.67	1.69
Vlakte van de Raan											
Disturbed	Stable	163	3.86	4.08	4.53	0.21	0.66	0.47	0.52	1.49	1.67
Disturbed	Unstable	353	8.09	8.74	9.22	0.65	1.13	0.92	0.91	1.53	1.81
Disturbed	Weakly stable	131	9.41	10.19	10.65	0.78	1.23	0.82	0.79	1.75	2.11
Undisturbed	Stable	3220	5.88	6.22	6.3	0.34	0.41	0.7	0.69	1.52	1.58
Undisturbed	Unstable	3078	8.42	9	9.01	0.57	0.59	0.89	0.89	1.38	1.38
Undisturbed	Weakly stable	1779	9.97	10.73	10.73	0.76	0.76	0.83	0.83	1.72	1.73
P11-B											
Undisturbed	Stable	2288	6.65	6.44	6.43	-0.21	-0.22	0.7	0.72	1.75	1.7
Undisturbed	Unstable	2881	8.45	9.16	9.15	0.71	0.7	0.81	0.82	2.03	2.01
Undisturbed	Weakly stable	1320	11.33	11.54	11.5	0.21	0.17	0.85	0.84	1.67	1.7
K13											
Undisturbed	Stable	2332	7.81	6.91	6.88	-0.9	-0.93	0.78	0.77	1.88	1.92
Undisturbed	Unstable	4468	9.59	9.32	9.32	-0.27	-0.26	0.92	0.92	1.29	1.31
Undisturbed	Weakly stable	1915	12.85	12.63	12.6	-0.21	-0.25	0.88	0.87	1.42	1.48
Lichteiland Goeree											
Undisturbed	Stable	2846	6.42	6.28	6.35	-0.14	-0.07	0.7	0.7	1.58	1.62
Undisturbed	Unstable	4033	9.11	9.22	9.27	0.1	0.15	0.91	0.91	1.27	1.26
Undisturbed	Weakly stable	1860	11.2	11.51	11.57	0.31	0.37	0.87	0.88	1.42	1.42

5 FINO1 and FINO3 Temperature, Humidity and Wind Speed measurements

On the North-Sea the FINO1 and FINO3 research platforms are the only locations were we can verify the offshore temperature and humidity profiles of HarmCy43. The FINO measurements are between ∼30-100m above mean sea level. Based on the stability regimes (stable, weakly stable and unstable) we will validate the temperature, humidity and wind speed profiles. The results for FINO1 and FINO3 are included in section 5.1 and 5.2, respectively. In the next chapter 6 we will continue with an extensive validation of the wind speed and wind direction of the lidar measurements.

5.1 FINO1

Figure 6 provides an overview of the FINO1 location. FINO1 is about 45km North of the German island Borkum. Figure 6B shows the research tower with the booms where the cup anemometers are mounted, on two sites of the tower. The towers positioning inside the wind farm zone is shown in figure 6C. FINO1 is surrounded by the operational wind farms *Alpha Ventus*, *Borkum Riffgrund I* and *TrianelWindpark Borkum*. Here we can validate the temperature, relative humidity and wind speed within the German wind park itself. West of the FINO1 tower is the KNMI/RWS measurement site BG-OHVS2, in the middle of the Gemini wind farm. Approximately 20km west of the Gemini wind farms the floating lidar of TNWB is positioned, which under stable conditions could measure the compound wake of the wind farms to its eastern side. The various wind parks surrounding FINO1 could cause a wake-wake interaction with western or easterly winds during stable conditions, possibly causing even lower wind speeds than expected from the one park only.

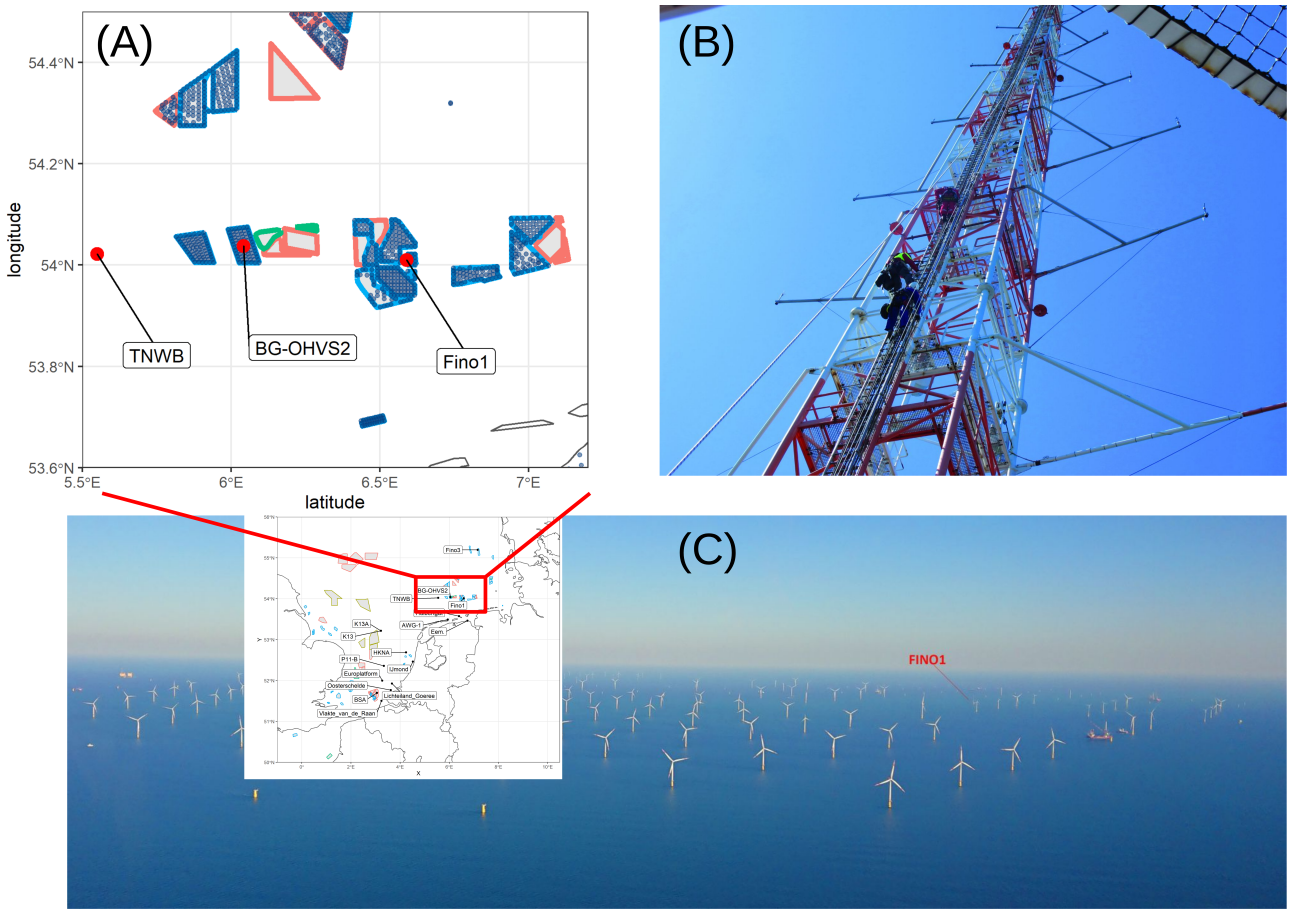

Figure 6: Overview of FINO1 research platform surrounded by German wind farms (*Alpha Ventus*, *Borkum Riffgrund I* and *TrianelWindpark Borkum*). The hub heights of the surrounding wind turbines is between 78-105m in 2019. (A) FINO1 with respect to the other measurement locations (KNMI/RWS measurement site BG-OHVS2 and the TNWB lidar) and wind farms. The operational wind farms are in blue. (B) The measurement tower with the cup anemometers at the end of the booms, mounted on two sides of the mast (source: www.FINO1.de). (C) Overview figure of the FINO1 tower inside the wind farms (source: www.FINO1.de).

The validation results of FINO1 are shown in Table 7:

Temperature: The temperature is measured at five different heights (figure not shown). The HarmCY43-WFP temperature between 34m and 101m has no significant bias ($< 0.1\,°C$) and correlates well with the observed temperature ($R^2 = 0.98$). The HarmCY43-CTL temperatures are negatively biased with $\sim 0.15\,°C$ in the lower 40 meters, which could indicate, averaged over the year 2019, a small warming of the lower atmosphere due to the wind farms.

Humidity: There are four sensors that measure the humidity. Although the sensor with the lowest humidity at 42m compares best with the models, it strongly deviates from the other observations. At all heights both HarmCY43-WFP and HarmCY43-CTL have a $(2 - 9\%)$ lower humidity. Figure 7 provides an overview of the relative humidity profiles under different stability regimes. For each stability regime there are enough profiles to draw conclusions. For (weakly) stable conditions the lowest underestimation was found. The bias was largest for unstable conditions.

Wind speed: The wind speed is measured at six different heights. As expected HarmCY43-CTL has the larger overestimation of the wind speed ~1.5m/s. HarmCY43-WFP overestimates the winds with on average ~0.4m/s between 60-90m and for more than 0.5m/s below 50m. Figure 8 shows the wind speed profiles under different stability regimes. Although most of the observations were for unstable atmospheric conditions (>2000 complete profiles) there are sufficient observations under stable (415 profiles) and weakly stable conditions (479 profiles) to draw conclusions. For stable conditions HarmCY43-WFP closely matches the observations. The overestimation of the wind speed was larger for weakly stable conditions. During unstable conditions the overestimation of the wind speed is largest.

Table 7: HarmCY43-WFP and HarmCY43-CTL validation at the FINO1 location including temperature, relative humidity and wind speed. The temperature is measured at 5 different heights, the humidity at 4 heights an the wind speed at 6 different heights. Note that the humidity sensor at 42m is biased compared with the other sensors. The measured values are denoted by OBS, the modelled values by CTL and WFP.

Variable	height	nr.	OBS	CTL	WFP	bias CTL	bias WFP	R^2 CTL	R^2 WFP	$RMSE$ CTL	$RMSE$ WFP
Temperature [°C]	34	8734	10.81	10.68	10.88	-0.13	0.07	0.98	0.98	0.74	0.71
Temperature [°C]	42	8734	10.81	10.64	10.81	-0.18	0.00	0.98	0.98	0.79	0.73
Temperature [°C]	52	8734	10.63	10.59	10.74	-0.04	0.11	0.98	0.98	0.78	0.73
Temperature [°C]	72	5054	13.13	13.06	13.11	-0.07	-0.02	0.98	0.98	0.64	0.63
Temperature [°C]	101	8734	10.41	10.43	10.50	-0.07	-0.09	0.98	0.98	0.78	0.73
Relative Humidity [−]	34	8733	0.85	0.79	0.77	-0.06	-0.08	0.54	0.63	0.11	0.11
Relative Humidity [−]	42	8733	0.81	0.78	0.77	-0.02	-0.04	0.63	0.68	0.09	0.09
Relative Humidity [−]	72	5054	0.86	0.77	0.77	-0.09	-0.09	0.75	0.75	0.11	0.11
Relative Humidity [−]	101	8733	0.83	0.78	0.78	-0.06	-0.06	0.69	0.70	0.10	0.09
Wind Speed $[m/s]$	41	2927	8.56	10.10	9.17	1.54	0.60	0.86	0.86	2.18	1.65
Wind Speed $[m/s]$	51	2927	8.72	10.22	9.23	1.50	0.51	0.86	0.87	2.17	1.62
Wind Speed $[m/s]$	61	2927	8.87	10.32	9.29	1.45	0.42	0.89	0.90	2.04	1.42
Wind Speed $[m/s]$	71	2927	8.93	10.40	9.34	1.47	0.41	0.89	0.90	2.07	1.43
Wind Speed $[m/s]$	81	2927	8.94	10.47	9.39	1.53	0.45	0.89	0.89	2.12	1.47
Wind Speed $[m/s]$	91	2927	9.02	10.53	9.44	1.51	0.42	0.89	0.89	2.13	1.49

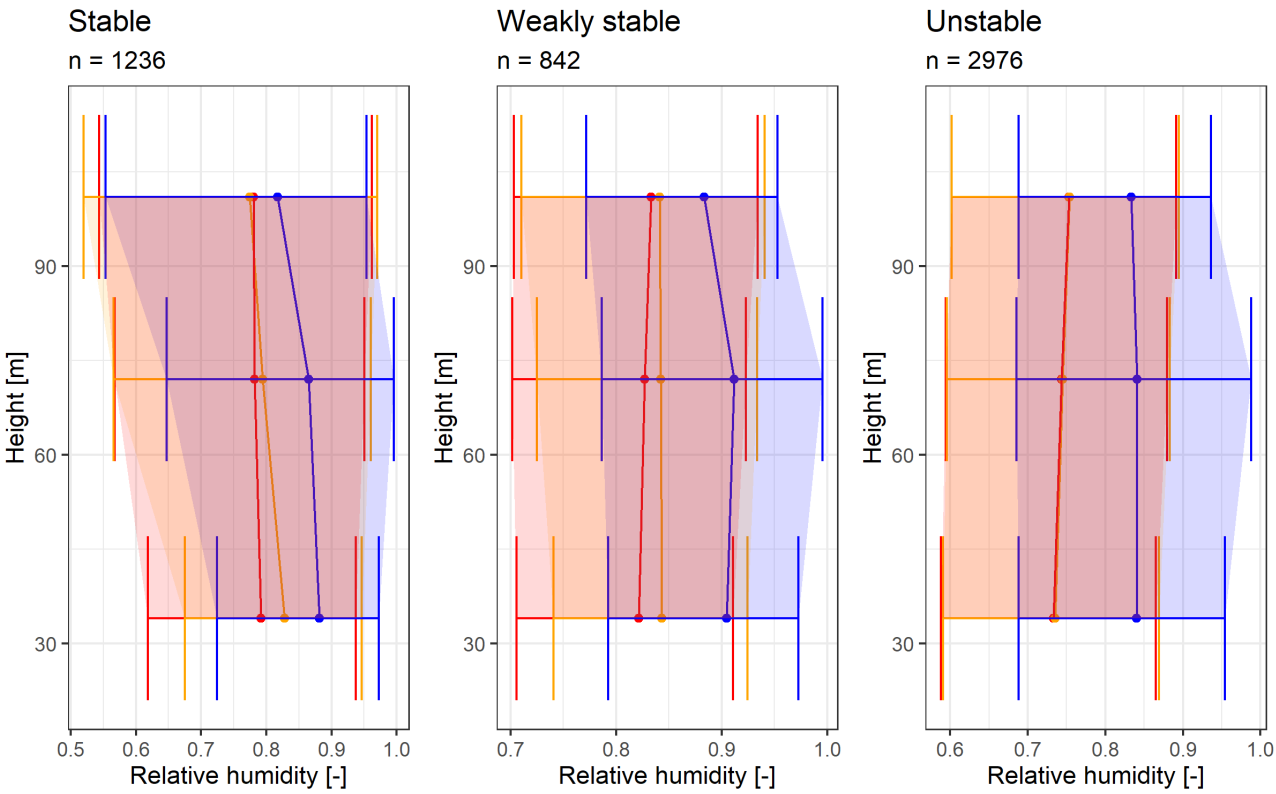

Figure 7: Overview of the relative humidity profiles at FINO1 in the middle of the wind farm, where n indicates the number of complete profiles. The relative humidity is measured at four different heights. The different flow regimes are based on the modelled Richardson number: ($Ri < 0.0$) unstable, ($0.0 <= Ri <= 0.25$) weakly stable and ($Ri > 0.25$) stable (see subsection 3.5.3 for more details). In blue the measurements, in yellow HarmCY43-CTL and in red HarmCY43-WFP. The horizontal lines indicate the 10-90% quantiles, calculated from a total of 5054 measurements at each height. *The relative humidity measurements at 42m strongly deviate from the other measurements and are therefore left out of this plot.

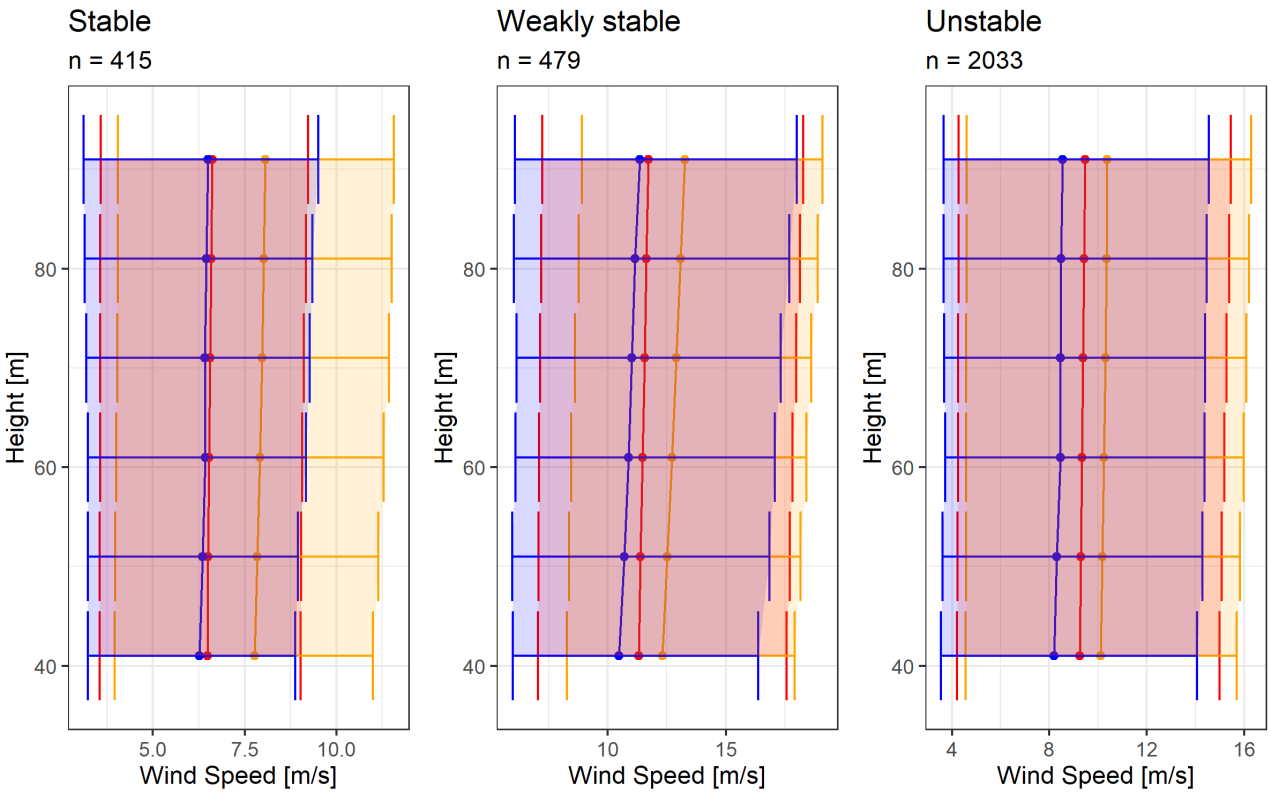

Figure 8: Overview of the wind speed profiles at FINO1 at the observation heights, where n indicates the number of complete profiles. The different flow regimes are based on the modelled Richardson number: ($Ri < 0.0$) unstable, ($0.0 <= Ri <= 0.25$) weakly stable and ($Ri > 0.25$) stable (see subsection 3.5.3 for more details). In blue the measurements, in yellow HarmCY43-CTL and in red HarmCY43-WFP. The horizontal lines indicate the 10-90% quantiles.

5.2 FINO3

Figure 9 provides an overview of the FINO3 research platform. FINO3 is located about 80km West of the Danish island Sylt. The FINO3 tower has one wind farm to the east (*DanTysk*) at 1km distance and another farm to the west (*Sandbank*) at less than 20km (Fig.9A). Due to its positioning so close to the farm the 2.5km model grid might not be the representative for this measurement site. South-western and north-western are not disturbed by either of the two farms. Compared with the FINO1 research platform we can also validate the temperature, humidity and wind speed profiles for non-disturbed wind directions.

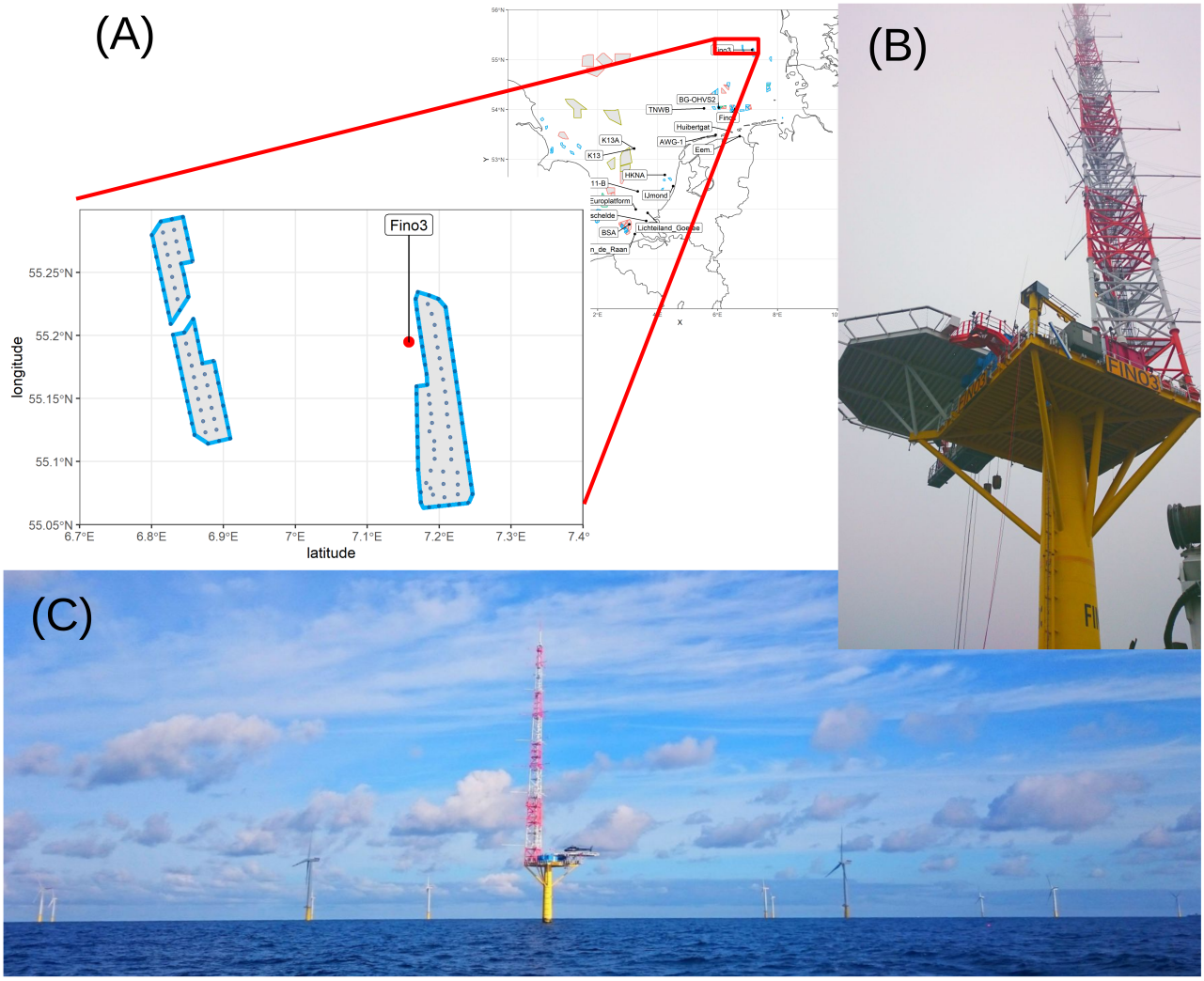

Figure 9: Overview of FINO3 next to the wind farms (*DanTysk* at 1km East and *Sandbank* at 20km East). The turbine hub height in these farms is between 88-95m in 2019. (A) The FINO3 site with respect to the other measurement locations and wind farms. Both wind farms were operational during the validation period. (B) The measurement platform with the cup anemometers at the end of the booms which are mounted on three sides of the tower (source: www.FINO3.de). (C) Overview figure of the FINO3 tower with the *DanTysk* wind farm in the background (source: www.FINO3.de).

Table 8 provides an overview of the temperature, relative humidity and wind speed validation at the FINO3 location for all wind directions:

Temperature: The temperature is measured at three different heights (29m, 55m and 95m) for the whole year (figure not shown). The HarmCY43-WFP temperatures are positively biased at all measurement heights, varying between 0.15 °C and 0.24 °C. For the HarmCY43-CTL the biasses are a bit smaller: ranging between 0.09 °C and 0.19 °C. With a measurement uncertainty of ~ 0.1 °C most of the biasses fall within the uncertainty range.

Humidity: The humidity is also measured at three different heights, similar to the temperature observations. The humidity in both runs is underestimated by $5-6\%$. The bias of HarmCY43-WFP is slightly larger than HarmCY43-CTL. Figure 10 provides an overview of the humidity profiles under different stability regimes. Most of the measurements were for undisturbed wind directions, though there are enough measurements from disturbed directions to draw conclusions. For unstable conditions the bias is similar for both HarmCY43 runs, here we also have the largest bias of 10% at 55m and 95m. For weakly stable conditions the bias is smaller, though larger for HarmCY43-WFP. We do not see a clear difference between the disturbed and undisturbed wind directions. However, for stable conditions the humidity underestimation of HarmCY43-WFP is larger for the disturbed wind directions than the undisturbed ones. At 95m we even observe a small overestimation.

Wind speed: The cup anemometers were installed at 51m, 71m and 91m. The measurements almost cover the entire validation year. The wind speed of HarmCY43-WFP has a positive bias of ~ 0.4 °C. In HarmCY43-CTL the bias is ~ 0.6 °C. Figure 11 provides an overview of the wind speed profiles for different stability regimes. During stable conditions which were not disturbed both models slightly over-predict the wind speeds. The bias is larger for disturbed wind directions. For weakly stable conditions the differences between HarmCY43-WFP and the measurements on average 1m/s.

Table 8: HarmCY43-WFP and HarmCY43-CTL validation at the FINO3 location including temperature, relative humidity and wind speed. The temperature and relative humidity measurements are at the same heights. The wind speed was measured at 3 different heights. The measured values are denoted by OBS, the modelled values by CTL and WFP.

Variable	height	nr.	OBS	CTL	WFP	bias CTL	bias WFP	R^2 CTL	R^2 WFP	*RMSE* CTL	*RMSE* WFP
Temperature [°C]	29	8424	10.44	10.53	10.61	0.09	0.16	0.98	0.98	0.72	0.70
Temperature [°C]	55	8425	10.17	10.36	10.41	0.19	0.24	0.98	0.98	0.77	0.75
Temperature [°C]	95	8425	10.01	10.17	10.16	0.16	0.15	0.97	0.97	0.80	0.78
Relative Humidity [−]	29	8424	0.84	0.79	0.78	-0.05	-0.06	0.75	0.75	0.08	0.09
Relative Humidity [−]	55	8425	0.83	0.78	0.78	-0.05	-0.05	0.74	0.75	0.08	0.09
Relative Humidity [−]	95	8425	0.84	0.78	0.78	-0.06	-0.06	0.72	0.72	0.09	0.09
Wind Speed [m/s]	51	8344	9.24	9.79	9.64	0.55	0.41	0.85	0.86	1.74	1.66
Wind Speed [m/s]	71	8344	9.43	10.04	9.86	0.61	0.43	0.84	0.86	1.84	1.72
Wind Speed [m/s]	91	8344	9.62	10.22	10.01	0.61	0.39	0.84	0.86	1.88	1.75

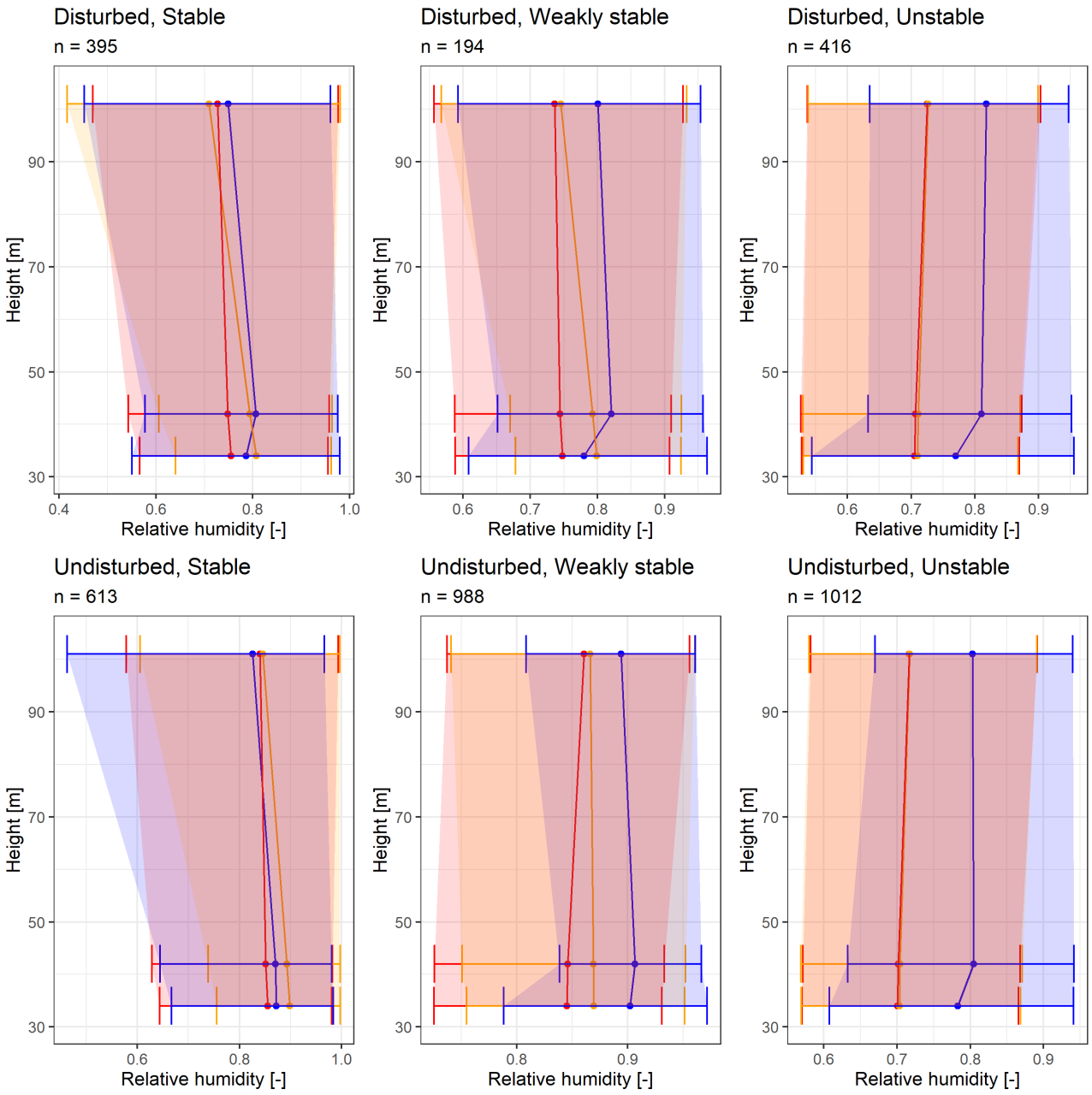

Figure 10: Overview of the relative humidity profiles at FINO3 at the border of the wind farm, where n indicates the number of complete profiles. The relative humidity is measured at four different heights. The different flow regimes are based on the modelled Richardson number: ($Ri < 0.0$) unstable, ($0.0 <= Ri <= 0.25$) weakly stable and ($Ri > 0.25$) stable (see subsection 3.5.3 for more details). In blue the measurements, in yellow HarmCY43-CTL and in red HarmCY43-WFP. The horizontal lines indicate the 10-90% quantiles, calculated from the number of profiles (n).

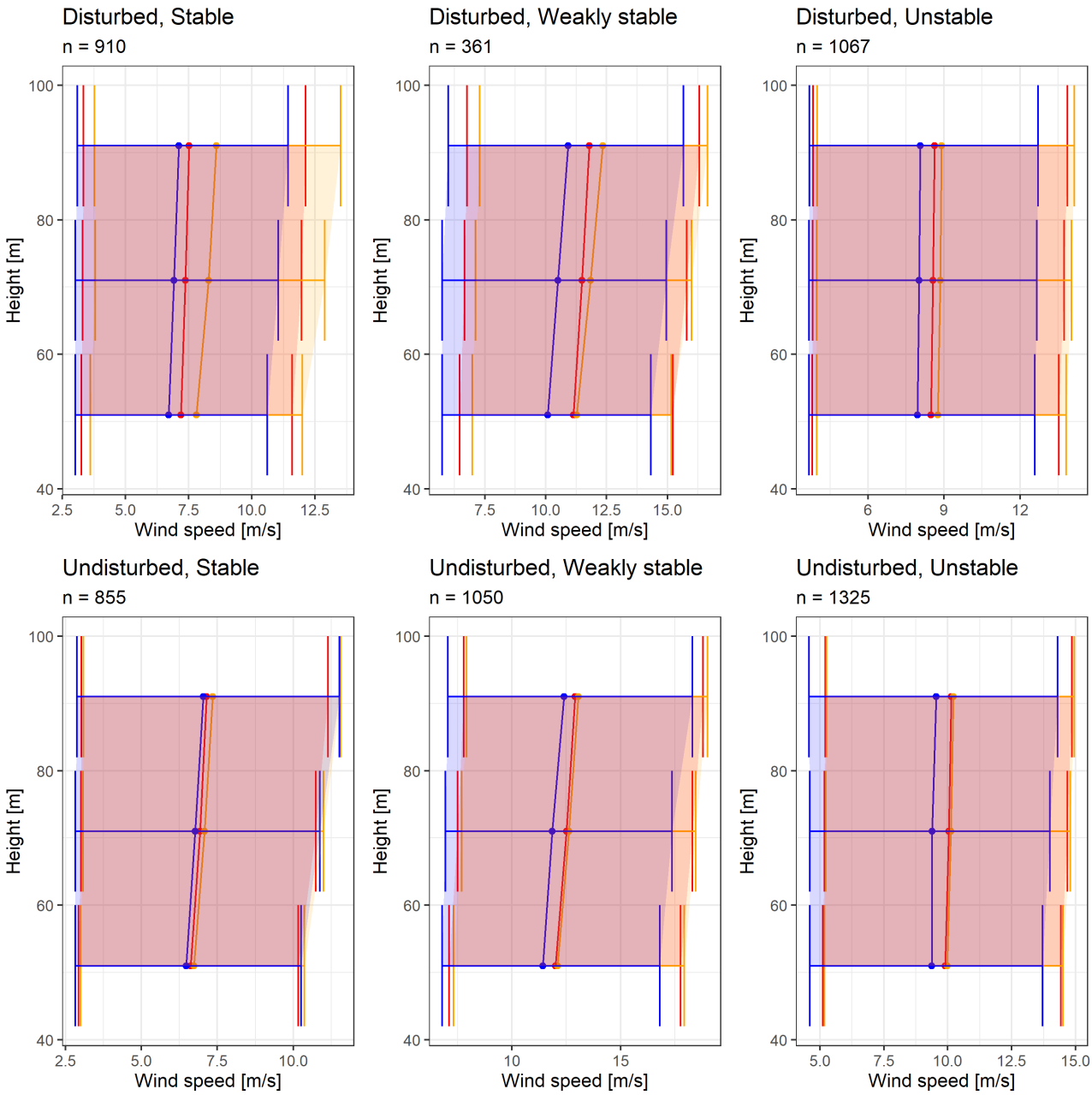

Figure 11: Overview of the wind speed profiles at FINO3 at the observation heights, where n indicates the number of complete profiles. The different flow regimes are based on the modelled Richardson number: ($Ri <$ 0.0) unstable, ($0.0 <= Ri <= 0.25$) weakly stable and ($Ri > 0.25$) stable (see subsection 3.5.3 for more details). In blue the measurements, in yellow HarmCY43-CTL and in red HarmCY43-WFP. The horizontal lines indicate the 10-90% quantiles, calculated from the number of profiles (n).

6 Model validation at the North Sea Lidar locations

In this chapter we will validate HarmCY43 wind at five lidar locations across the North Sea. We will validate both the wind speed profiles and wind directions of HarmCY43-CTL and HarmCY43-WFP. We will compare the diurnal variation and directional variations of the wind speed. Additionally, we will validate the modelled wind speeds for wind directions which are disturbed and undisturbed under different stability regimes. Based on the Richardson number these are here defined as: unstable ($Ri < 0.0$), weakly stable ($0.0 <= Ri <= 0.25$) and stable ($Ri > 0.25$).

The wind directions of the lidars were compared with both model runs. The ZephIR300 lidar, measuring with Doppler, sometimes have a 180^o error. After correcting for this error we will correlate the lidar directions to HarmCY43-CTL and HarmCY43-WFP. The correction for the directional error is included in Appendix C.

The validation results of HarmCY43-CTL and HarmCY43-WFP at each lidar location are included in the next paragraphs. These include the lidars BSA (sec.6.1), K13A (sec.6.2), HKNA (sec.6.3), TNWB (sec.6.4) and Eemshaven (sec.6.5).

6.1 BSA

Figure 12 gives the locations of the BSA lidar compared to the operational Belgian wind farms in 2019 (blue). Note that the red wind farm areas, including the Dutch Borssele wind farm zone, are not yet operational during the validation period. In 2019 the Belgian wind farms had a total capacity of 1.6GW. The BSA lidar is installed on the Tennet platform (Fig.12B) about 10km from the operational Belgian wind farms. The two separate measurement campaigns were in autumn 2019 (Fig.4). During the measurement period of BSA the approved new wind farms were not yet in operation (the red areas in figure 12A), this would have placed the lidars in the middle of the wind farm (the red areas in Figure 12). The short range lidar at BSA measures wake effects of the operational parks with a south-western wind.

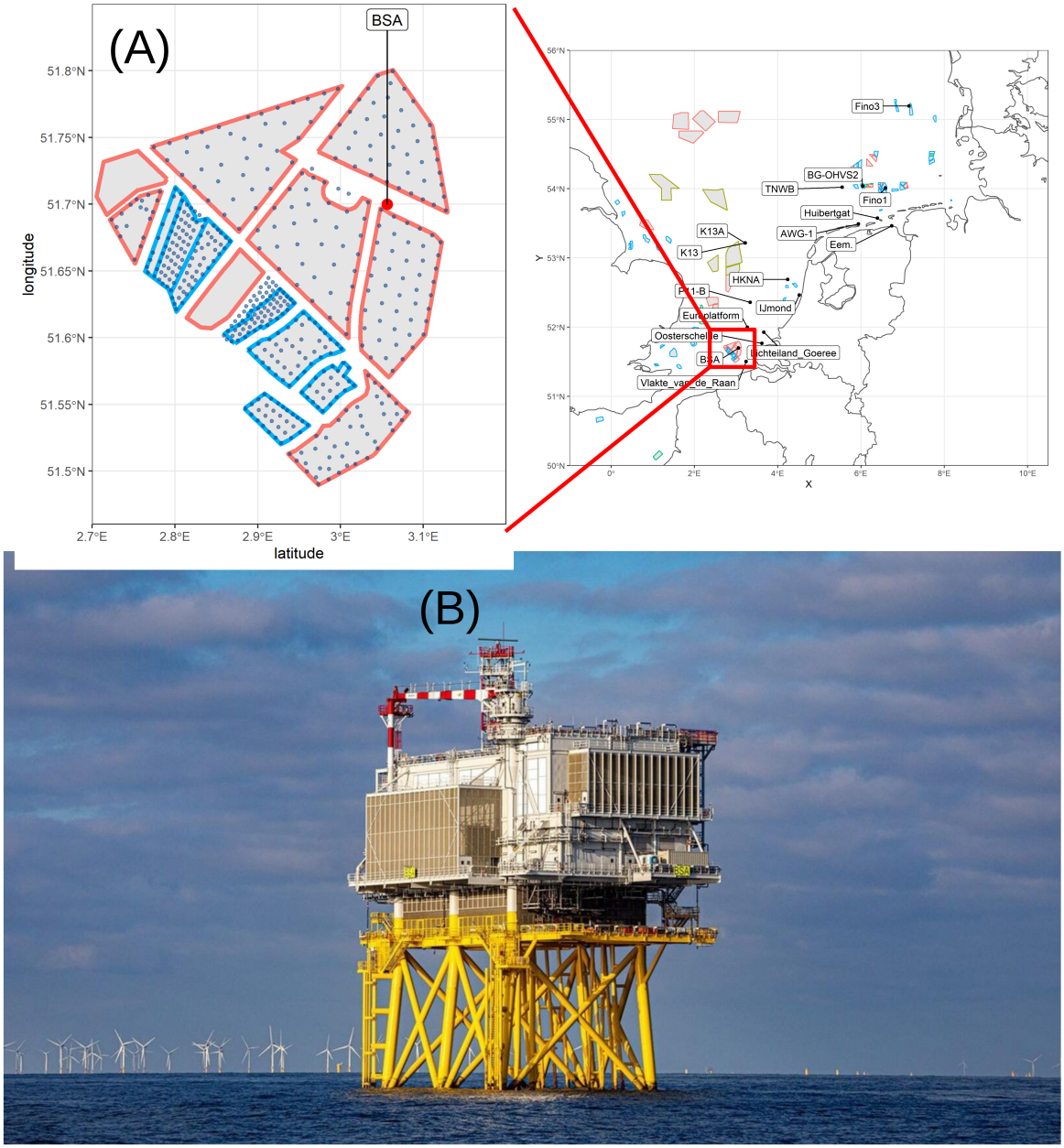

Figure 12: The location of the BSA lidar. (A) The wind farms in blue were operational in 2019. The hub heights of these turbines are between 71-94m. The wind farms in red were not operational during the validation period. (B) The Tennet platform on which the BSA lidar was mounted (source: www.tennet.eu).

We have validated the HarmCY43 wind speeds and directions between 59-295m at the BSA site. During the second measurement period in September the lidar measured at slightly different heights, which were interpolated to the measurements heights of the first campaign. Table 9 provides an overview of the model validation for

all directions and stabilities. HarmCY43-CTL has the largest bias between 150-300m of >0.7m/s. The WFP reduced this bias to approximately 0.4m/s, below 150m the bias is close to zero. The bias of HarmCY43-CTL is also a bit smaller below 150m and ranges between 0.3-0.6m/s. The squared correlation coefficient of HarmCY43 is above 0.8 for all measurement heights. The RMSE ranges between 1.7-2.1m/s

Directional wind speed profile: Figure 13 provides an overview of the averaged wind speed profile for each 5^o wind direction section. Both the interpolated model heights and measurement heights were interpolated to a constant interval of 50m. Figure 13F shows that during the measurement period the south-westerly winds were dominant, from the other wind directions there are not enough observations to drawn conclusions from. The winds from a south-westerly directions are ∼2m/s overestimated by HarmCY43-CTL. This can be expected since the wind farms are 10km upstream. The bias is almost reduced to zero by the WFP.

Diurnal wind speed profile: Figure 14 show the diurnal profiles of HarmCY43-WFP and HarmCY43-CTL. As expected there is almost no variation in the wind speed throughout the day. The measurements have been averaged for each hour. The number of observations for each hour is similar (Fig. 14F) and limited to 330-350 observations per bin. Both runs show an underestimation of the wind speed during the early hours of the day. During the afternoon HarmCY43-WFP underestimates the wind speed. The under- and overestimation of ∼1m/s do seem to have small variations with height.

Stability profiles: Based on the stability regimes and disturbed wind directions we have compared the wind profiles (Fig.15). The number of profiles for weakly stable conditions too small to draw any conclusions. The disturbed unstable winds were best represented with almost 600 and 300 complete profiles. The wind speed for disturbed stable conditions is underestimated by HarmCY43-WFP. The shape of the wind profile under weakly stable conditions are a bit steeper for HarmCY43. It is unclear if this is a consistent pattern due to the limited number of profiles. During unstable conditions the shape of the wind profiles matches. For unstable conditions the HarmCY43 wind speeds closely match the measurements.

Wind directions: The ZephIR300 directional errors are described in Appendix C, here figure 33 provides an overview of the wind directional errors per wind speed group. The wind directions of the BSA lidar had an error in 9.7% of the cases. After correcting the bias of HarmCY43-WFP and HarmCY43-CTL equaled 2.3^o and 1.5^o.

Table 9: Validation of HarmCY43 at the BSA lidar location for the 11 measurement heights, between 59m and 295m. The measurement heights are in units meters above mean sea level. The measured values are denoted by OBS, the modelled values by CTL and WFP.

Height	nr.	OBS	CTL	WFP	bias CTL	bias WFP	R^2 CTL	R^2 WFP	$RMSE$ CTL	$RMSE$ WFP
m	-	m/s	m/s	m/s	m/s	m/s	m/s	m/s	m/s	m/s
59	1354	9.11	9.46	9.02	0.35	-0.10	0.86	0.84	1.66	1.67
84	1355	9.21	9.66	9.21	0.45	0.00	0.85	0.84	1.77	1.74
112	1358	9.33	9.86	9.41	0.53	0.08	0.85	0.84	1.82	1.77
121	1358	9.35	9.91	9.46	0.57	0.12	0.85	0.84	1.85	1.79
143	1357	9.36	10.03	9.59	0.67	0.23	0.84	0.83	1.97	1.87
168	1353	9.45	10.16	9.72	0.71	0.27	0.84	0.83	2.04	1.92
194	1347	9.58	10.29	9.86	0.71	0.28	0.84	0.83	2.06	1.95
225	1350	9.58	10.38	9.97	0.80	0.39	0.83	0.83	2.16	2.02
205	1347	9.59	10.33	9.90	0.74	0.31	0.84	0.83	2.09	1.97
245	1350	9.60	10.42	10.03	0.82	0.43	0.83	0.83	2.19	2.05
295	1346	9.77	10.52	10.17	0.74	0.39	0.84	0.84	2.12	2.01

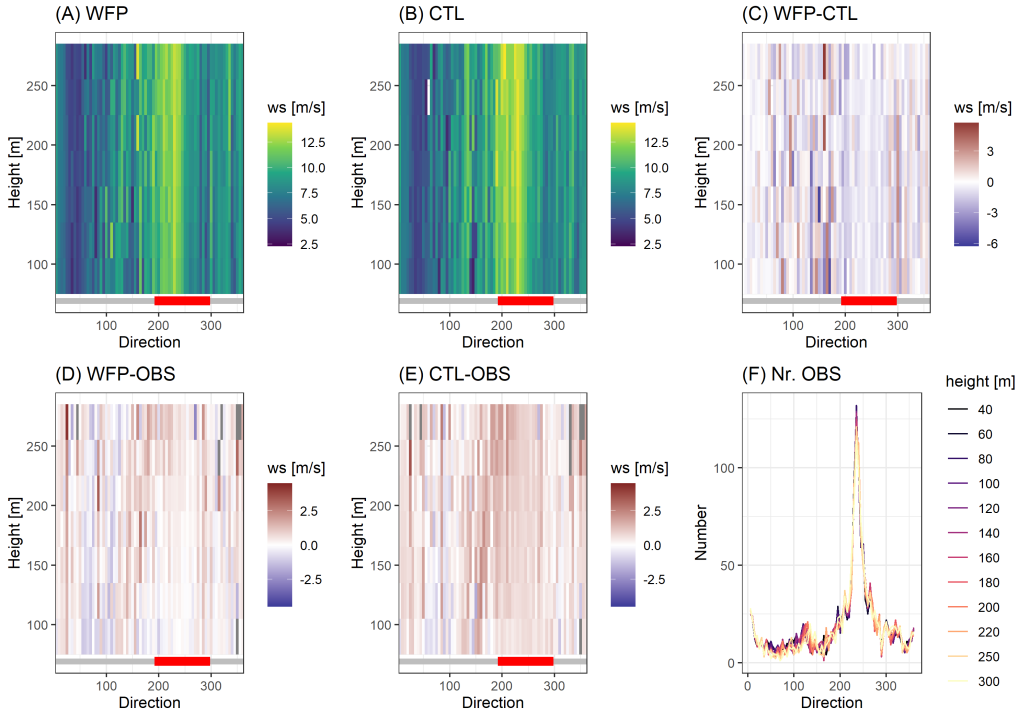

Figure 13: The wind speeds for the HarmCY43-WFP (a) and HarmCY43-CTL (b). (c) the difference between HarmCY43-WFP and HarmCY43-CTL with the varying wind direction. The bias of HarmCY43-WFP (d) and HarmCY43-CTL (e) with the measurements. The number of measurements for 5^o is included in subplot (f).

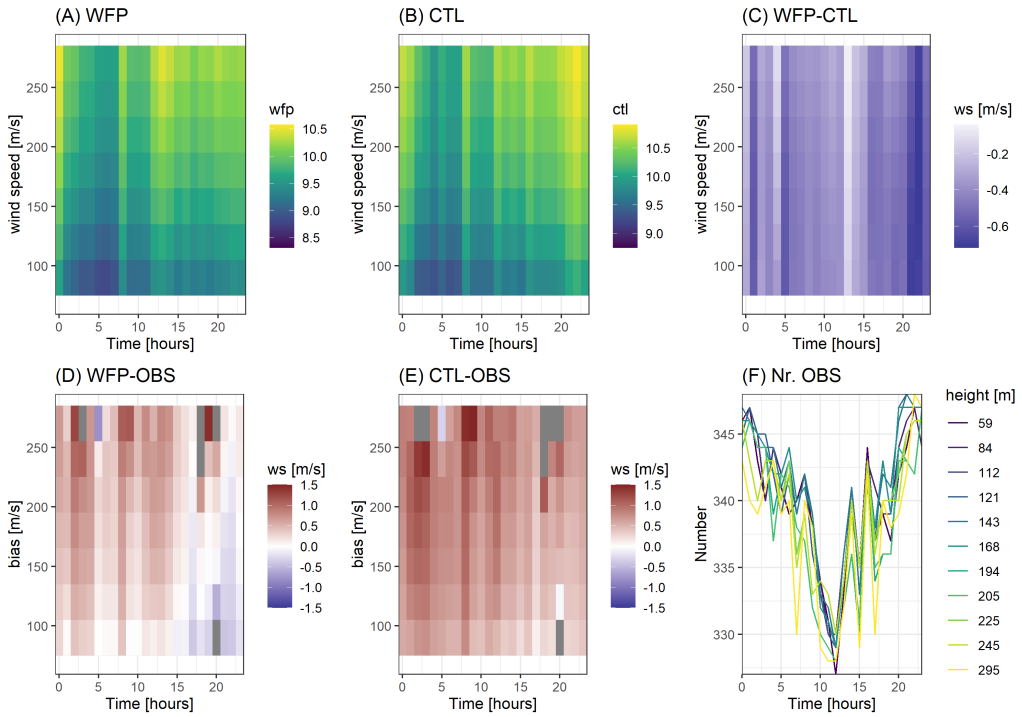

Figure 14: Diurnal profiles of the HarmCY43-WFP (a) and HarmsCY43-CTL (b) and the difference between the reanalysis (c). The lower subplots indicate the model bias with the BSA lidar for HarmCY43-WFP (d) and HarmCY43-CTL (e). The number of measurements for each hour is included in subplot (f).

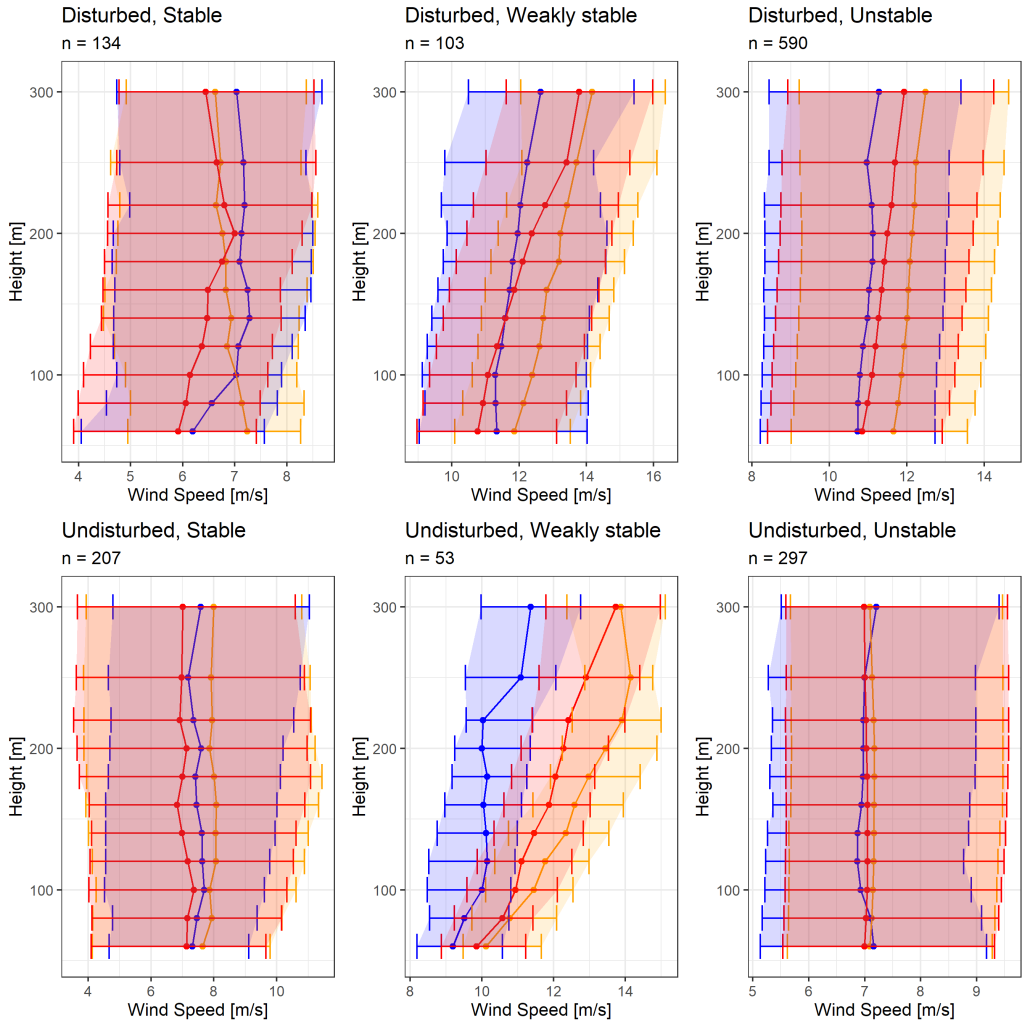

Figure 15: Wind profiles at the BSA location, where n indicates the number of complete profiles. In blue the observed wind speed, in red the modelled wind speed by HarmCY43-WFP and in yellow the HarmCY43-CTL wind speed. The horizontal lines indicate the 30-70% quantiles. The data is organized in disturbed wind directions and undisturbed wind directions. The subplots indicate the different flow regimes based on the modelled Richardson number ($Ri < 0.0$) unstable, ($0.0 <= Ri <= 0.25$) weakly stable and ($Ri > 0.25$) stable flow (see subsection 3.5.3 for more details).

6.2 K13A

Figure 16 provides an overview of the K13A lidar. The K13A lidar is positioned in the central part of the Dutch continental shelf, at the same latitude as the Dutch Northern islands. At the oil rig where the K13A lidar is mounted (Fig.16B) there is also a KNMI meteorological site (see section 4 for the results of K13). The wind at lower elevations (typically less than 30m) could be disturbed by the oil rig. The lidar, which starts measuring at 63m above mean sea level, is expected to be undisturbed. Several areas surrounding the stations have been allocated for the construction of future wind farms (Fig.16A). Though, currently there are no operational wind farms in its proximity. Therefore the location is ideal for the benchmarking of HarmCY43-WFP and HarmCY43-CTL, which should behave similar.

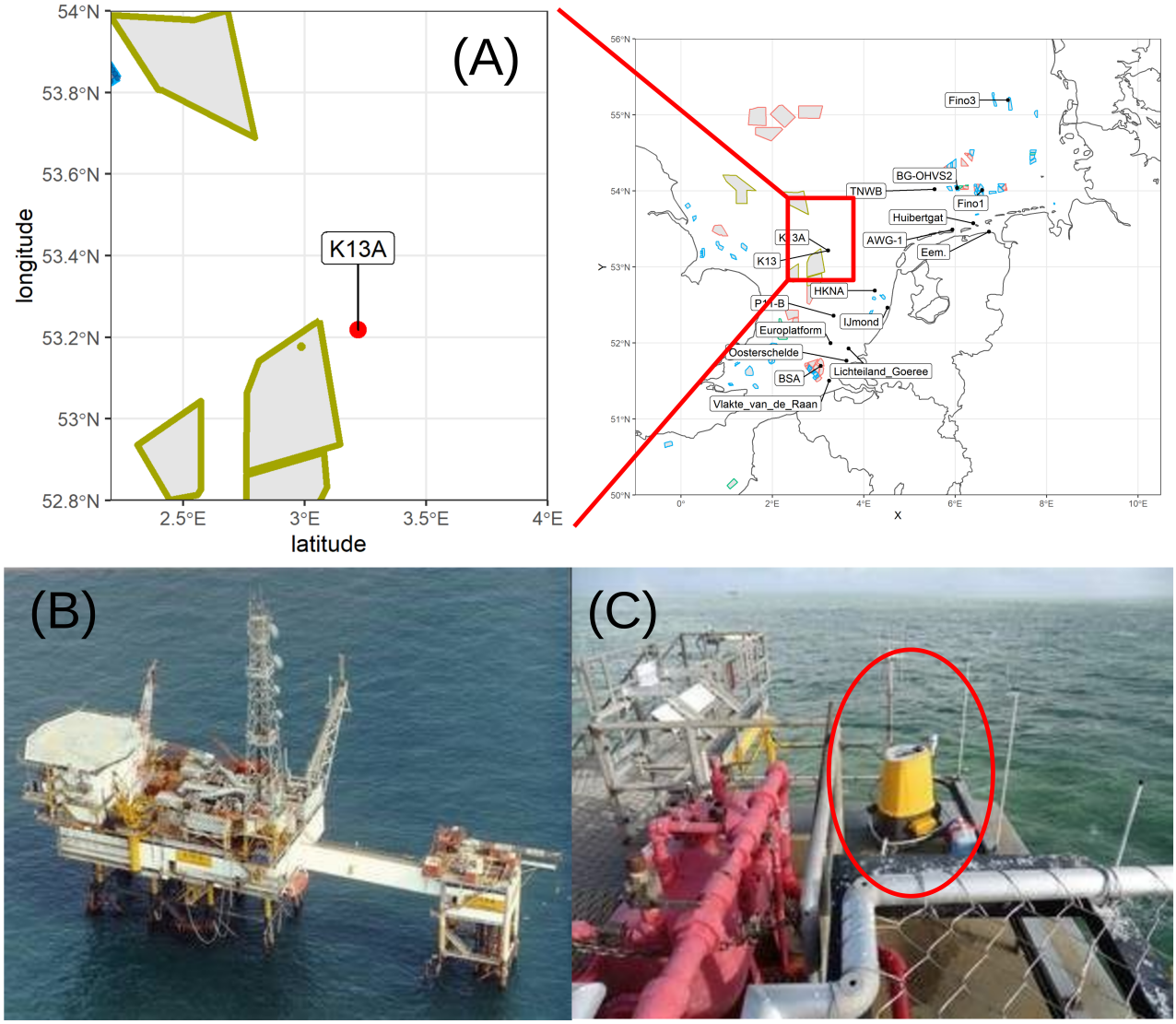

Figure 16: (A) Location of the K13A Lidar and the construction areas in yellow. There are no approved or operational wind farms in the proximity. (B) The oil rig with the lidar mounted on the right hand side (www.windopzee.net). (C) Highlighted in red the yellow ZephIR300 lidar (www.windopzee.net).

Table 10 provides an overview of the validation of HarmCY43 at the ten measurements heights of the K13A lidar. As expected, the differences between the wind speed from HarmCY43-WFP and HarmCY43-CTL are small and within the range of the measurement error. Both runs have a small underestimation of the wind speed around 100m of 0.2m/s. Above 200m both runs are unbiased. With a squared correlation coefficient around 0.9 and a RMSE of 1.5m/s the performance is good.

Directional wind speed profile: Figure 34 compares the wind speeds for different wind directions, group by 5^o. There were less 100 measurements per bin from the East while the Southern winds are better represented with up to 250 measurements. Generally, the wind speeds from the various directions are well represented in the model with only small deviations for southern and northern wind directions. Wind between $100 - 200^o$ are underestimation with 0.5m/s. The northern wind directions, which inherit a large fetch, have an overestimation of 0.5m/s.

Diurnal wind speed profile: Figure 18 shows the diurnal cycle, as expected there are as good as no variations in the wind speed during the day. With more than 2100 measurements per hour and height we can draw conclusions. HarmCY43 closely matches the diurnal wind speeds. The diurnal profile has a small overestimation of the wind speed in the first 10 hours of the day above 200m. Similarly an underestimation of the wind speed below 200m is observed at the end of the day. Both are in the order of 0.2m/s.

Stability profiles: Figure 19 shows the wind profiles at K13A for different stabilities. There is more than enough data per stability regime to draw conclusions. For stable conditions there were about 100 days of hourly data, for weakly stable conditions approximately 80 days and for unstable conditions 190 days were available for the validation of HarmCY43. As expected the profiles from HarmCY43-WFP and HarmCY43-CTL are similar for all stability regimes. For stable atmospheric conditions the wind speeds are underestimated by HarmCY43 with approximately 0.5m/s. During weakly stable conditions the modelled wind speeds closely match the measurements, with a 0.1m/s overestimation below 75m and above 200m. For unstable conditions the profiles closely match, only below 100m there is a 0.1m/s overestimation which is within the measurement error range.

Wind directions: The ZephIR300 directional errors are described in Appendix C, here figure 34 provides an overview of the directional errors per wind speed class. In 4% of the cases the wind direction at K13A had a directional error. After correcting the bias of HarmCY43-WFP and HarmCY43-CTL was low with 1.5^o and 1.3^o.

Table 10: HarmCY43 validation at the K13A lidar location for the 10 measurement heights between 63m and 291m. The measurement heights are in meters above mean sea level. The measured values are denoted by OBS, the modelled values by CTL and WFP.

Height	nr.	OBS	CTL	WFP	bias CTL	bias WFP	R^2 CTL	R^2 WFP	*RMSE* CTL	*RMSE* WFP
m	-	m/s	m/s	m/s	m/s	m/s	m/s	m/s	m/s	m/s
63	8728	9.32	9.23	9.24	-0.10	-0.08	0.89	0.90	1.47	1.43
91	8728	9.71	9.52	9.53	-0.19	-0.18	0.89	0.90	1.54	1.50
116	8729	9.94	9.75	9.75	-0.20	-0.19	0.90	0.90	1.55	1.52
141	8728	10.10	9.94	9.95	-0.16	-0.15	0.90	0.90	1.56	1.53
166	8729	10.21	10.10	10.11	-0.11	-0.10	0.90	0.91	1.57	1.54
191	8729	10.29	10.24	10.24	-0.06	-0.05	0.90	0.91	1.59	1.56
216	8729	10.35	10.34	10.34	-0.01	-0.01	0.91	0.91	1.61	1.58
241	8729	10.40	10.42	10.42	0.02	0.02	0.91	0.91	1.63	1.60
266	8729	10.44	10.47	10.47	0.04	0.03	0.91	0.91	1.65	1.63
291	8727	10.46	10.51	10.51	0.05	0.05	0.91	0.91	1.67	1.64

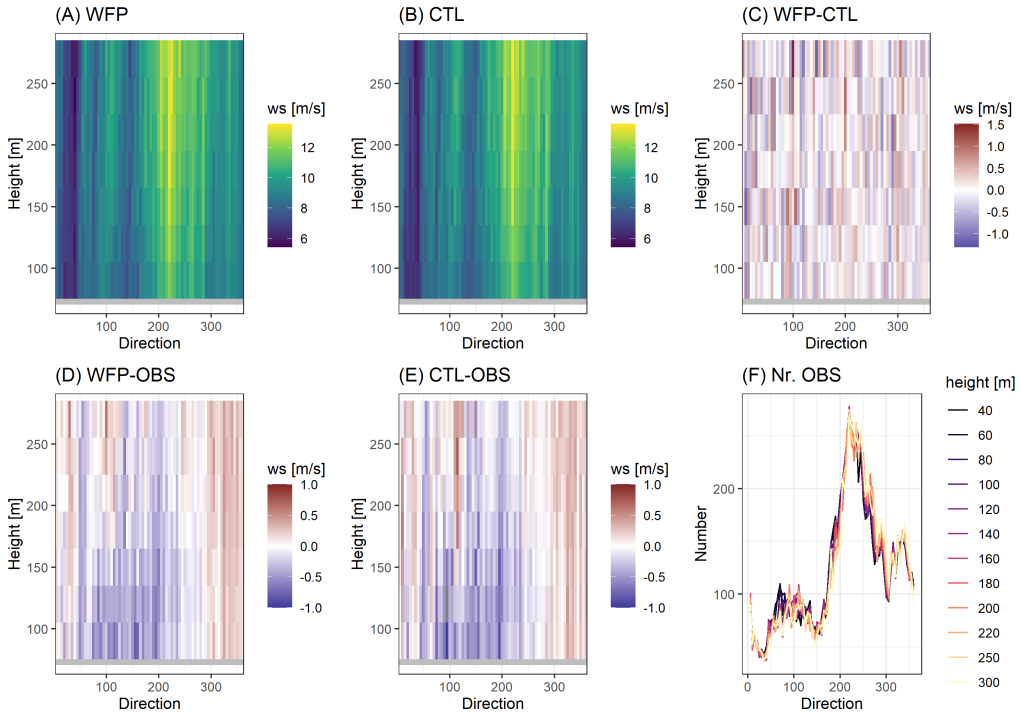

Figure 17: Wind direction bias profile of the K13A lidar. The wind speeds for the HarmCY43-WFP (a) and HarmCY43-CTL (b) and the difference between HarmCY43-WFP and HarmCY43-CTL (c). In the lower plots the bias of HarmCY43-WFP (d) and HarmCY43-CTL (e) with the measurements is shown. The number of measurements for each 5^o angle is included in (f).

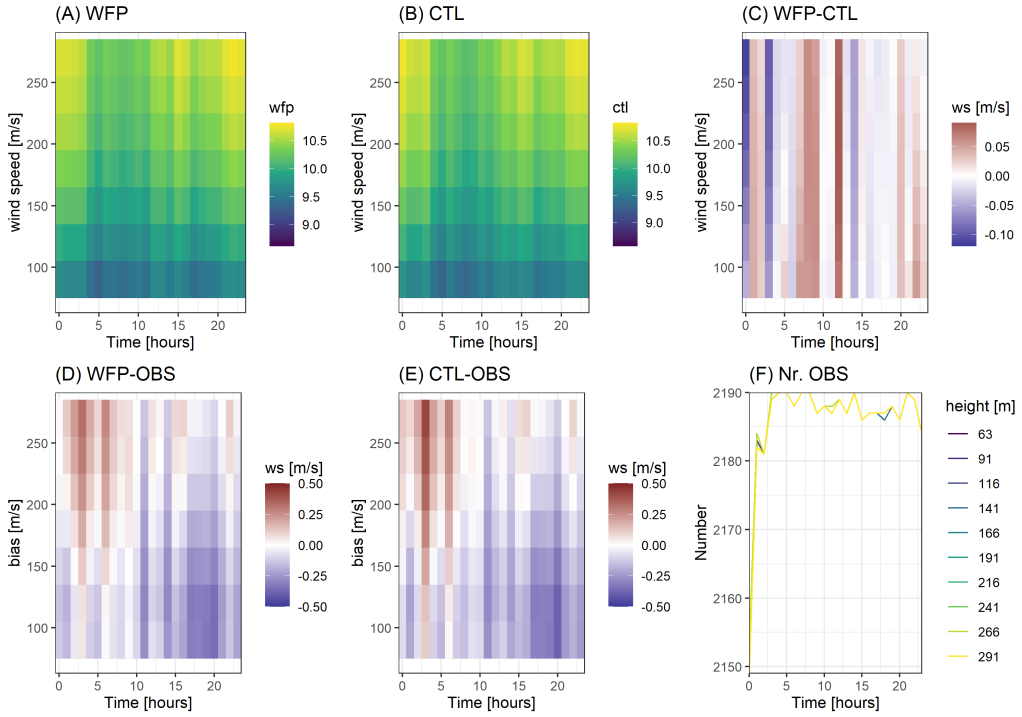

Figure 18: Diurnal profiles of the HarmCY43-WFP (a) and HarmsCY43-CTL (b) and the differences (c). In the lower plots the bias of HarmCY43-WFP (d) and HarmCY43-CTL (e) with the K13A measurements is included. The number of measurements is almost constant with time (f).

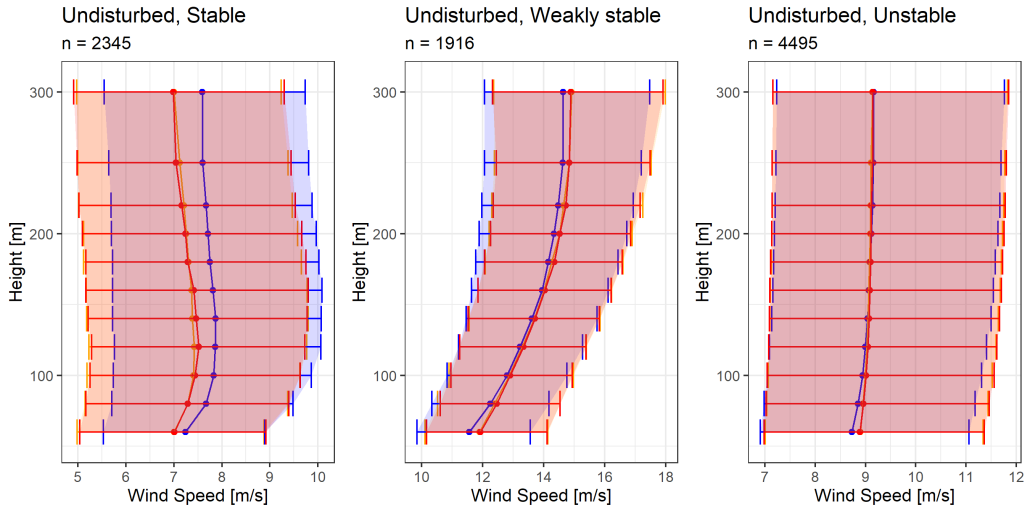

Figure 19: Wind profiles at the K13A location, where n indicates the number of complete profiles. The horizontal lines indicate the 30-70% quantiles. In blue the observed wind speed and, in red and orange respectively the HarmCY43-WFP and HarmCY43-CTL wind speed. The profiles are divided into disturbed and undisturbed wind directions as well as stability regimes. The different flow regimes are based on the modelled Richardson number: ($Ri < 0.0$) unstable, ($0.0 <= Ri <= 0.25$) weakly stable and ($Ri > 0.25$) stable (see subsection 3.5.3 for more details).

6.3 HKNA

The lidar at HKNA is positioned about 22km offshore. Measurements of HKNA are near the parks *Amalia* (9km), *OWEZ* (10km) and *Luchterduinen* (29km), which have a production capacity of respectively 120MW, 108MW and 129MW. Moving from the HKNA lidar to the South and behind the *Amalia* wind farm the *Luchterduinen* wind farm is positioned (Fig.20A). Figure 20B shows that the wind farms are visible from the floating lidar location during fair weather. Under (weakly) stable conditions it is expected that these farms will disturb the wind measurements of the HKNA lidar.

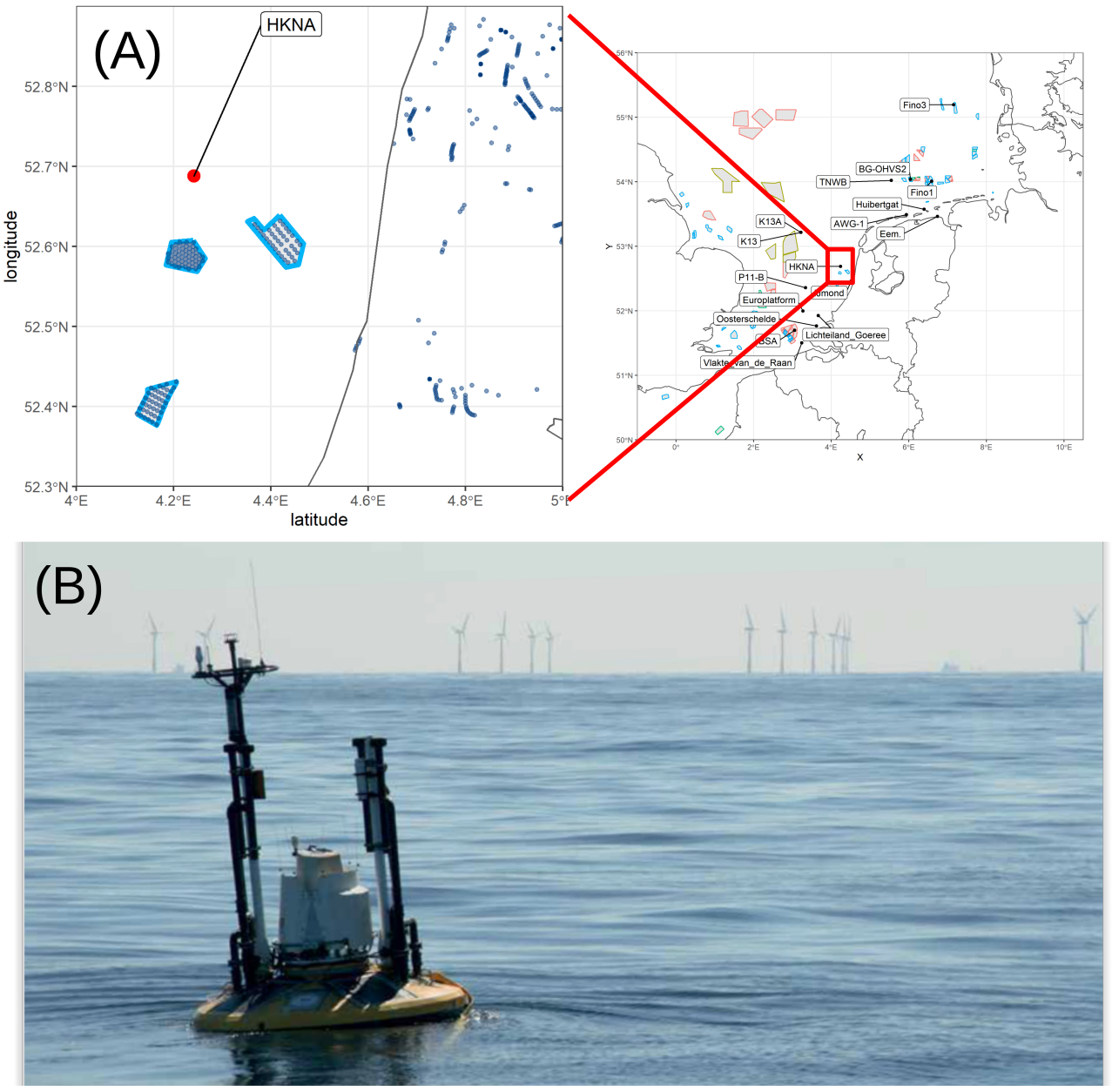

Figure 20: (A) Zoomed in on the location of the HKNA lidar, located 22km West of the coastline. The hub heights of the turbines in the operational wind farms are between 59-81m in 2019. (B) The floating lidar with the wind farms near the Dutch coastline (offshorewind.rvo.nl).

Table 11 provides an overview of the HarmCY43 validation at the measurement heights of the HKNA lidar. There are about 1700 hourly averaged observations at each measurement height. The differences between the HarmCY43-WFP and HarmCY43-CTL at HKNA are small. The measurements at 30m and 40m show a larger biases for both runs of respectively 0.35m/s and 0.19m/s for HarmCY43-CTL and 0.34m/s and 0.18m/s for HarmCY43-WFP. It is expected that measurements below 50m are biased. Above 50m the biases are smaller. The positive bias is smallest when the WFP is included, varying between 0.02m/s and 0.18m/s. The squared correlation coefficient of HarmCY43 is ∼0.95 and RMSE values vary around 1.2m/s for both runs.

Directional wind speed profile: Figure 21 provides an overview of the wind speeds averaged over each 5^o wind direction. The amount of measurements from HKNA are limited to on average 50 cases for south-western wind directions. The limited number of measurements from the (north-)eastern wind directions makes the validation even more uncertain. Possibly due to the limited number of observations there is no clear wake effect visible. The wakes from the *OWEZ* farm (red bar) are not visible from the differences between HarmCY43-WFP, HarmCY43-CTL and the measurements. However, for the other two farms (orange bar) we do see a small positive bias in HarmCY43-CTL.

Diurnal wind speed profile: Figure 22 provides an overview of the diurnal cycle at HKNA. The number of observations per hour varies between 420 and 510. As expected there is almost no variation during the day. The diurnal variations in wind speed are well captured by HarmCY43. The biasses with the measurements are smaller than 0.5m/s and the differences between HarmCY43-WFP and HarmCY43-CTL are less than 0.1m/s (Fig.22C). Most of the biases are within the measurement error range.

Stability profiles: Figure 23 shows the profiles for the disturbed and undisturbed wind directions for different stabilities. Most of the measurements are from undisturbed wind directions (about 15-30 days of hourly data per stability). For disturbed conditions the number of measurements was limited to 60-100 profiles, which is not enough to drawn any solid conclusions. During unstable conditions the HarmCY43 profiles show the best match with the measurements. For weakly stable conditions the wind speeds are slightly overestimated by the HarmCY43, also for undisturbed winds. During stable conditions HarmCY43 has a small underestimation of the wind speed, for the disturbed wind we also see a similar underestimation when the WFP is included.

Wind directions: The lidars directional errors are shown in figure 35. After correcting for the directional error (which occurred in 3.6% of the cases) HarmCY43-WFP and HarmCY43-CTL had a bias of respectively -2.3^o and -2.6^o.

Table 11: HarmCY43 validation at the HKNA lidar location for the 10 measurement heights, which are between 30m and 200m. The measurement heights are in meters above mean sea level. The measured values are denoted by OBS, the modelled values by CTL and WFP.

Height	nr.	OBS	CTL	WFP	bias CTL	bias WFP	R^2 CTL	R^2 WFP	*RMSE* CTL	*RMSE* WFP
m	-	m/s	m/s	m/s	m/s	m/s	m/s	m/s	m/s	m/s
30	1723	10.10	10.45	10.43	0.35	0.34	0.94	0.95	1.19	1.18
40	1723	10.42	10.61	10.59	0.19	0.18	0.95	0.95	1.16	1.15
60	1722	10.83	10.91	10.90	0.08	0.07	0.95	0.95	1.17	1.16
80	1722	11.16	11.20	11.18	0.04	0.02	0.95	0.95	1.21	1.19
100	1720	11.42	11.45	11.44	0.03	0.02	0.95	0.95	1.23	1.22
120	1723	11.63	11.69	11.67	0.05	0.04	0.95	0.95	1.24	1.23
140	1723	11.82	11.90	11.88	0.08	0.07	0.95	0.95	1.24	1.23
160	1723	11.97	12.09	12.07	0.12	0.10	0.95	0.96	1.25	1.24
180	1723	12.09	12.26	12.24	0.16	0.14	0.96	0.96	1.27	1.26
200	1723	12.20	12.40	12.38	0.20	0.18	0.96	0.96	1.29	1.29

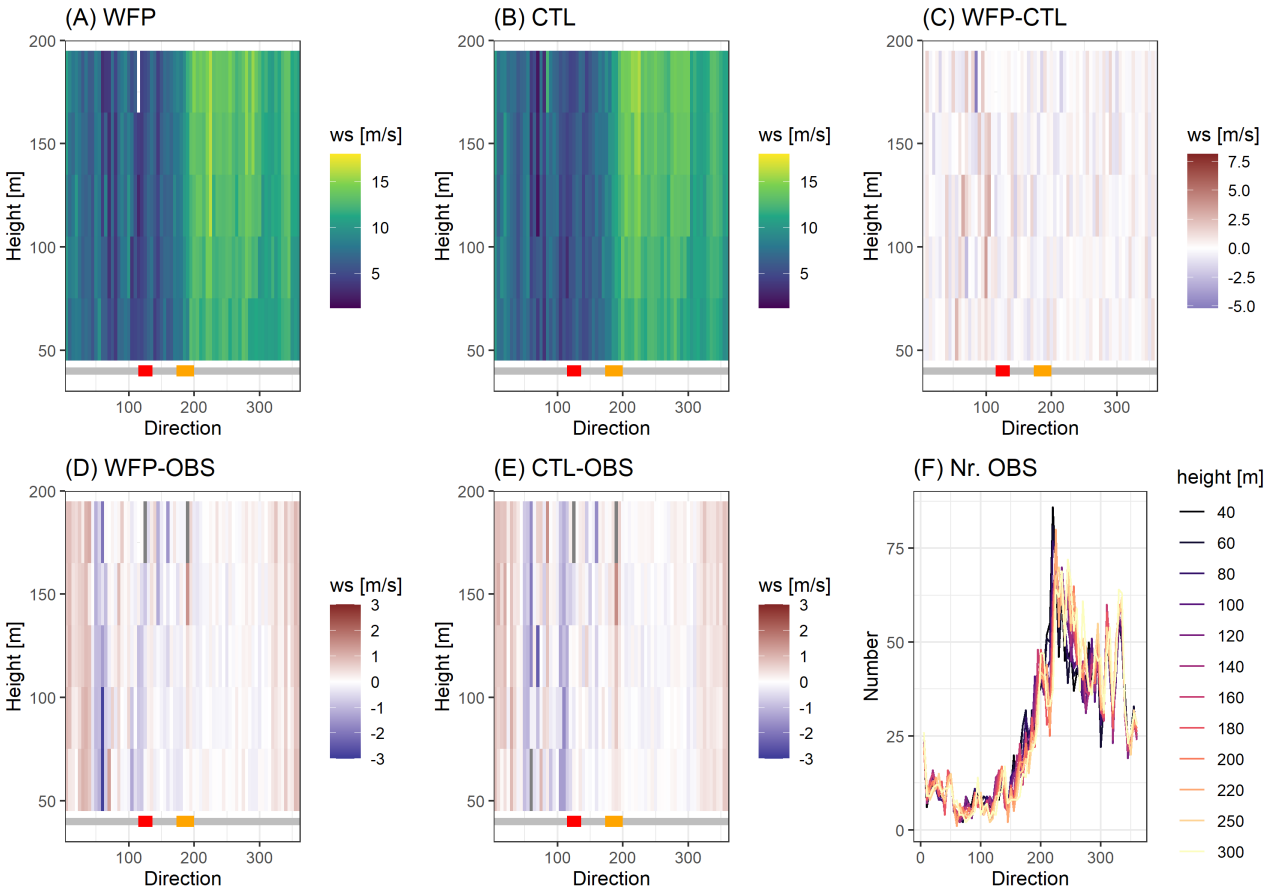

Figure 21: Overview of the directional wind profiles at heights of the HKNA lidar. The red and orange colour bars denote the wind farms. The farm is within distances of approximately 10km. Wind speed at various heights per 5^o from HarmCY43-WFP (a), HarmCY43-CTL (b) and the difference between them (c). Differences between the predicted and observed wind speed for HarmCY43-WFP (d) and HarmCY43-CTL (e). The number of measurements for each direction is included in (f).

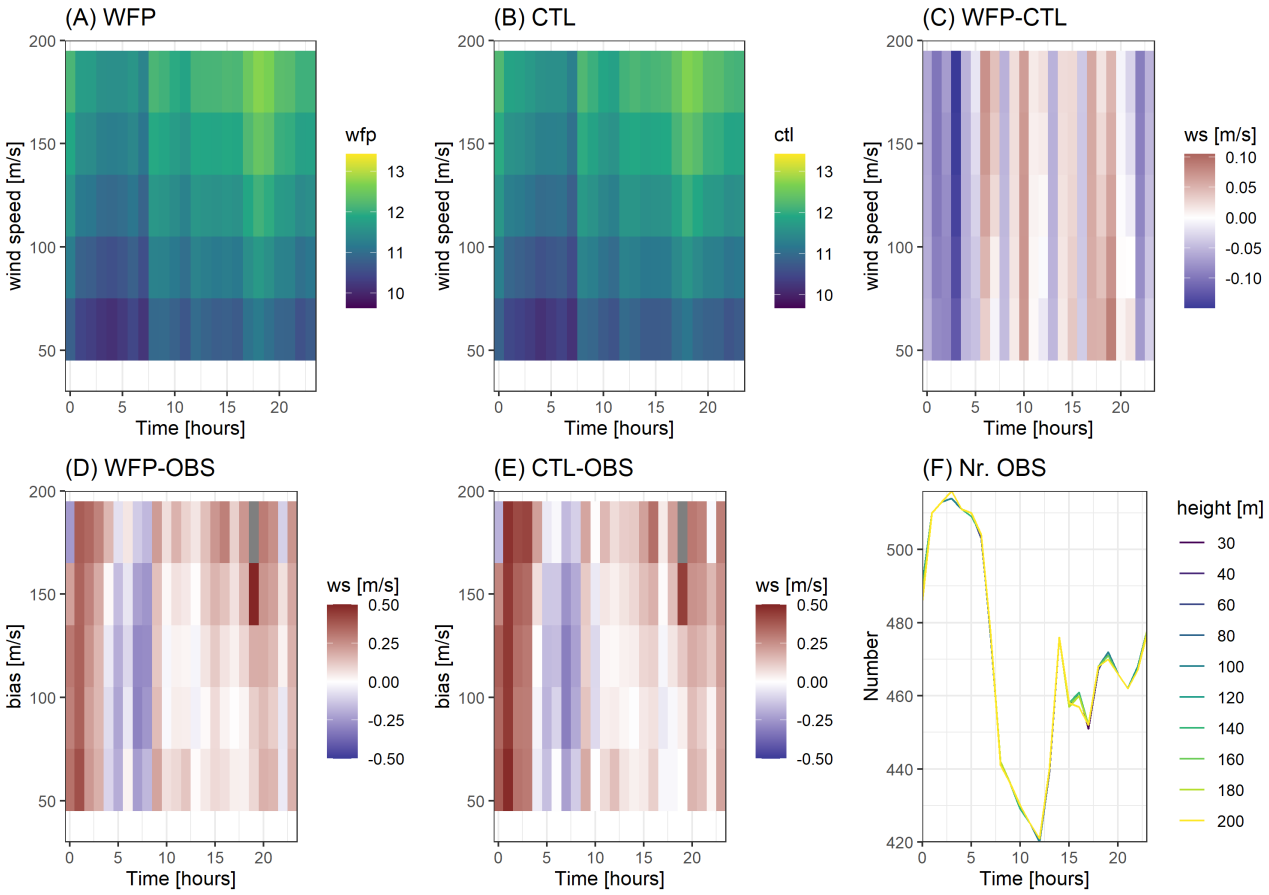

Figure 22: Overview of the diurnal cycle in HarmCY43-WFP and HarmCY43-CTL compared with the measurements at HKNA. Wind speed at various heights for each hour from HarmCY43-WFP (a), HarmCY43-CTL (b) and their differences (c). The model biases at the HKNA location for HarmCY43-WFP (d) and HarmCY43-CTl (e). The number of measurements for each hour is included in (f).

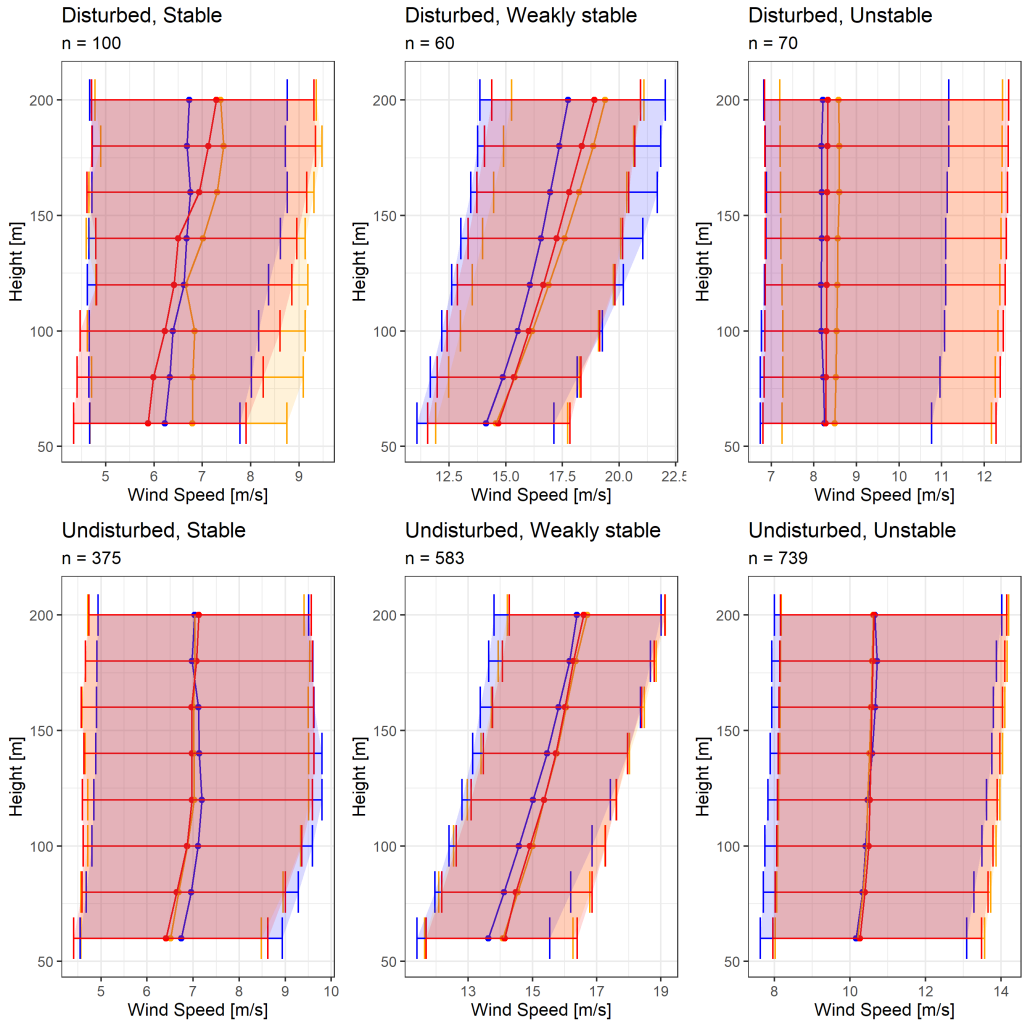

Figure 23: Wind profiles at the HKNA location, where n indicates the number of complete profiles. The horizontal lines indicate the 30-70% quantiles. In blue the observed wind speed and, in red and orange respectively the HarmCY43-WFP and HarmCY43-CTL wind speed. The profiles are divided into disturbed and undisturbed wind directions as well as stability regimes. The different flow regimes are based on the modelled Richardson number: ($Ri < 0.0$) unstable, ($0.0 <= Ri <= 0.25$) weakly stable and ($Ri > 0.25$) stable (see subsection 3.5.3 for more details).

6.4 TNWB

The TNWB lidar is floating North of the Dutch islands, about 65km offshore. The lidar at TNWB is with an easterly wind in the wake of the Gemini wind parks, which have a total installed capacity of 600MW. The Gemini *ZeeEnergie* wind farm is closest at a distance of 18km, the Gemini park *Buitengraads* is at a distance of 30km. TNWB is in the wake of these farm for the wind directions $77 - 95^o$. About 60km East the German wind parks with the FINO1 research platform are located, the various active wind farms could possibly cause a combined wake effect during stable conditions.

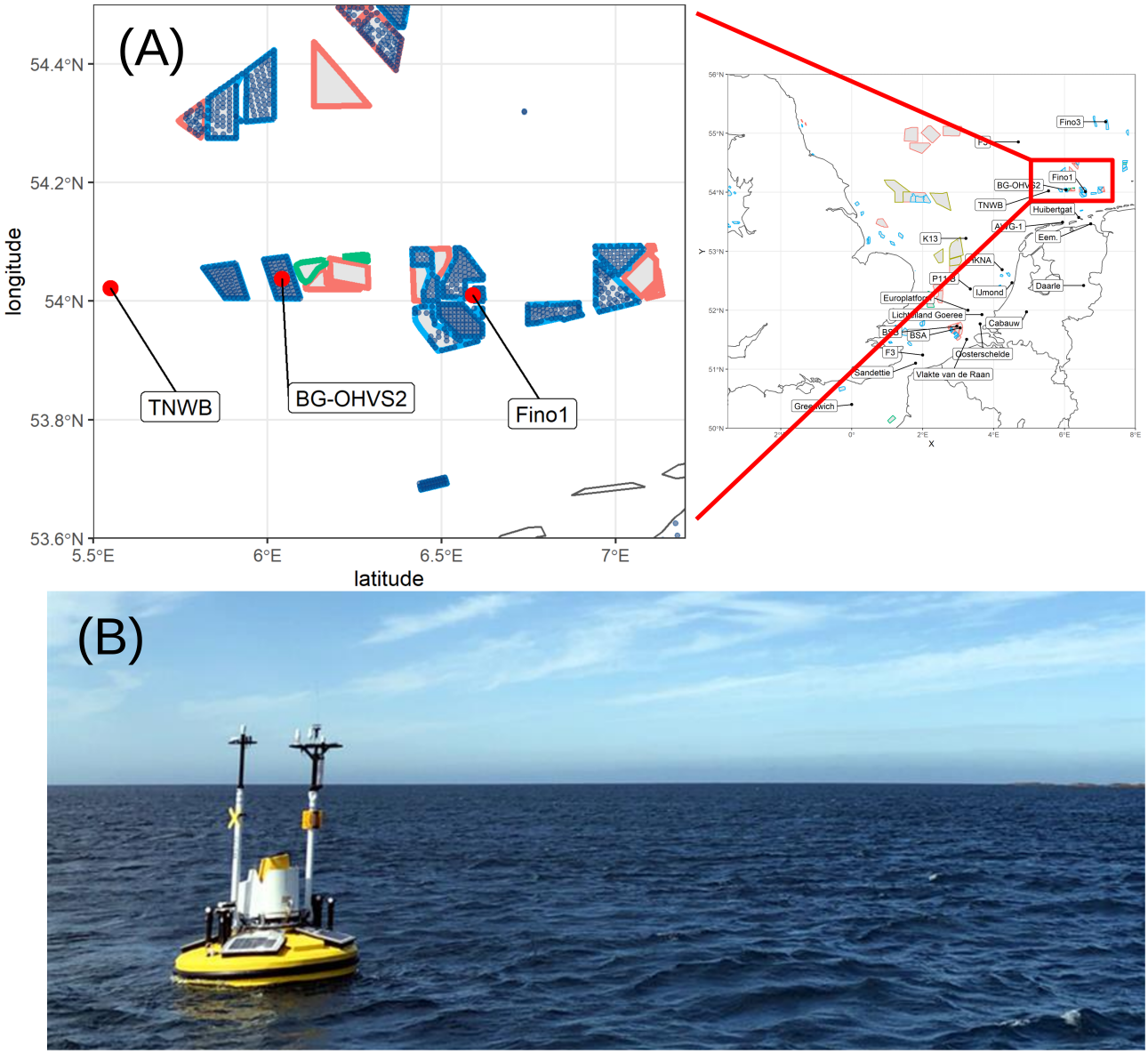

Figure 24: (A) Zoomed in on the location *Ten Noorden van de Wadden*, where the TNWB lidar is west of the wind farms. The turbine hub height in the nearest wind farm is 89m in 2019. (B) Impression of the Fugro floating lidar (source: www.fugro.com).

Table 12 provides an overview of the HarmCY43 validation at the measurement heights of the TNWB lidar. The TNWB lidar measured between 30-250m. The lowest measurement at 30m deviates from the others, this is as expected since the lidar measurements below 50m are less accurate. The wind speeds are underestimated by HarmCY43-CTL. With the WFP the bias is about 0.03m/s larger. Though, with a bias of less than 0.2m/s both runs fall within the measurement uncertainty range. The RMSE of 1.3-1.5m/s and squared correlation coefficient of 0.9 are similar for HarmCY43-WFP and HarmCY43-CTL.

Directional wind speed profile: Figure 25 shows the wind speeds for different wind directions, grouped by 5^o. The number of observations from the disturbed wind directions is limited to about 25 per directional bin, which makes it hard to draw any general conclusions. From the undisturbed southern wind directions there are more than 50 measurements. HarmCY43-CTL shows a clear bias around 90^o, this is where we expect the wake effect from the upstream wind farms. With the WFP the bias is reduced to almost zero. Based on the averaged difference between HarmCY43-WFP and HarmCY43-CTL the wake is on average around 1m/s for this single day of measurements.

Diurnal wind speed profile: Figure 26 shows the diurnal variations (which are negligible on Sea) in wind speed. There are sufficient measurement to state that the diurnal cycle of HarmCY43 is in good agreement with the measurements. Both HarmCY43-WFP and HarmCY43-CTL have a small negative bias of 0.1-0.2m/s. The differences between both model runs are small.

Stability profiles: Figure 26 provides an overview of the wind profiles under disturbed and undisturbed wind directions. Most of the profiles were for undisturbed wind directions: 28 days of hourly measurements under stable conditions, 19 days for weakly stable conditions and 111 days for unstable conditions. For disturbed conditions the data was limited to less than 139 hourly profiles per class, which is not sufficient to draw general conclusions. The undisturbed measurements of both HarmCY43 runs were in close agreement. The HarmCY43 profiles are in good agreement with the measurements during undisturbed unstable conditions. During stable undisturbed conditions the wind speeds were underestimated with 0.3 m/s by HarmCY43, while for weakly stable conditions the wind speeds were overestimated. A similar pattern was found for the disturbed wind directions.

Wind directions: The TNWB lidars wind directions had a 180^o Doppler error in 3.1% of the measurements. An overview of the wind directional errors of TNWB is included in figure 36. After correcting for the directional error HarmCY43-WFP and HarmCY43-CTL are found to have a bias of respectively 1.2^o and 1.0^o.

Table 12: HarmCY43 validation at the TNWB lidar location for the 11 measurement heights (between 30-250m). The measurement heights are in meters above mean sea level. The measured values are denoted by OBS, the modelled values by CTL and WFP.

Height	nr.	OBS	CTL	WFP	bias CTL	bias WFP	R^2 CTL	R^2 WFP	$RMSE$ CTL	$RMSE$ WFP
m	-	m/s	m/s	m/s	m/s	m/s	m/s	m/s	m/s	m/s
30	3328	9.13	9.18	9.15	0.05	0.02	0.89	0.89	1.31	1.31
40	3327	9.31	9.27	9.25	-0.04	-0.07	0.89	0.89	1.33	1.34
60	3327	9.59	9.45	9.42	-0.14	-0.17	0.89	0.89	1.40	1.40
80	3325	9.76	9.61	9.58	-0.15	-0.18	0.89	0.89	1.44	1.44
100	3324	9.89	9.75	9.72	-0.14	-0.17	0.89	0.89	1.46	1.46
120	3328	10.01	9.88	9.85	-0.13	-0.16	0.89	0.89	1.47	1.47
140	3327	10.11	9.99	9.96	-0.11	-0.15	0.90	0.90	1.47	1.47
160	3328	10.19	10.09	10.06	-0.11	-0.14	0.90	0.90	1.48	1.47
180	3327	10.27	10.17	10.14	-0.10	-0.13	0.90	0.90	1.48	1.47
200	3326	10.34	10.25	10.21	-0.10	-0.13	0.90	0.90	1.48	1.48
250	3320	10.49	10.37	10.34	-0.12	-0.15	0.91	0.91	1.48	1.47

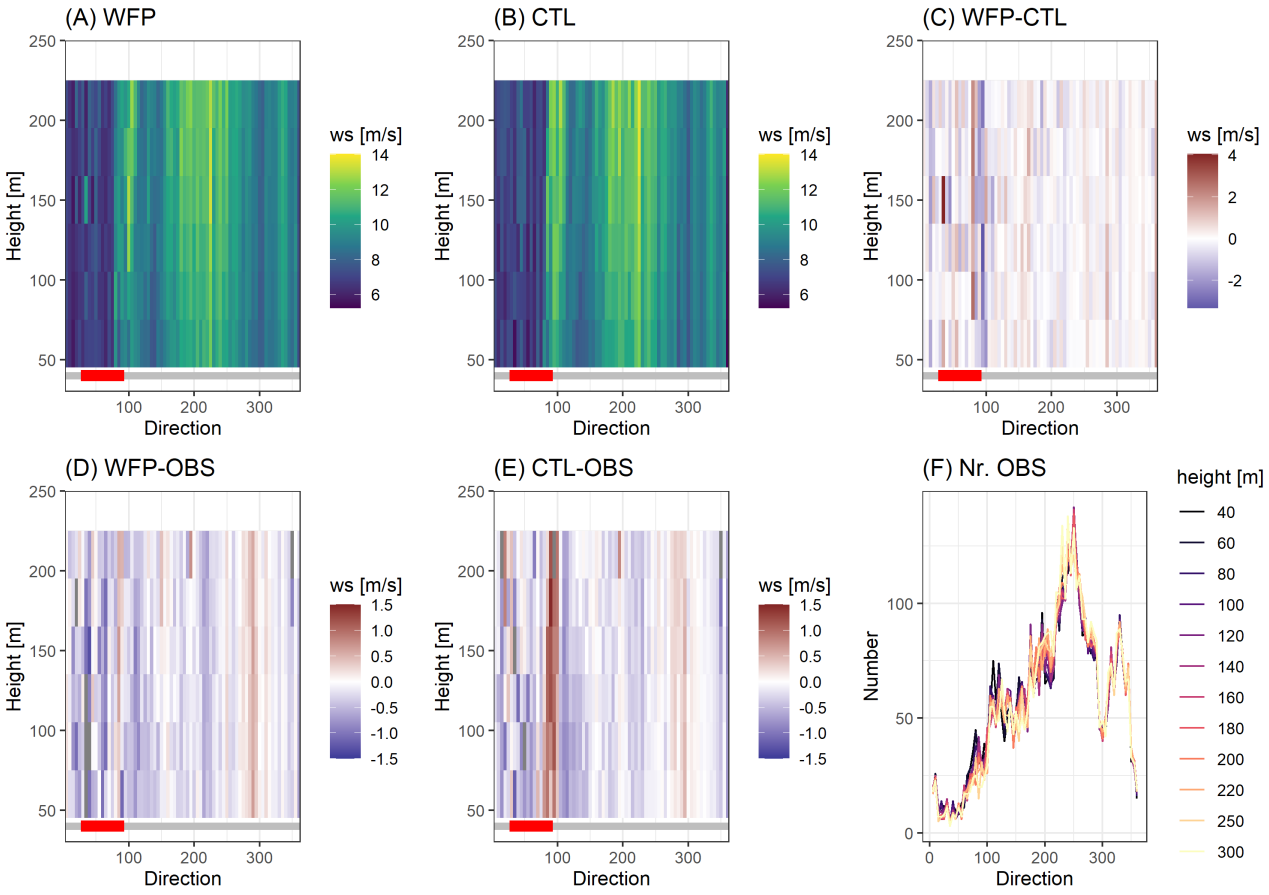

Figure 25: Overview of the directional wind profiles at heights of the TNWB lidar. The red colour indicates the direction of the *Gemini* wind farm. The farms are within distances of approximately 5km and 30km. Wind speed at various heights per 5^o from HarmCY43-WFP (a), HarmCY43-CTL (b) and the differences (c). The bias with the measurements for HarmCY43-WFP (d) and HarmCY43-CTL (e). The number of measurements for each wind direction is included in (f).

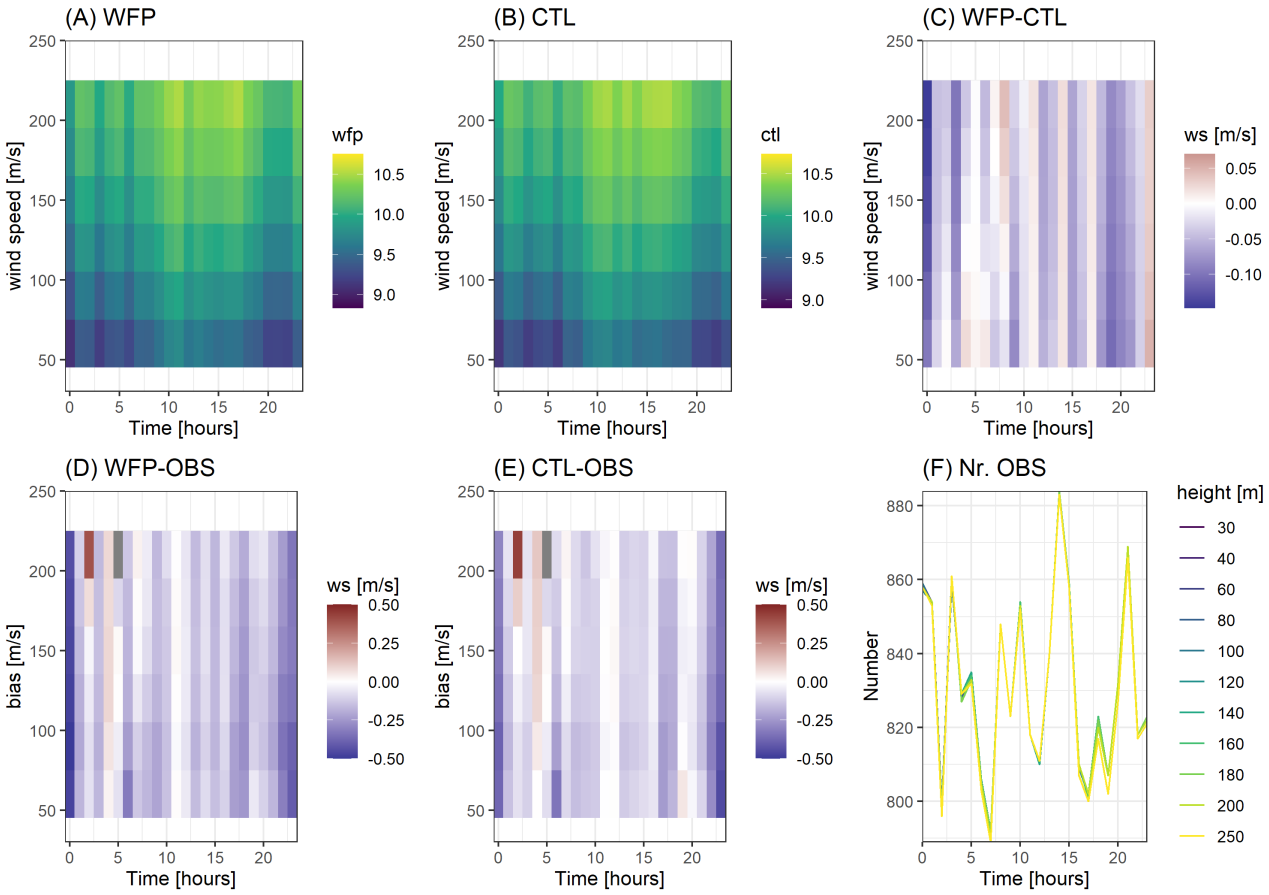

Figure 26: Diurnal cycle at the location of the TNWB lidar for HarmCY43-WFP (a), HarmCY43-CTL (b) and the differences between HarmCY43-WFP and HarmCY43-CTL (c). The bias with the measurements for HarmCY43-WFP (d) and HarmCY43-CTL (e). The number of measurements at each of the lidar measurement heights (f).

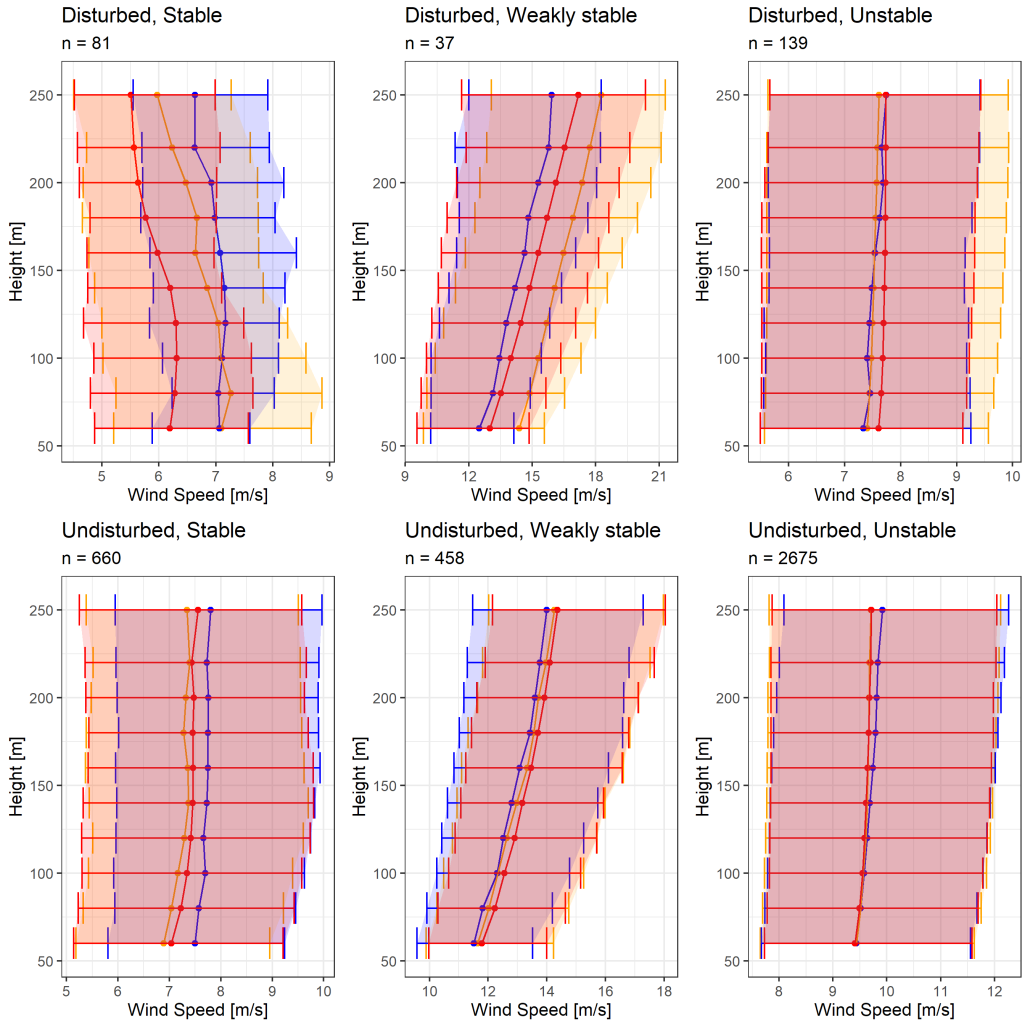

Figure 27: Wind profiles at the TNWB location, where n indicates the number of complete profiles. The horizontal lines indicate the 30-70% quantiles. In blue the observed wind speed and, in red and yellow respectively the modelled wind speed of HarmCY43-WFP and HamCY43-CTL. The data is organized in disturbed and undisturbed wind directions as well as stability. The different flow regimes are based on the modelled Richardson number: ($Ri < 0.0$) unstable, ($0.0 <= Ri <= 0.25$) weakly stable and ($Ri > 0.25$) stable (see subsection 3.5.3 for more details).

6.5 Eemshaven

In the north-eastern part of the Netherlands near the German border the lidar of Eemshaven is located. The Eemshaven windcube lidar from Pondera is positioned on the shoreline near the port of Eemshaven (Fig.28A). Figure 28B shows the lidar behind the sea dike in front of the solar panels. The wind farm is at a distance of 1km from the lidar and has about 150 installed turbines, covering the eastern angles $93 - 161^o$. The position on the shore line complicates the model validation since we expect local coastal effects due to the land/sea transition.

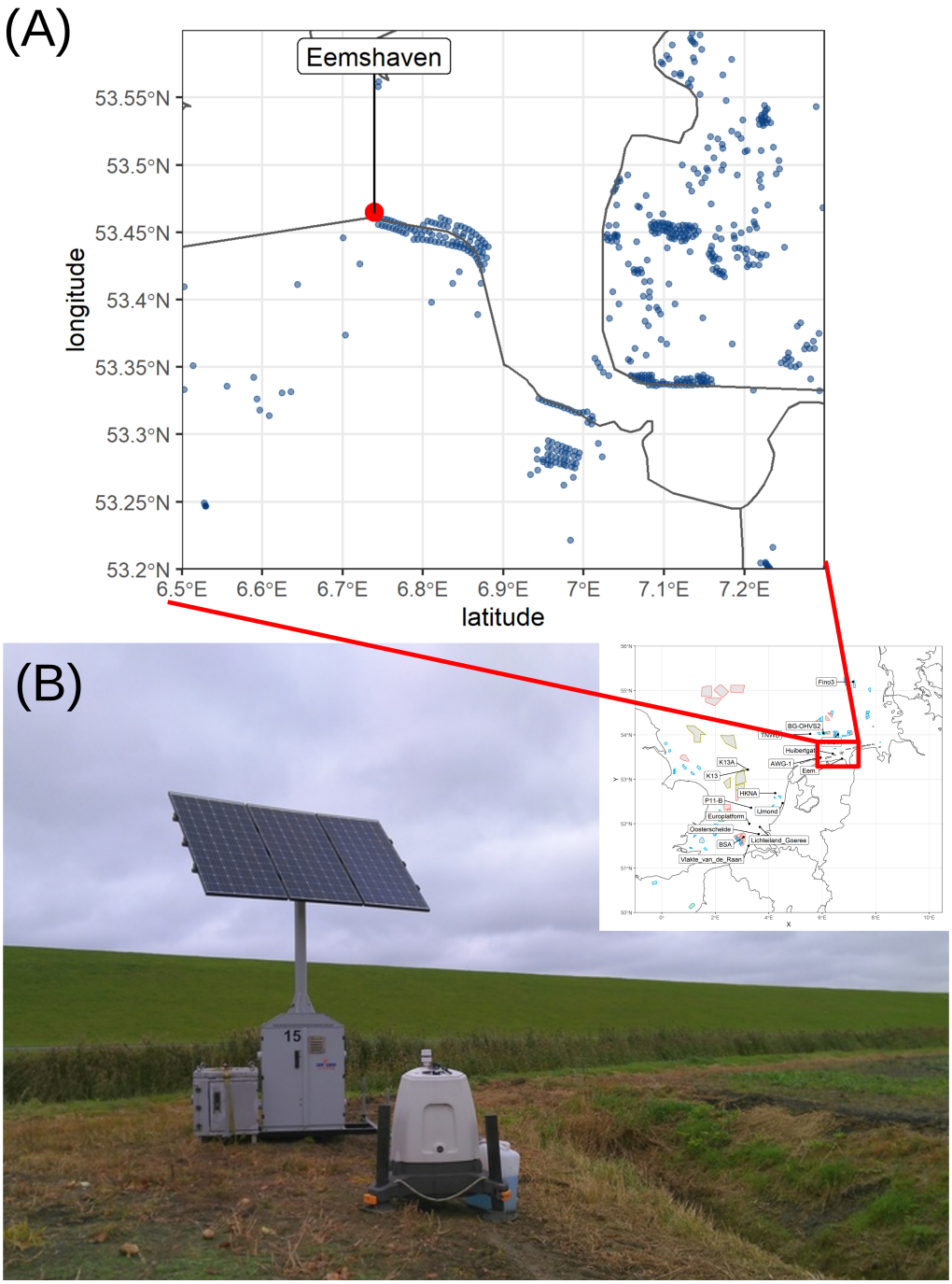

Figure 28: (A) The Eemshaven windcube lidar is positioned on the shoreline of the *Waddenzee* with on the western side the estuary of the river Eems. The blue dots are the individual wind turbines which all have a hub height of 100m in 2019. (B) The windcube Lidar from Pondera (source: ponderaconsult.com).

Table 13 provides an overview of the HarmCY43 validation at the 12 measurement heights of the Eemshaven lidar. The bias of HarmCY43-CTL is negative, the wind speeds are underestimated with 0.1-0.3m/s. With the WFP the underestimation is 0.15m/s larger. The squared correlation coefficient is high and above 0.9. The RMSE varies between 1.2-1.3m/s.

Directional wind speed profile: Figure 29 compares the model performance for different wind directions. Most observations are from a south-western wind direction (20-40), with the short measurement campaign it is hard to draw general conclusions. The red bar indicates the directions of the upstream Eemshaven wind farm. Within the wake the wind speed is overestimated by HarmCY43-CTL. With the WFP the overestimation is smaller. For Southern winds both models underestimate the wind speed, while for a Northern direction the wind speeds are overestimated. From the South the winds are from land, while the Northern winds are from sea. Though it is hard to verify if winds from sea are systematically overestimated since the number of observations is limited to 0-20 per bin.

Diurnal wind speed profile: Figure 30 shows the diurnal cycle of HarmCY43. There is little variation in the wind speed, though during the day the winds are a bit stronger. Most of the time the bias of HarmCY43-WFP varies between 0.1m/s and 0.8m/s. For HarmCY43-CTL the bias is a bit smaller.

Stability profile: Figure 31 shows the wind profiles for different stabilities. The number of measurements for the disturbed wind directions is limited (13-66 hourly profiles), this is not sufficient to draw general conclusions. For undisturbed stable and unstable conditions there were respectively 179 and 49 hourly profiles. Most of the measurements were under undisturbed weakly stable conditions (715). Here, we see a clear underestimation of the wind speed by HarmCY43. Also under stable undisturbed conditions we find an underestimation of the wind speed. This underestimation was not observed for the disturbed directions.

Wind directions: The wind directions from the wind cube don't inherit the same directional error as the ZephIR300 instruments. With low wind speeds we still observe directional differences between HarmCY43 and the lidar in 1.7% of the cases. It it possible that the wind near the shoreline is variable, causing differences with the model. The bias of HarmCY43-WFP and HarmCY43-CTL was -4.7^o and -4.2^o, respectively.

Table 13: Validation at the Eemshaven lidar location for the 12 measurement heights, which were between 42m and 200m. The measurement heights are in meters above mean sea level. The measured values are denoted by OBS, the modelled values by CTL and WFP.

Height	nr.	OBS	CTL	WFP	bias CTL	bias WFP	R^2 CTL	R^2 WFP	*RMSE* CTL	*RMSE* WFP
m	-	m/s	m/s	m/s	m/s	m/s	m/s	m/s	m/s	m/s
42	1054	9.13	8.84	8.73	-0.28	-0.40	0.92	0.92	1.13	1.16
58	1054	9.63	9.30	9.17	-0.33	-0.46	0.92	0.92	1.18	1.21
71	1054	9.97	9.65	9.51	-0.32	-0.46	0.92	0.92	1.22	1.24
84	1053	10.26	9.98	9.84	-0.28	-0.42	0.92	0.92	1.26	1.26
96	1053	10.51	10.27	10.12	-0.25	-0.39	0.91	0.92	1.29	1.28
109	1053	10.77	10.55	10.40	-0.22	-0.37	0.91	0.92	1.31	1.30
121	1053	11.01	10.81	10.66	-0.19	-0.34	0.92	0.92	1.32	1.30
133	1053	11.22	11.05	10.90	-0.18	-0.33	0.92	0.93	1.32	1.29
146	1050	11.46	11.30	11.15	-0.16	-0.32	0.92	0.93	1.32	1.29
158	1047	11.66	11.51	11.36	-0.14	-0.30	0.92	0.93	1.31	1.28
183	1031	12.07	11.96	11.80	-0.12	-0.28	0.93	0.93	1.32	1.30
200	1017	12.36	12.25	12.09	-0.11	-0.27	0.93	0.93	1.33	1.31

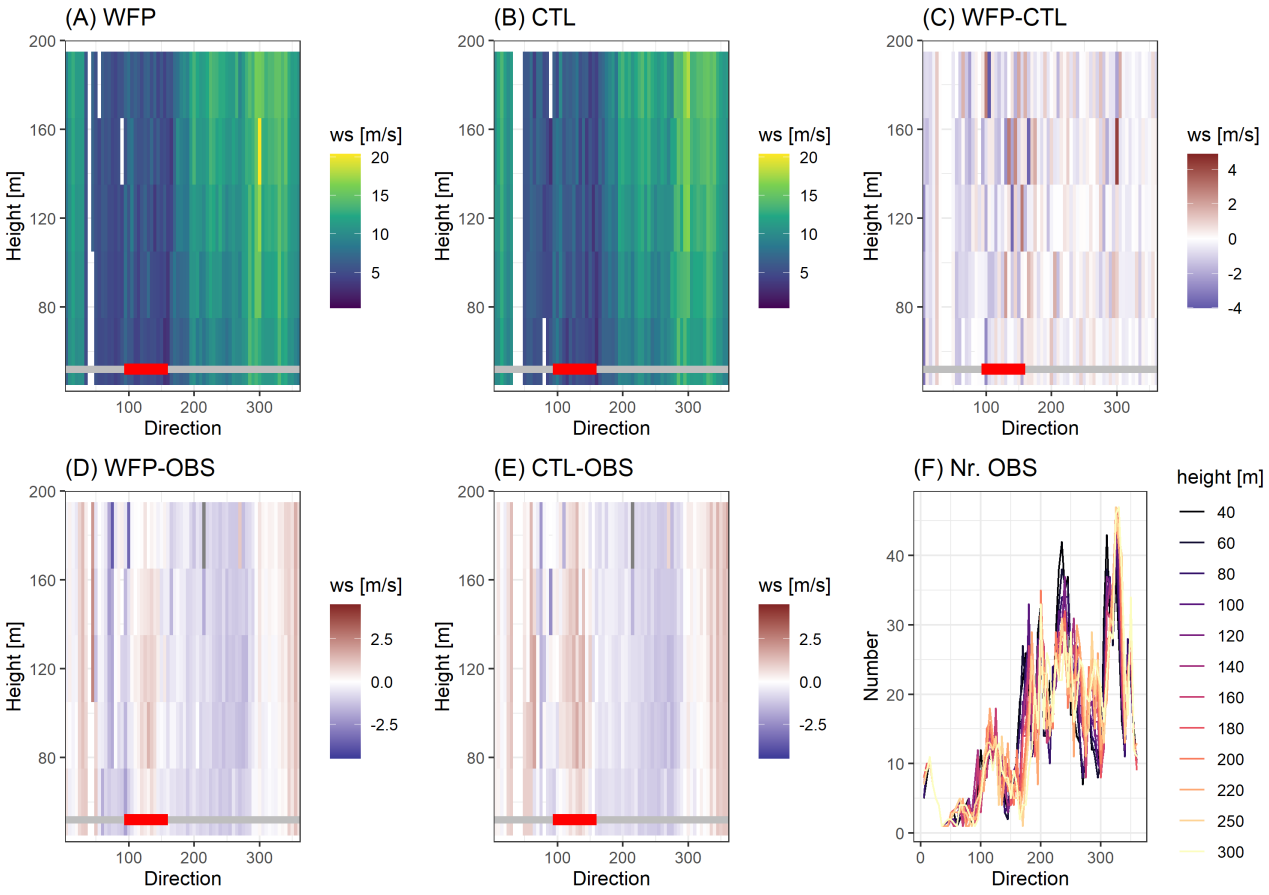

Figure 29: Overview of the directional wind profiles at heights of the Eemshaven lidar. The red color bar indicates the directions of the *Eemshaven* wind farm. The wind speed at interpolated to a constant height per 5^o for HarmCY43-WFP (a), HarmCY43-CTL (b) and their differences (c). The bias with the measurements for HarmCY43-WFP (d) and HarmCY43-CTL (e). The number of measurements for each direction is included in (f).

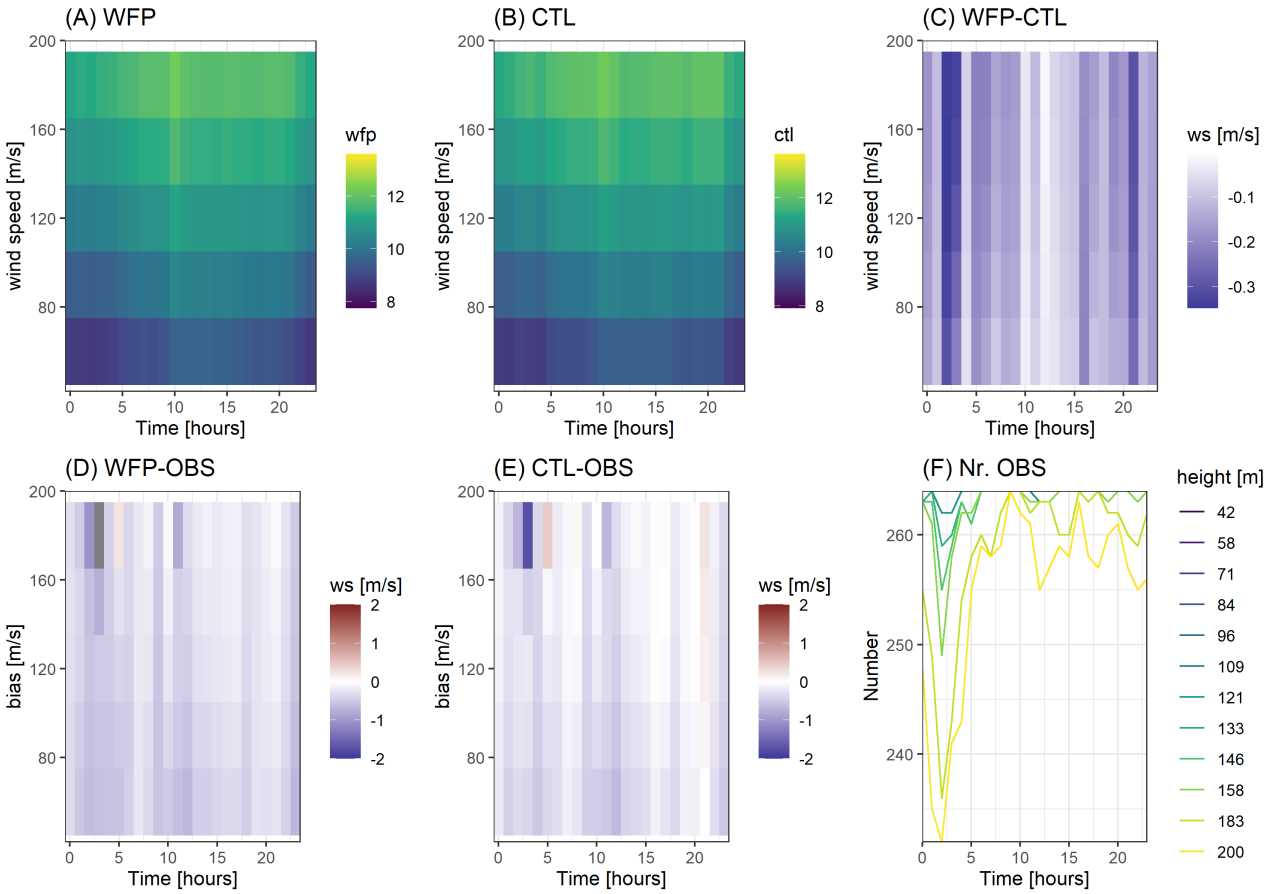

Figure 30: Diurnal cycle at the location of the Eemshaven lidar for HarmCY43-WFP (a), HarmCY43-CTL (b) and their differences (c). The hourly bias with the measurements for HarmCY43-WFP (d) and HarmCY43-CTL (e). The number of measurements for each hour is included in (f).

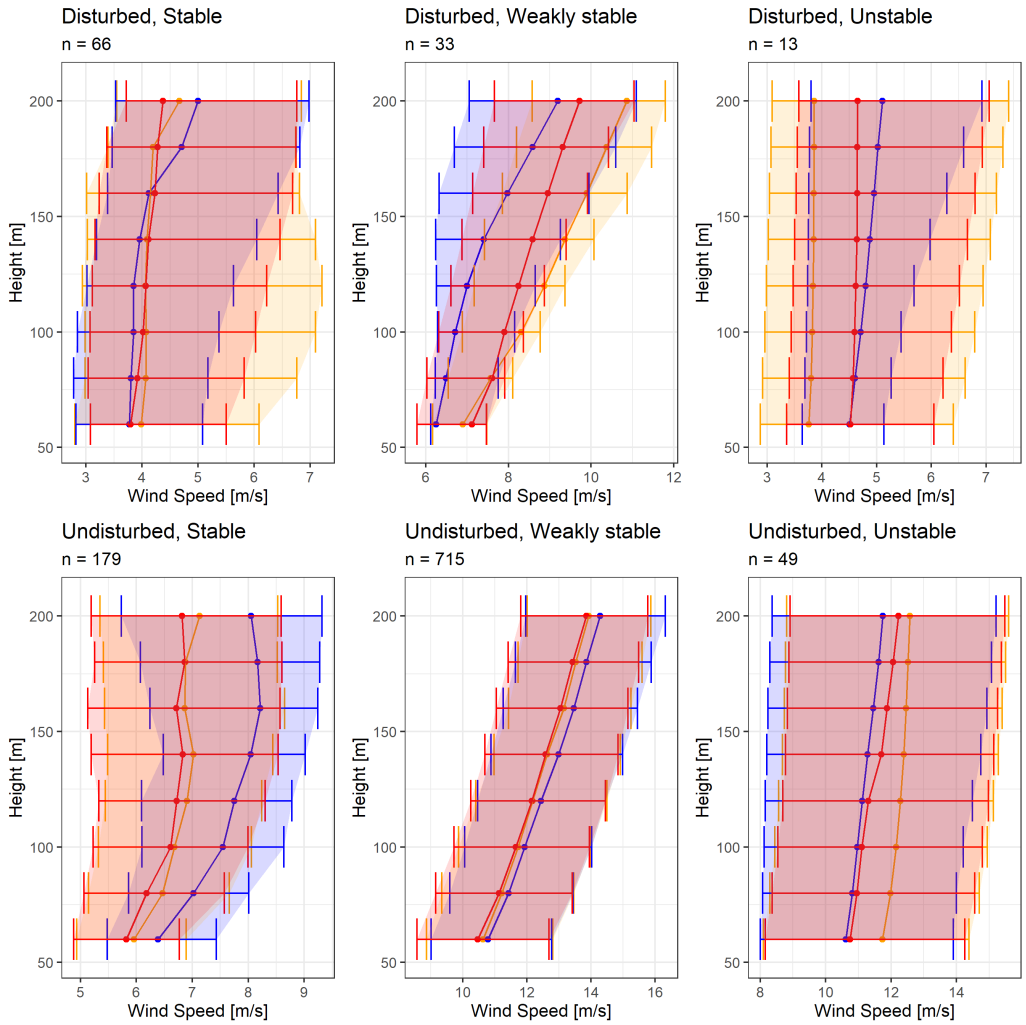

Figure 31: Wind profiles at the Eemshaven location with the measurements in blue, HarmCY43-WFP in red and HarmCY43-CTL in yellow. The subtitle n indicates the number of complete profiles. The horizontal lines indicate the 30-70% quantiles. The data is organized in disturbed and undisturbed wind directions as well as stability. The different flow regimes are based on the modelled Richardson number: ($Ri < 0.0$) unstable, ($0.0 <= Ri <= 0.25$) weakly stable and ($Ri > 0.25$) stable (see subsection 3.5.3 for more details).

7 Discussion

7.1 Methodology

With regard to the methodology it is important to realize we made several assumptions about:

1. Optimal wind farm operation and wind turbine performance. Wind turbines may not perform conform the turbine specific power curve or rotor blades may not be turning at all because of maintenance or legislation. There are not many publications about the downtime of turbines, for the *OWEZ* wind farm the downtime is about 20% (Cevasco et al., 2021; Faulstich et al., 2011). We have no way to verify this assumption: disturbed wind direction most likely are not disturbed all the time.

2. Selection of disturbed wind direction. The disturbed wind directions have been defined as the upstream angles of the productive wind farms from 2019 less than 50km from the measurement site. This method did not account for (1) long wakes with a velocity deficit beyond the 50km boundary, (2) meandering of the wakes due to for example turning wind directions or the Coriolis force. Since the undisturbed wind profiles in HarmCY43-WFP and HarmCY43-CTL are generally similar, we have reason to believe that the disturbed wind direction selection works most of the time. For example: figure 32 shows the directional wind speed bias at BSA calculated as the difference between HarmCY43-WFP and HarmCY43-CTL. The disturbed wind directions (wind directions downwind Belgian wind farms) are shaded in green. As expected we observe no wind speed bias for undisturbed wind directions and a negative wind speed bias for disturbed wind directions. However, the selection of the disturbed wind directions is not perfect: for the undisturbed (not green) wind directions between 170 and 190 degrees HarmCY43-WFP is lower than in HarmCY43-CTL.

3. The minimum number of cases required before we can draw conclusions about the comparison between HarmCY43-WFP and HarmCY43-CTL. In several cases the number of measurements per stability regime was low. All cases were included in the results, but when the number of cases was below 100 we did not draw any conclusions. Also, some of the measurement campaigns we used for validation were too short to draw any conclusions. For example the data availability of the BSA lidar was only four months.

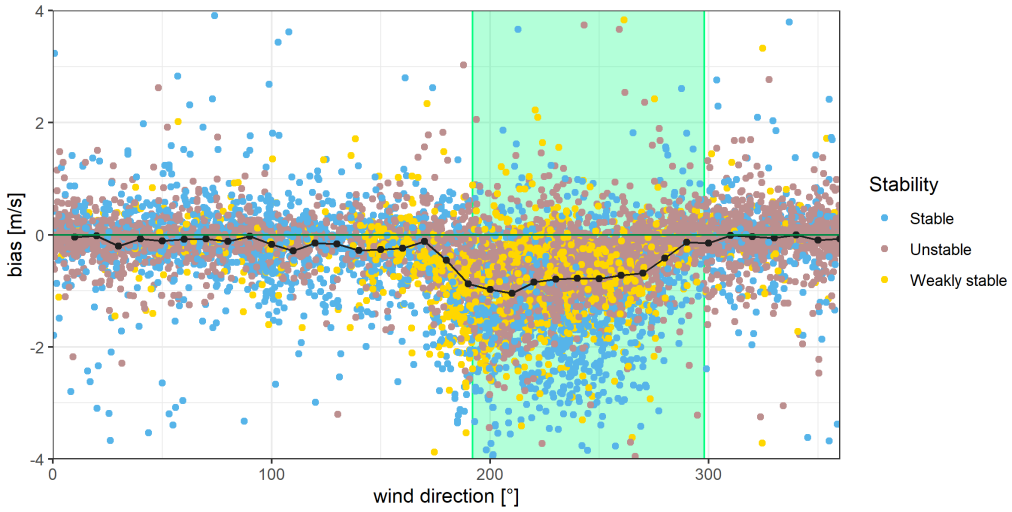

Figure 32: Bias for each wind direction calculated as HarmCY43-WFP minus HarmCY43-CTL at BSA. The black line indicates the mean bias averaged over each 5^o bin, the green shaded area highlights the directions of the upstream Belgium wind farms. The different flow regimes are based on the modelled Richardson number: ($Ri < 0.0$) unstable, ($0.0 <= Ri <= 0.25$) weakly stable and ($Ri > 0.25$) stable (see subsection 3.5.3 for more details).

These assumptions complicate the validation of the WFP: differences between HarmCY43-CTL and HarmCY43-WFP may be caused by the quality of the WFP, but can also be the result of the assumptions we made.

7.2 Results

We will now discuss the results of the validation work based on the research questions:

Q1: How well is the wind (speed, direction) represented over the North Sea by HARMONIE-AROME?

Table 14 and 15 provide a summary of the lidar and cup anemometer validation results. The Lidar and FINO1 and FINO3 measurements are averaged over all measurement heights, the KNMI/RWS measurement are just for one height. Measurements at FINO3 and K13A are for the entire year 2019, but at the other sites the measurement campaigns are shorter (FINO1 4 months, TNWB 4 months, HKNA 4 months, BSA 4 months and Eemhaven 2 months). Most of the KNMI stations have measured the entire year.

Wind speed: Table 14 gives a summary of the wind speed evaluation. The quality of the fit is determined by the bias (systematic error) and the squared correlation coefficient (random error). The squared correlation coefficient is high (0.8 or higher) and not affected by the WFP. If there is no wind farm nearby, the bias of HarmCY43-WFP compared to the bias of HarmCY43-CTL does not change significantly. However, for most sites with wind farms nearby we see that the WFP improves the bias. This confirms the result of an earlier study for 2016 by van Stratum et al. (2021). The WFP does not improve the bias for:

- Huibertgat: 12km from the wind farm, but can only affect the measurement for a 20^o wind direction range from the North.
- IJmond: 13km from the wind farm, 20^o wind direction range from the north-west.
- Vlakte van de Raan: 17km from the wind farms, 25^o from the West-northwest.
- HKNA: 9km from the wind farms, 45^o from a south-easterly direction.
- TNWB: 18km from the wind farm, 17^o from a East-northeasterly direction.
- Eemshaven: 1km from the wind farm, 70^o from the East to south-east.

For all these sites the prevailing wind direction is West-southwest, so the measurements are not often in the wind farm wake. Table 6 also shows that the number of disturbed measurements at these sites is low.

All measurement sites included in the validation are at least 2.5km away from the coast (except for Eemshaven). This means that HarmCY43 grid boxes at these locations are proper water grid boxes, so without mixing in a bit of land. In general we see a larger overestimation closer to the coast than further offshore. For the stations within 20km from the coast, Oosterschelde, Vlakte van de Raan and IJmond the wind speed bias is 0.3-0.6m/s, for Huibertgat and AWG1 0.1-0.2m/s. For most measurement sites in or at the edge of wind farms (BG-OHVS2, FINO1 and FINO3) we see a particularly large overestimation. This is what we expect because HarmCY43 has a 2.5x2.5km resolution which means the model is not suitable for inside wind farms. Inside these wind farms HarmCY43-WFP overestimates the wind speed by $\sim$0.5m/s. Eemshaven is also on the edge of the wind farm. Here we see a small underestimation of the wind speed, but the number of disturbed cases is really small.

For the lidar sites the HarmCY43-WFP bias is smaller than 0.25m/s for all sites. The WFP gives a significant improvement at BSA. This confirms results of an earlier study for 2016 (van Stratum et al., 2021). Compared to this study from 2016 the bias for 2019 is a bit smaller (0.6m/s). In 2016 this was 0.7-0.9m/s. During the measurement period in 2016 the lidar was much closer to the wind farm, and with similarly prevailing south-westerly winds the wake effects are expected to be stronger. For the lidar sites (K13A, HKNA and TNWB) that are further away from wind farms and therefore not (that often) disturbed, the WFP does not affect the averaged bias, as to be expected.

Wind direction: Table 15 gives a summary of the wind direction evaluation with the lidar measurements. For the evaluation of the wind direction we used a circular coordinate system. The Zephir300 lidars at BSA, K13A, HKNA and TNWB have been corrected for the 180^o Doppler error which occurs mostly at low wind speeds (Appendix C). We assume that the Zephir300 lidars have this error if the wind direction measurement differs more than 90^o with the model value (Knoop et al., 2018). The lidar measurements at BSA may be disturbed by flow distortions caused by the wind masts on the platform. How much depends mainly on the wind direction.

Table 14: Overview of the HarmCY43-CTL and HarmCY43-WFP validation at lidar and cup measurement sites on the North Sea. For the lidars the statistics are the profile averaged values, ranging between 50m up to a maximum height of 200-300m above sea level (depending on the lidar). The number is the total sum of hourly averaged measurements used to evaluate HarmCY43. The column z denotes the hub height (range) of the turbines in the nearest wind farm(s). There is no value at K13(A) because the wind farm is 95km away.

name	WF	z	nr.	OBS	CTL	WFP	bias CTL	bias WFP	R^2 CTL	R^2 WFP	$RMSE$ CTL	$RMSE$ WFP
units	km	m	-	m/s	m/s	m/s	m/s	m/s			m/s	m/s
KNMI/RWS measurements												
AWG1	39	78-105	8709	8.54	8.77	8.76	0.24	0.23	0.78	0.78	1.84	1.85
BG-OHVS2	0	89	8742	8.04	9.51	8.55	1.47	0.51	0.87	0.88	2.14	1.56
Europlatform	45	71-94	8655	8.65	8.79	8.75	0.14	0.10	0.88	0.88	1.46	1.45
Huibertgat	12	78-105	8739	8.11	8.23	8.22	0.12	0.11	0.86	0.86	1.32	1.33
IJmond	13	59-81	8619	7.79	8.16	8.11	0.37	0.32	0.87	0.87	1.46	1.45
K13	95		8715	9.81	9.37	9.38	-0.43	-0.42	0.89	0.90	1.53	1.49
Lichteiland Goeree	59	71-94	8739	8.67	8.80	8.74	0.13	0.07	0.89	0.89	1.42	1.41
Oosterschelde	47	71-94	8723	7.75	8.37	8.30	0.63	0.55	0.87	0.88	1.56	1.51
P11-B	53	59-81	6489	8.40	8.67	8.69	0.27	0.28	0.83	0.82	1.84	1.86
Vlakte van de Raan	17	71-94	8724	7.71	8.30	8.23	0.59	0.53	0.86	0.86	1.57	1.52
Research platforms												
FINO1	0	78-105	17562	8.84	10.34	9.31	1.5	0.47	0.88	0.89	2.12	1.51
FINO3	1	88-95	25032	9.43	10.02	9.84	0.59	0.41	0.84	0.86	1.82	1.71
Lidar sites												
BSA	10	71-94	13840	9.45	10.10	9.67	0.65	0.22	0.84	0.83	1.98	1.89
K13A	95		79380	10.15	10.08	10.09	-0.07	-0.06	0.90	0.90	1.57	1.54
HKNA	9	59-81	15416	11.17	11.38	11.36	0.22	0.20	0.90	0.91	1.74	1.72
TNWB	18	89	41140	10.08	10.03	10.00	-0.05	-0.08	0.86	0.86	1.75	1.75
Eemshaven	1	100	7385	10.94	10.84	10.68	-0.10	-0.25	0.87	0.87	1.68	1.68

Averaged over the whole period (depending on the site 2-12 months in 2019) and over all available heights (depending on the lidar 50-200m or 50-300m), the wind direction bias is similar for HarmCY43-CTL and HarmCY43-WFP and varies between $1-5^o$. The HarmCY40-CTL bias for Cabauw was of similar magnitude (Knoop et al., 2019). In our report we looked at all wind directional data, but Knoop et al. (2019) left out low wind speeds (<0.5m/s), which generally amounts to less than 1% of the hourly averaged data. The differences between the wind speed climatology in HarmCY40 and HarmCY43 are described in Theeuwes et al. (2021a), offshore at hub height the differences were less than 2%. However, there is no information about how HarmCY40 and HarmCY43 compare for wind direction. Just like for wind speed, the wind direction correlation is not affected by the WFP (R^2 remains about 0.8).

Table 15: Overview of the HarmCY43-CTL and HarmCY43-WFP wind direction validation at lidar measurement sites on the North Sea. The wind directions have been transformed into circular coordinates to calculate mean wind direction, bias, R^2 and $RMSE$. The statistics are based on the profile averaged values, between 50m and 200-300m above sea level. The number of measurements is the sum of the hourly averaged measurements used to evaluate with HarmCY43. If the difference between both model runs and the measurements is more than 90^o the Zephir300 Doppler lidars have a directional error, which is included in the last column. *For the correlation of the Eemshaven lidar we left out the measurements with a deviating direction of more than 90^o, which were in total 197/11505 cases or 1.7%, in order to make a similar comparison as with the Zephir300 lidars.

name	nr.	OBS	CTL	WFP	bias CTL	bias WFP	R^2 CTL	R^2 WFP	$RMSE$ CTL	$RMSE$ WFP	error $> 90^o$
units	-	^{o}	^{o}	^{o}	^{o}	^{o}			^{o}	^{o}	%
BSA	14831	241	241	237	1.5	2.3	0.77	0.77	5.8	5.7	9.7
K13A	87265	244	244	238	1.3	1.5	0.80	0.82	5.4	5.5	4.0
HKNA	13746	263	263	254	-2.6	-2.3	0.84	0.83	5.6	5.6	3.6
TNWB	29734	232	232	231	1.0	1.2	0.82	0.82	5.4	5.3	3.1
Eemshaven*	11308	259	259	253	-4.7	-4.2	0.93	0.94	5.6	5.6	1.7

Q2: How well is the diurnal cycle of the wind represented by HARMONIE-AROME?

We only verified the diurnal cycle of HarmCY43 at the lidar locations. HarCY43 captures the diurnal cycle very well and the WFP does not affect this. As to be expected, the diurnal cycle is almost absent offshore. A small effect is visible at coastal site Eemshaven, although this might not be significant. The bias at BSA is larger, but due to the limited number of measurements we cannot draw conclusions.

Q3: How does the wake effect depend on vertical stability and wind speed?

Based on the Bulk Richardson number we have divided the measurements in three different flow regimes: unstable flow ($Ri < 0.0$), weakly stable flow ($0.0 <= Ri <= 0.25$) and stable flow ($Ri > 0.25$). We distinguish between disturbed and undisturbed winds, where we assume wind measurements to be disturbed for wind directions with upstream wind farms within 50 km from the measurement location (Tab. 1,2).

The measurement campaigns at BSA, HKNA, TNWB and Eemshaven lasted only a few months, which makes the interpretation of the results difficult. Mainly for the stable and weakly stable stability classes the number of measurements is limited, which makes it hard to draw any robust conclusions.

HarmCY43-CTL is validated for undisturbed conditions, so only wind directions that are not disturbed by the wind farm (note that both Eemshaven and FINO3 possibly measure the blockage effect because they are within 1km from wind farms):

- During stable undisturbed conditions HarmCY43-CTL underestimates the wind speeds at 6/9 KNMI/RWS measurement sites (generally less than 0.3m/s, with a maximum of 0.9m/s). Also the lidars at the BSA, K13A, HKNA, TNWB and Eemshaven show an underestimation of the wind speed. The K13A lidar has the longest record and matches the underestimation at KNMI/RWS measurement site K13.

- For weakly stable undisturbed conditions we find a clear overestimation of the wind speeds for 7/9 KNMI/RWS measurement sites (between 0.3-0.9m/s). At half of the lidar locations (BSA, HKNA and TNWB) we also observe an overestimation. At BSA there were not enough profiles to draw conclusions from, at HNKA and TNWB the overestimations was ≈0.5m/s. Also at FINO3 the wind speeds are overestimated (≈0.5m/s).

- For unstable undisturbed conditions 8/9 KNMI/RWS measurement sites overestimate the wind speed with 0.1-0.7m/s. At FINO3 the wind speeds were overestimated with ≈0.6m/s. At the lidar locations all sites show different results. At Eemshaven we observe a overestimation (≈0.5m/s above 130m). At HKNA HarmCY43-CTL overestimates the wind speed at all levels, while at K13A HarmCY43-CTL underestimates the wind speed at all levels. At BSA and TNWB HarmCY43-CTL underestimates the wind speed at higher levels. Around hub height (100m) there is however good agreement between HarmCY43-CTL and the lidar measurements at BSA and TNWB. The same goes for the measurements below 125m at TNWB. Below 100m HarmCY43-CTL overestimates the wind speed at BSA.

Due to the limited number of disturbed measurements per stability class we have also taken into account cases with less that 100 measurements in the next paragraph (note that we did leave out BG-OHVS2 and FINO1 because they do measure inside the wind farm). HarmCY43-WFP is validated for disturbed conditions (so only wind directions that are disturbed by the wind farm):

- During stable disturbed conditions the WFP overestimates the wind speed for the majority of the KNMI/RWS measurement sites (4/6). At FINO3 the wind speeds were overestimated with ≈0.6m/s. At the lidar sites (allemaal genoeg metingen?) we observe the opposite: HarCY43-WFP underestimates the wind speed at all locations and for all levels, except at HKNA above 150m: BSA (0.1-1.0m/s), HKNA (below 150m: 0.1-0.3m/s) and TNWB (≈1m/s). There are no disturbed winds at K13A and there is therefore no difference between HarmCY43-WFP and HarmCY43-CTL for that location. Elsewhere we clearly see that the WFP decreases the wind speed for all levels.

- For weakly stable and unstable disturbed conditions the WFP still overestimates the wind speed for 5/6 KNMI/RWS measurement sites (but less than HarmCY43-CTL). At BSA, HKNA, TNWB and FINO3 the wind speeds are also overestimated. Since the undisturbed wind speeds were already too high for most of the cases, this could also partially explain the overestimation.

HarmCy43-WFP may underestimate wind speeds because in the WFP we assume that wind turbines are harvesting energy conform the power curve provided by the manufacturer. They may not (any more) if they are old or badly maintained. And it is possible that wind turbines are not turning because of other reasons that the wind, e.g. maintenance or legislation about bird/bat migration. In the WFP the only reason for wind turbines not to turn is too little or too much wind. If the turbines do not turn for another reason, the WFP will overestimate the wake effect and underestimate the wind.

There are still improvements to be made for HarmCY43: in general HarmCY43-CTL underestimates undisturbed winds in stable conditions and overestimates winds for weakly stable and unstable conditions. For the undisturbed stable conditions we clearly observe an underestimation of the wind speed at the KNMI/RWS measurement sites. But, based on the analyses above, we cannot draw a clear conclusion on the performance of HarmCY43-WFP under disturbed stable conditions, possibly due to the limited number of observation under these conditions. Though, at the lidar locations we can observe that the WFP makes this underestimation worse. HarmCY43-WFP overestimates disturbed winds under weakly stable and unstable conditions (the overestimation is less than for HarmCY43-CTL). In conclusion, after comparing wind speed, directions, diurnal wind profiles, directional wind profiles and stability regimes, the HarmCY43-WFP clearly outperformed HarmCY43-CTL.

Q4: How strong and how long is the wake effect of the wind farms?

We expect the strongest and longest wakes under stable conditions. We have defined the averaged wake effect as the difference between HarmCY43-WFP and HarmCY43-CTL. This implies that we assume that the wake effects are unbiased in the model. If we would calculate the wake effect as the difference between HarmCY43-CTL and the measurements the model bias during stable conditions would result in an underestimation of the wake effect. From the validated sites with more than 100 disturbed cases for stable stratification we can conclude that:

- FINO3: The nearest wind farm is 1km away and the average wind speed is around 7m/s. Here we observe an average wake effect of 1.3m/s around 90m. The average wake effect is the wake effect averaged over all disturbed wind directions and measurement heights.
- HKNA: The nearest wind farm is 9km away and the average wind speed is 6.5m/s. Here we observe an average wake effect of ≈0.5m/s above 100m, below 100m the velocity deficit was around 1m/s.
- BSA: The nearest wind farm is 10km away and the average wind speed is 7m/s. Around 150m we observe a velocity deficit of 0.5m/s, just below 100m the velocity deficit increases to above 1m/s.
- IJmond: The nearest wind farm is 13km away and the average wind speed is 4.5m/s. Here we observe an average wake effect of 0.15m/s (within the measurement uncertainty range).
- Vlakte van de Raan: The nearest wind farm is 17km away and the average wind speed is 4m/s. Here we observe an average wake effect of 0.45m/s.
- Europlatform: The nearest wind farm is 45km away and the average wind speed is around 6m/s. Here a wake effect of 0.25m/s was predicted by the WFP.
- Oosterschelde: The nearest wind farm is 47km away and the average wind speed is 5m/s. The WFP predicts a wake effect of 0.4m/s.

So, only looking at stable stratification we can can conclude: (1) even at Oosterschelde, which is 47km away from the wind farm we observe a wake effect. Based on this, the 50km limit seems reasonable. (2) In all cases we see that the WFP decreases the wind speed, only at BSA the WFP did not improve the model bias, basically because HarmCY43-CTL already underestimates the wind speed. (3) At FINO3 we observed the largest wake effect averaged over the measurement period are in the order of 1.3m/s.

For unstable disturbed conditions, the wake effects at BSA are very large: 2m/s, which is about 20% of the average wind speed at these sites. At BSA the flow is disturbed for a lot of wind directions: a range of $\sim 100^o$. This might explain why the disturbance is so large. At HKNA, where the wind farm is just as close, the disturbed wind direction range and the wake effects are both much smaller. This is not only because a smaller wind sector affects the measurements, but also because a meandering wake might easily miss the measurement site.

7.3 Future Research

In this study we made use of existing measurements for validation of the WFP. The results are promising, but the number of measurements in wind farm wakes remains limited. For future research we strongly recommend targeted measurement campaigns in wind farm wakes and to use these measurements for further model validation. However, by comparing HarmCY43-WFP and HarmCY43-CTL we can isolate the wake and build a wake propagation model.

8 Conclusion

HARMONIE-AROME simulations, including the parametrisation of operational wind farms (referred to as HarmCY43-WFP), are part of the WINS50 project. In this report we will focus on the validation of HarmCY43-WFP for the year 2019. We validated wind speed and wind direction with five lidars and wind speed with cup anemometers at KNMI/RWS measurement sites and the FINO1 and FINO3 research platforms. All of the lidars, except for the one at Eemshaven, are Zephir300 lidars and provide wind profiles up to a height of 200-300m (Fig.3). Only the wind speed and wind direction measurements above 50m are used for validation because measurements at lower heights are too disturbed by the platforms. The KNMI/RWS measurement sites measure at a height between 17-74m. The FINO1 and FINO3 measurements were at several heights between 30-100m. The lidars and cup anemometers are deployed at different distances from operational wind farms, from 10 km (FINO3, BSA and Eemshaven), to 20km (Huibertgat, IJmond, Vlakte van de Raan, HKNA and TNWB) or even further away (AWG1, Europlatform, P11-B, K13, Lichteiland Goeree, Oosterschelde and K13A).

In all cases we see that the wind farm parametrisation (WFP) decreases the wind speed, as expected. For the lidar sites the HarmCY43-WFP bias is smaller than 0.25m/s for all sites, which is in the similar order of magnitude as the measurement uncertainty. For the lidar sites that are further away from wind farms and therefore not (that often) disturbed, the WFP does not affect the averaged bias, as to be expected.

Despite the fact that the WFP is not suitable for wake parametrisation in a wind farm we still compared HarmCY43-WFP to measurements within wind farms *Gemini* and a German wind farm cluster. Inside the wind farms HarmCY43-WFP overestimates the wind speed by $\sim$0.5m/s, which is an improvement compared with the reference run without WFP (HarmCY43-CTL).

From the averaged stable profiles we can conclude that wind farm wake effects from HarmCY43-WFP, in some cases, are up to a distance of 50km. This is in line with previous studies (e.g. Platis et al. (2018)). The largest averaged wake effects were within 10km from the wind farms; under stable conditions this was in the order of 1m/s.

Although this was not the focus of this report, we also compared the HarmCY43 temperature and humidity profiles to measurements at FINO1 and FINO3. The validation results indicate that both HarmCY43-CTL and HarmCY43-WFP give a good representation of the temperature profile (generally within the 0.1 °C measurement uncertainty range), but underestimate the relative humidity at all levels with approximately 5% (the difference between HarmCY43-CTL and HarmCY43-WFP was small).

There are still improvements to be made for HarmCY43-WFP with respect to the parametrisation under stable and weakly stable conditions. In conclusion, after comparing wind speed, directions, diurnal wind profiles, directional wind profiles and stability regimes, the HarmCY43-WFP clearly outperformed HarmCY43-CTL.

Acknowledgements

First of all the authors would like to thank Andrew Stepek for his expert knowledge on the cup anemometer measurements and corrections. We would like to thank Steven Knoop for sharing the lidar data and his feedback. Thanks to Markus Kreklau we have been able to validate our model results at the FINO locations. Thanks to Erik Holtslag and his colleges from Pondera we have been able to validate the model at the coastal site of Eemshaven. There were many different people involved when we were gathering the lidar measurements, for those we have not mentioned in person: thank you for making the data available for this research.

Appendices

A Project deliverables WP5 & WP6

The validation of wakes is part of work package 5 of the WINS50 project which has as key deliverables:

- Use existing datasets for model validation with the focus on (far) wakes.
- Validation datasets must include: floating lidar measurements, synthetic aperture radar (SAR), offshore met masts and offshore platform weather stations.
- The goal is to quantify coastal wind gradient, stability and other effects on power production and wake evolution.
- For the BWFZ the energy production will be validation with power production time series. Also the farm farm interaction between the UK and western Dutch wind farms will be analyzed.

During work package 6 other variations of the wind farm parameterization will be investigated. The future scenario's for 2050 and sensitivity for spacing, number and type of turbines will be explored.

B Wind measurements and validation

The wind measurements from meteorological masts, lidar, aircraft and Doppler radar are often available on short averaged time-scales of around 10-15 minutes. Their spatial coverage varies between one specific point location and an a $10km^2$ average. The Synthetic Aperture Radar (SAR) measurements are collected twice a day over the North Sea covering an area of about 250x250km. The ASCAT coastal product has two overpasses a day and has a swath width of more than 500km (Duncan et al., 2019a). The model output from HARMONIE-AROME in this report is instantaneous on hourly basis and the validation domain covers the Dutch part of the North Sea.

B.0.1 SAR

The Synthetic aperture radar (SAR) (Hasager et al., 2005) provides a snap shot of the wind field at high resolution, typically below 100m. Though, due to noise the data requires averaging over a larger area of 500m (Ahsbahs et al., 2020). The Sentinel 1A and 1B satellites, with SAR on board, pass over the North Sea twice a day at an elevation of 400-700km. SAR measures the backscatter from the oceans short wind generated waves and eddies. SAR is thus a proxy of the near surface winds, representing the 10m winds above the water surface.

A quantitative comparison between SAR and model/measurement data is proven to be difficult. Most of the studies focus on a qualitative comparison (Hasager et al., 2015). Compared with Advanced scatterometers (ASCAT) the SAR wind fields are within the standard deviation boundaries of 2m/s (Monaldo et al., 2016). The benchmarking studies from Ahsbahs et al. (2020) also shows promising results. Compared with the Doppler radar measurements the SAR measurements are found to inherit a 4% smaller velocity deficit. Additionally, the quality of the retrieved wind speeds depends on the atmospheric stability. The agreement with the Doppler radar was best under unstable conditions. The SAR data is available free of charge and thereby does provide opportunities for the validation of wake structures in reanalysis.

B.0.2 Doppler radar

Horizontal scanning Doppler radars are the sole ground based measurements capturing spatial wake development. With the high spatial resolution the wake effects of individual turbines can be observed. This poses an additional challenge for wake modelling. To predict the development of individual wakes the Park model can be used during stable conditions Nygaard and Christian Newcombe (2018). On average their model results were in good agreement with the measurements, though the individual wakes were underestimate by approximately 1m/s.

Potentially the Doppler radar could provide short term power forecasts for wind farms (Valldecabres et al., 2018). Limiting though is the spatial coverage of the data, which is not large enough to capture the full inflow conditions of large wind farms. Possibly, combined with SAR measurements the full inflow conditions could be reconstructed. To study cluster wakes Schneemann et al. (2020) analysed the Doppler and SAR measurements together. In a (weakly) stable atmosphere they observed wakes of at least 55km long with an average flow reductions of $21 - 25\%$.

B.0.3 Aircraft measurements

The availability of aircraft measurements are limited (Lampert et al., 2020). The flights can capture detailed transects behind the wind farms. The wind structure of the wakes was well presented in Weather Research and Forecasting model WRF (Siedersleben et al., 2018b), also the warming and drying of the air in the wake can be observed (Siedersleben et al., 2018a). They however did observe an underestimation of the upwind wind speed (with a maximum bias of 1.9m/s) and the wind speed within the wake.

C Zephir300 Directional corrections

The Zephir300 lidars at BSA, K13A, HKNA and TNWB have been corrected for the 180^o Doppler error. We assume that the Zephir300 lidars have this error if the wind direction measurement differs more than 90^o with the model value (Knoop et al., 2018). Compared with Knoop et al. (2018) we used HarmCY43-WFP and HarmCY43-CTL for the correction: in case both models have an error of more than 90^o we applied the 180^o correction.

In order to calculate the error, without having issues with the $360 - 0^o$ transition, the directions have been transformed into a circular coordinate system. Next, the hourly averaged wind direction was compared with the closed HarmCY43 grid point. We will examine the directional error for all the wind speeds and for four groups: (1) <=4m/s, (2) 4-8m/s, (3) 8-12m/s, (4) >12m/s.

BSA: The directional errors for the BSA lidar are mainly observed between $290^o - 350^o$, for higher wind speeds the 180^o error was also observed around 100^o (Fig.33). Most of the directional errors are found for wind speeds below 4m/s, with an occurrence of 14.4% within this wind speed group. The directional error for low wind speeds (<=4m/s) around 300^o equals 100% of the cases, this is also the direction within which the mast wake effects are expected. If both the HarmCY43-WFP and HarmCY43-CTL were deviating more than 90^o compared with the observed wind direction, than the 180^o was assumed.

K13A: The wind directions for wind speeds above 4m/s are well represented in the model (Fig.34). Though, in 10% of the cases a directional error was found for wind speeds <=4m/s. The largest directional errors were observed for the Northern wind directions, with a maximum scaled occurrence of 42%. The errors are consistent for all wind speeds which makes wake effects from a mast plausible.

HKNA: The wind directions from the models compare well with the HKNA lidar, especially for wind speeds above 4m/s (Fig.35). For wind speeds <=4m/s almost 14% of the cases show a directional error. Most of the errors are observed for Northern wind directions, which is consistent for all wind speeds.

TNWB: The wind directions of TNWB compare well with the modelled wind directions of HarmCY43-WFP and HarmCY43-CTL (Fig.36). The smallest errors are observed for wind speeds >4m/s, which are on average less than 4% of the cases. The errors of the low wind speeds (<=4m/s) gradually decrease from North to South and are smallest for a Southern wind directions after which they increase again from South to North. For the Northern wind direction the largest errors are also observed for wind speeds >4m/s.

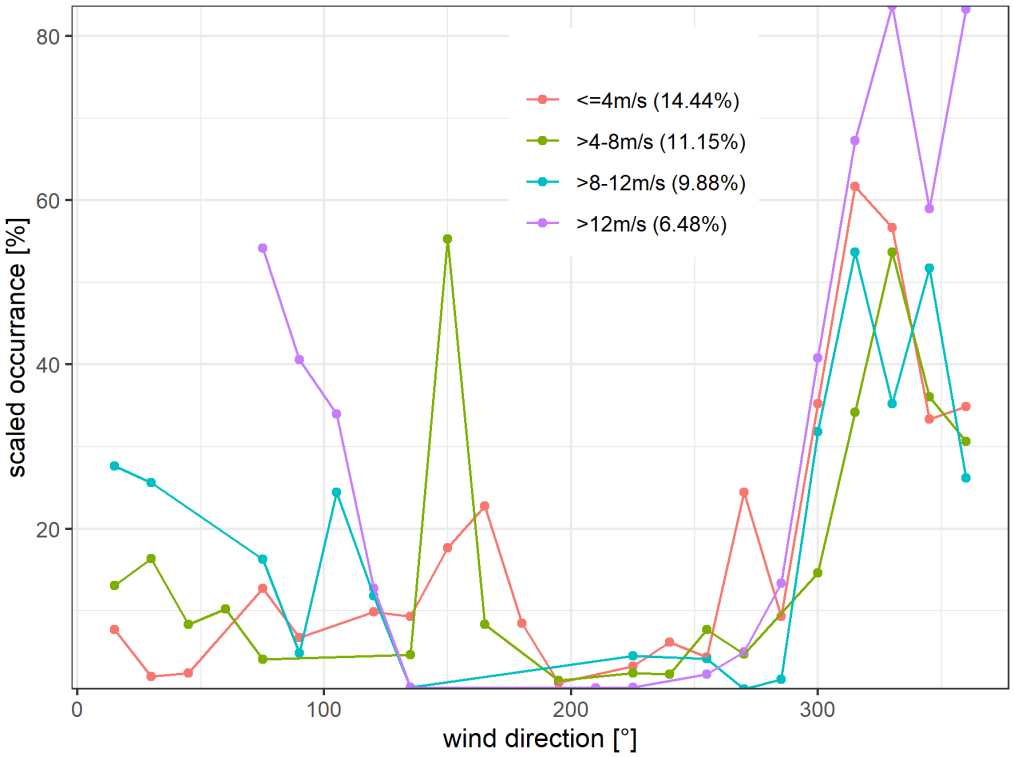

Figure 33: Directional errors of the wind speed for the BSA lidar. The wind directions combined into groups of 15^o each. The occurrences are scaled to the number of cases in the measurements for the wind speed and directions class. In the legend the precentral occurrence of the error compared to the total number of measurements in the wind speed ground are included.

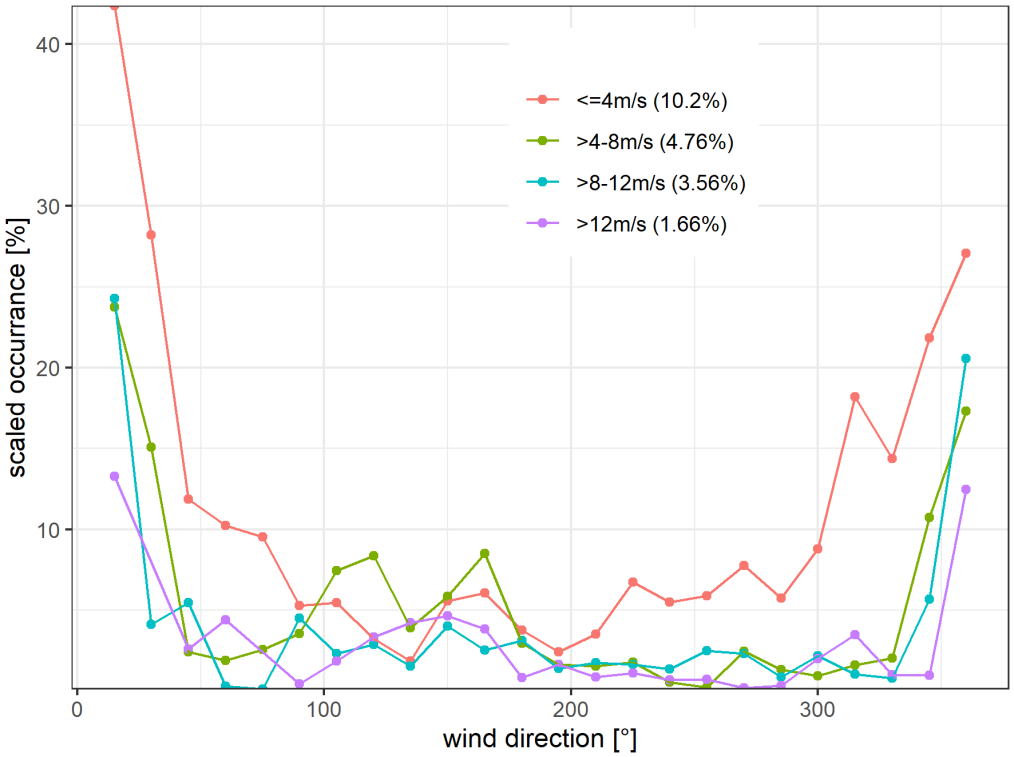

Figure 34: Directional errors of the wind speed for the K13A lidar. The wind directions combined into groups of 15^o each. The occurrences are scaled to the number of cases in the measurements for the wind speed and directions class. In the legend the precentral occurrence of the error compared to the total number of measurements in the wind speed ground are included.

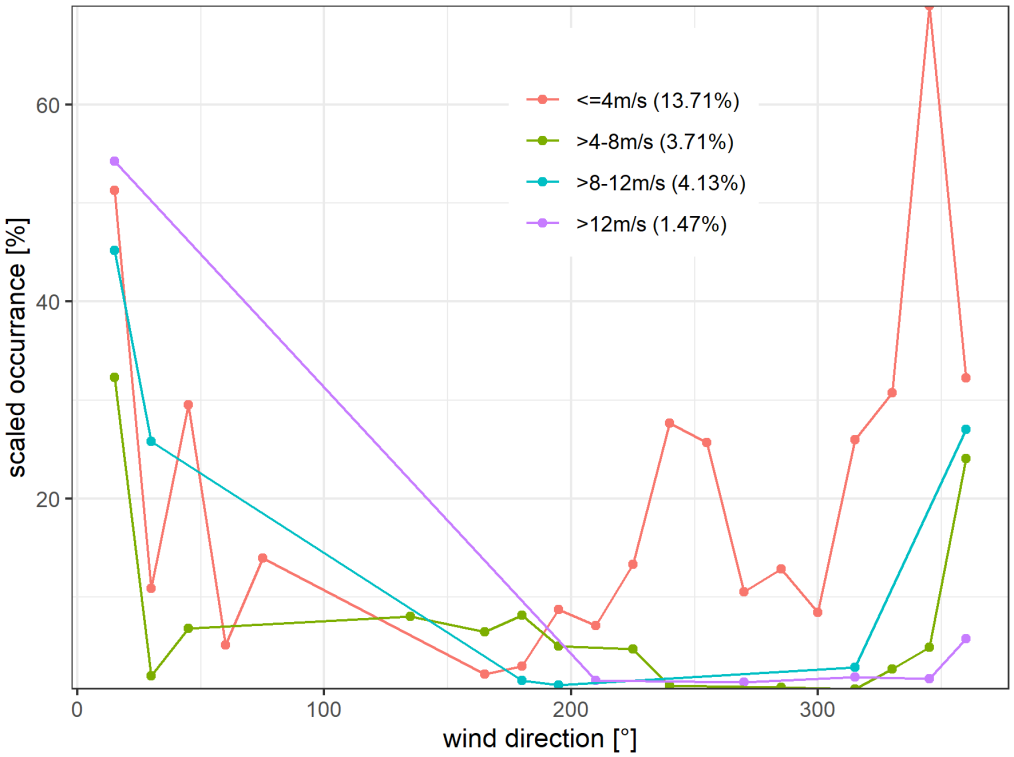

Figure 35: Directional errors of the wind speed for the HKNA lidar. The wind directions combined into groups of 15^o each. The occurrences are scaled to the number of cases in the measurements for the wind speed and directions class. In the legend the precentral occurrence of the error compared to the total number of measurements in the wind speed ground are included.

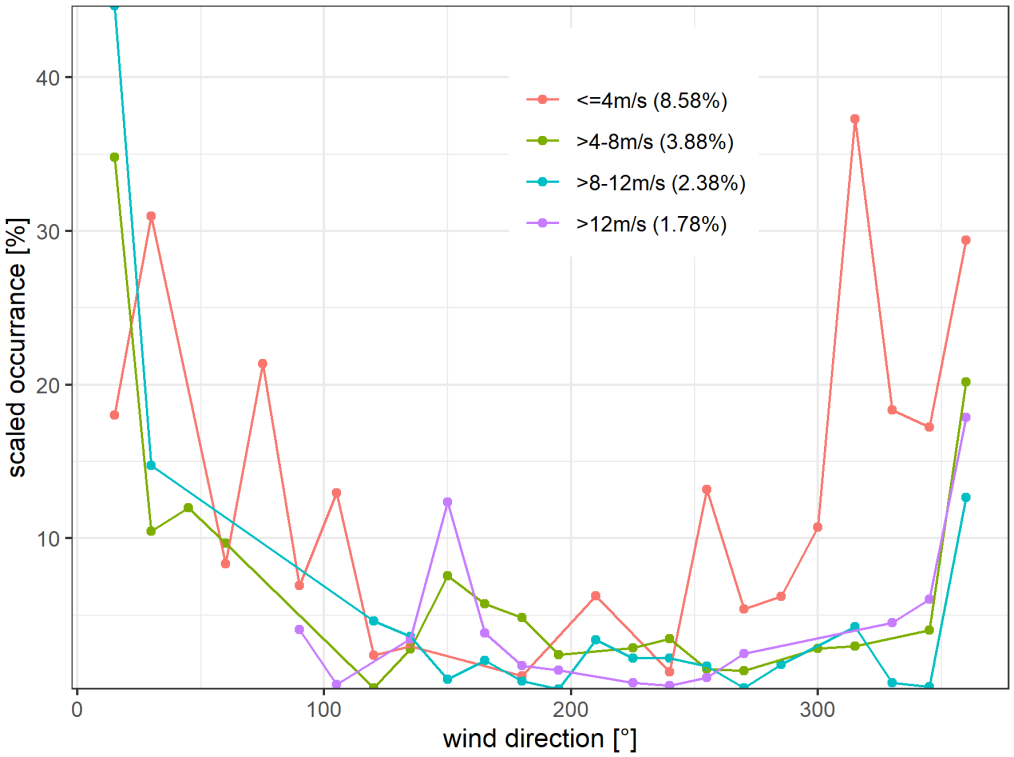

Figure 36: Directional errors of the wind speed for the TNWB lidar. The wind directions combined into groups of 15^o each. The occurrences are scaled to the number of cases in the measurements for the wind speed and directions class. In the legend the precentral occurrence of the error compared to the total number of measurements in the wind speed ground are included.

References

T. Ahsbahs, N. G. Nygaard, A. Newcombe, and M. Badger. Wind farm wakes from SAR and doppler radar. *Remote Sensing*, 12(3):1–22, 2020. ISSN 20724292. 10.3390/rs12030462.

P. Baas, S. R. de Roode, and G. Lenderink. The scaling behaviour of a turbulent kinetic energy closure model for stably stratified conditions. *Boundary-Layer Meteorology*, 127(1):17–36, 2007. ISSN 00068314. 10.1007/s10546-007-9253-y.

L. Bengtsson, U. Andrae, T. Aspelien, Y. Batrak, J. Calvo, W. de Rooy, E. Gleeson, B. Hansen-Sass, M. Homleid, M. Hortal, K. I. Ivarsson, G. Lenderink, S. Niemelä, K. P. Nielsen, J. Onvlee, L. Rontu, P. Samuelsson, D. S. Muñoz, A. Subias, S. Tijm, V. Toll, X. Yang, and M. Ø. Køltzow. The HARMONIE-AROME model configuration in the ALADIN-HIRLAM NWP system. *Monthly Weather Review*, 145(5):1919–1935, may 2017. ISSN 15200493. 10.1175/MWR-D-16-0417.1. URL https://journals.ametsoc.org/view/journals/mwre/145/5/mwr-d-16-0417.1.xml.

J. Bleeg, M. Purcell, R. Ruisi, and E. Traiger. Wind farm blockage and the consequences of neglecting its impact on energy production. *Energies*, 11(6), 2018. ISSN 19961073. 10.3390/en11061609.

P. Brousseau, L. Berre, F. Bouttier, and G. Desroziers. Background-error covariances for a convective-scale data-assimilation system: AROME-France 3D-Var. *Quarterly Journal of the Royal Meteorological Society*, 137(655):409–422, jan 2011. ISSN 00359009. 10.1002/qj.750. URL http://doi.wiley.com/10.1002/qj.750.

D. Cevasco, S. Koukoura, and A. J. Kolios. Reliability, availability, maintainability data review for the identification of trends in offshore wind energy applications, feb 2021. ISSN 18790690.

M. B. Christiansen and C. B. Hasager. Wake effects of large offshore wind farms identified from satellite SAR. *Remote Sensing of Environment*, 98(2-3):251–268, 2005. ISSN 00344257. 10.1016/j.rse.2005.07.009.

S. De Haan. High-resolution wind and temperature observations from aircraft tracked by Mode-S air traffic control radar. *Journal of Geophysical Research Atmospheres*, 116(10):10111, may 2011. ISSN 01480227. 10.1029/2010JD015264. URL https://onlinelibrary-wiley-com.tudelft.idm.oclc.org/doi/full/10.1029/2010JD015264https://onlinelibrary-wiley-com.tudelft.idm.oclc.org/doi/abs/10.1029/2010JD015264https://agupubs-onlinelibrary-wiley-com.tudelft.idm.oclc.org/doi/10.1029/2010JD015264.

S. De Haan. Estimates of Mode-S EHS aircraft-derived wind observation errors using triple collocation. *Atmospheric Measurement Techniques*, 9(8):4141–4150, aug 2016. ISSN 18678548. 10.5194/AMT-9-4141-2016.

J. B. Duncan, G. J. Marseille, and I. L. Wijnant. DOWA validation against ASCAT satellite winds. Technical report, TNO, 2019a. URL www.tno.nl.

J. B. Duncan, I. L. Wijnant, and S. Knoop. DOWA validation against offshore mast and LiDAR measurements. Technical report, KNMI, De Bilt, 2019b. URL https://www.dutchoffshorewindatlas.nl/publications/reports/2019/12/05/knmi-report---dowa-validation-coastal-wind-lidarhttps://www.dutchoffshorewindatlas.nl/binaries/dowa/documents/reports/2019/05/21/tno-report---dowa-validation-against-offshore-mast-and-.

S. Faulstich, B. Hahn, and P. J. Tavner. Wind turbine downtime and its importance for offshore deployment. *Wind Energy*, 14(3):327–337, apr 2011. ISSN 10954244. 10.1002/we.421.

J. Fischereit, R. Brown, X. G. Larsén, J. Badger, and G. Hawkes. Review of Mesoscale Wind-Farm Parametrizations and Their Applications. *Boundary-Layer Meteorology*, 2021. ISSN 0006-8314. 10.1007/s10546-021-00652-y. URL https://doi.org/10.1007/s10546-021-00652-y.

A. C. Fitch. Notes on using the mesoscale wind farm parameterization of Fitch et al. (2012) in WRF, sep 2016. ISSN 10991824.

A. C. Fitch, J. B. Olson, J. K. Lundquist, J. Dudhia, A. K. Gupta, J. Michalakes, and I. Barstad. Local and mesoscale impacts of wind farms as parameterized in a mesoscale NWP model. *Monthly Weather Review*, 140(9):3017–3038, 2012. ISSN 00270644. 10.1175/MWR-D-11-00352.1.

A. C. Fitch, J. B. Olson, and J. K. Lundquist. Parameterization of wind farms in climate models. *Journal of Climate*, 26(17):6439–6458, 2013. ISSN 08948755. 10.1175/JCLI-D-12-00376.1.

A. A. Grachev, E. L. Andreas, C. W. Fairall, P. S. Guest, and P. O. G. Persson. The Critical Richardson Number and Limits of Applicability of Local Similarity Theory in the Stable Boundary Layer. *Boundary-Layer Meteorology*, 147(1):51–82, apr 2013. ISSN 00068314. 10.1007/s10546-012-9771-0.

C. B. Hasager, M. Nielsen, P. Astrup, R. Barthelmie, E. Dellwik, N. O. Jensen, B. H. Jørgensen, S. C. Pryor, O. Rathmann, and B. R. Furevik. Offshore wind resource estimation from satellite SAR wind field maps. *Wind Energy*, 8(4):403–419, 2005. ISSN 10954244. 10.1002/we.150.

C. B. Hasager, P. Vincent, R. Husson, A. Mouche, M. Badger, A. Peña, P. Volker, J. Badger, A. Di Bella, A. Palomares, E. Cantero, and P. M. Correia. Comparing satellite SAR and wind farm wake models. In *Journal of Physics: Conference Series*, volume 625. Institute of Physics Publishing, jun 2015. 10.1088/1742-6596/625/1/012035.

T. H. Joosten and A. Stepek. Wessels' wind measurement corrections : Applied to rigs on the North Sea. Technical report, KNMI Internal report IR-2019-02, De Bilt, 2019.

S. Knoop and I. L. Wijnant. DOWA validation against coastal wind lidar measurements. Technical report, KNMI, 2019.

S. Knoop, W. Koetse, and F. Bosveld. Wind LiDAR measurement campaign at CESAR Observatory in Cabauw: Preliminary results. *arXiv*, pages 1–13, 2018. ISSN 23318422.

S. Knoop, P. Ramakrishnan, and I. L. Wijnant. DOWA validation against Cabauw meteomast wind measurements. Technical report, KNMI, De Bilt, 2019.

S. Knoop, P. Ramakrishnan, and I. Wijnant. Dutch offshore wind atlas validation against cabauw meteomast wind measurements. *Energies*, 13(24):6558, dec 2020. ISSN 19961073. 10.3390/en13246558. URL https://www.mdpi.com/1996-1073/13/24/6558/htmhttps://www.mdpi.com/1996-1073/13/24/6558.

S. Knoop, F. C. Bosveld, M. J. de Haij, and A. Apituley. A 2-year intercomparison of continuous-wave focusing wind lidar and tall mast wind measurements at Cabauw. *Atmospheric Measurement Techniques*, 14(3):2219–2235, mar 2021. 10.5194/amt-14-2219-2021.

A. Lampert, K. Bärfuss, A. Platis, S. Siedersleben, B. Djath, B. Cañadillas, R. Hunger, R. Hankers, M. Bitter, T. Feuerle, H. Schulz, T. Rausch, M. Angermann, A. Schwithal, J. Bange, J. Schulz-Stellenfleth, T. Neumann, and S. Emeis. In situ airborne measurements of atmospheric and sea surface parameters related to offshore wind parks in the German Bight. *Earth System Science Data*, 12(2):935–946, apr 2020. ISSN 1866-3516. 10.5194/essd-12-935-2020. URL https://essd.copernicus.org/articles/12/935/2020/.

T. Leiding, B. Tinz, L. Gates, R. Gudrun, K. Herklotz, C. Senet, O. Outzen, A. Lindenthal, T. Neumann, R. Frühmann, F. rich Wilts, F. Bégué3, P. Schwenk, D. Stein, I. Bastigkeit, B. hard Lange, S. Hagemann, S. Müller, and J. Schwabe. Standardisierung und vergleichende Analyse der meteorologischen FINO-Messdaten (FINO123). 2016.

G. Lenderink and A. A. Holtslag. An updated length-scale formulation for turbulent mixing in clear and cloudy boundary layers. *Quarterly Journal of the Royal Meteorological Society*, 130(604):3405–3427, oct 2004. ISSN 1477-870X. 10.1256/QJ.03.117. URL https://onlinelibrary.wiley.com/doi/full/10.1256/qj.03.117https://onlinelibrary.wiley.com/doi/abs/10.1256/qj.03.117https://rmets.onlinelibrary.wiley.com/doi/10.1256/qj.03.117.

G. Marseille and A. Stoffelen. Toward Scatterometer Winds Assimilation in the Mesoscale HARMONIE Model. *IEEE JOURNAL OF SELECTED TOPICS IN APPLIED EARTH OBSERVATIONS AND REMOTE SENSING*, pages 1–19, 2016.

F. Monaldo, C. Jackson, X. Li, and W. G. Pichel. Preliminary Evaluation of Sentinel-1A Wind Speed Retrievals. *IEEE Journal of Selected Topics in Applied Earth Observations and Remote Sensing*, 9(6):2638–2642, jun 2016. ISSN 21511535. 10.1109/JSTARS.2015.2504324.

N. G. Nygaard and A. Christian Newcombe. Wake behind an offshore wind farm observed with dual-Doppler radars. *Journal of Physics: Conference Series*, 1037(7), 2018. ISSN 17426596. 10.1088/1742-6596/1037/7/072008.

A. Platis, S. K. Siedersleben, J. Bange, A. Lampert, K. Bärfuss, R. Hankers, B. Cañadillas, R. Foreman, J. Schulz-Stellenfleth, B. Djath, T. Neumann, and S. Emeis. First in situ evidence of wakes in the far field behind offshore wind farms. *Scientific Reports*, 8(1):2163, dec 2018. ISSN 2045-2322. 10.1038/s41598-018-20389-y. URL http://www.nature.com/articles/s41598-018-20389-y.

F. Porté-Agel, M. Bastankhah, and S. Shamsoddin. Wind-Turbine and Wind-Farm Flows: A Review. *Boundary-Layer Meteorology*, 174(1):1–59, jan 2020. ISSN 15731472. 10.1007/s10546-019-00473-0.

J. Schneemann, A. Rott, M. Dörenkämper, G. Steinfeld, and M. Kühn. Cluster wakes impact on a far-distant offshore wind farm's power. *Wind Energy Science*, 5(1):29–49, jan 2020. ISSN 2366-7451. 10.5194/wes-5-29-2020. URL https://wes.copernicus.org/articles/5/29/2020/.

Y. Seity, P. Brousseau, S. Malardel, G. Hello, P. Bénard, F. Bouttier, C. Lac, and V. Masson. The AROME-France Convective-Scale Operational Model. *Monthly Weather Review*, 139(3):976–991, mar 2011. ISSN 0027-0644. 10.1175/2010MWR3425.1. URL http://journals.ametsoc.org/doi/abs/10.1175/2010MWR3425.1.

S. K. Siedersleben, J. K. Lundquist, A. Platis, J. Bange, K. Bärfuss, A. Lampert, B. Cañadillas, T. Neumann, and S. Emeis. Micrometeorological impacts of offshore wind farms as seen in observations and simulations. *Environmental Research Letters*, 13(12):124012, nov 2018a. ISSN 1748-9326. 10.1088/1748-9326/aaea0b. URL https://iopscience.iop.org/article/10.1088/1748-9326/aaea0b.

S. K. Siedersleben, A. Platis, J. K. Lundquist, A. Lampert, K. Bärfuss, B. Cañadillas, B. Djath, J. Schulz-Stellenfleth, J. Bange, T. Neumann, and S. Emeis. Evaluation of a wind farm parametrization for mesoscale atmospheric flow models with aircraft measurements. *Meteorologische Zeitschrift*, 27(5):401–415, 2018b. ISSN 16101227. 10.1127/metz/2018/0900.

A. Stepek, M. Savenije, and I. L. Wijnant. Validation of KNW atlas with publicly available mast observations (Phase 3 of KNW project). 2015.

B. Stratum, S. Basu, I. L. Wijnant, J. Barkmeijer, J. Onvlee, and A. P. Siebesma. Wind turbine parametrisation in HARMONIE-AROME. pages 1–28, 2019. URL https://www.dutchoffshorewindatlas.nl/publications/reports/2019/12/06/knmi-report---wind-turbine-parameterisation.

N. Theeuwes, J. Barkmeijer, B. Van Ulft, and I. Wijnant. Comparison DOWA and WINS50-data. Technical report, KNMI, De Bilt, 2021a. URL www.wins50.nl.

N. Theeuwes, J. Barkmeijer, B. Van Ulft, and I. Wijnant. Comparison DOWA and WINS50-data. Technical Report June, 2021b. URL https://wins50.nl/downloads/MemoComparisonDOWAandWINS50.pdf.

C. D. Valk and I. L. Wijnant. Uncertainty analysis of climatological parameters of the Dutch Offshore Wind Atlas (DOWA). Technical report, KNMI, De Bilt, 2019. URL https://www.dutchoffshorewindatlas.nl/publications/reports/2019/12/10/knmi-report---uncertainty-analysis-of-climatological-parameters.

L. Valldecabres, N. Nygaard, L. Vera-Tudela, L. von Bremen, and M. Kühn. On the Use of Dual-Doppler Radar Measurements for Very Short-Term Wind Power Forecasts. *Remote Sensing*, 10(11):1701, oct 2018. ISSN 2072-4292. 10.3390/rs10111701. URL http://www.mdpi.com/2072-4292/10/11/1701.

B. van Stratum, N. E. Theeuwes, J. Barkmeijer, B. van Ulft, and I. Wijnant. A year-long evaluation of a wind-farm parameterisation in HARMONIE-AROME. 2021. URL https://doi.org/10.1002/essoar.10509415.1.

A. Westerhellweg and T. Neumann. Comparison of lidar and UAM-based offshore mast effect corrections. In *EWEA 2011*, number May, page 1:10, Brussels, 2019.

A. Westerhellweg, T. Neumann, and D. Gmbh. FINO1 Mast Correction. *DEWI Magazin*, (40):60–66, 2012.

I. L. Wijnant, G. J. Marseille, A. Stoffelen, H. W. Van Den Brink, and A. Stepek. Validation of KNW atlas with scatterometer winds (Phase 3 of KNW project). Technical report, 2015.

I. L. Wijnant, B. Van Ulft, B. Van Stratum, J. Barkmeijer, J. Onvlee, C. De Valk, S. Knoop, S. Kok, G. J. Marseille, H. Klein Baltink, and A. Stepek. The Dutch Offshore Wind Atlas (DOWA): description of the dataset. 2019.